Title
Understanding Autoinhibition of Drosophila Formin Cappuccino in vitro and in vivo

Author
Bor, Batbileg

Publication Date
2014

Peer reviewed|Thesis/dissertation

UNIVERSITY OF CALIFORNIA

Los Angeles

Understanding Autoinhibition of *Drosophila* Formin Cappuccino *in vitro* and *in vivo*

A dissertation submitted in partial satisfaction of the

Requirements for the degree Doctor of Philosophy

in Molecular Biology

By

Batbileg Bor

2014

ABSTRACT OF THE DISSERTATION

Understanding Autoinhibition of *Drosophila* Formin Cappuccino *in vitro* and *in vivo*

By

Batbileg Bor

Doctor of Philosophy in Molecular Biology

University of California, Los Angeles, 2014

Professor Margot E. Quinlan, Chair

Cappuccino (Capu) is an actin assembly factor that is necessary to establish *Drosophila* oocyte polarity. Disrupting normal polarity leads to female sterility. It is thought that Capu helps establish oocyte polarity by creating a mesh-like actin structure that spans the oocyte during early stages of development. Disappearance of this actin mesh in later stages of oogenesis coincides with rapid coordinated flows of the cytoplasm, referred to as cytoplasmic streaming. When cytoplasmic streaming starts prematurely, as occurs in *capu* null mutants, many polarity determinants fail to localize properly. In this dissertation, I describe the discovery and analysis of autoinhibitory regulation of Capu using both *in vitro* and *in vivo* approaches. The N-terminal half of Capu (Capu-NT, aa1-466) potently inhibits nucleation and binding to the barbed end of elongating filaments by the C-terminal half of Capu (aa467-1059). We identified residues 1-222 as the Capu Inhibitory Domain (CID) using various biochemical techniques such as pyrene polymerization, limited proteolysis and polarization anisotropy assays. This domain is sufficient to bind the short sequence C-terminal to the FH2 domain called Capu-Tail and inhibits the FH2 domain. Based on our biochemical data, we over-expressed a constitutively active form of Capu, CapuΔN (Capu271-1059), in *Drosophila* oocytes. Only 18% of eggs laid by flies expressing CapuΔN hatched, compared to 47% fertility for flies over-expressing full-length Capu. From this we concluded that loss of autoinhibition is deleterious to the developing egg.

Closer examination of CapuΔN-expressing oocytes revealed that the actin mesh persisted beyond stage 10B and the onset of cytoplasmic streaming was delayed. We quantified cytoplasmic streaming using Particle Image Velocimetry and found that streaming is significantly slowed or absent in flies expressing CapuΔN. Supporting that CapuΔN lost its autoinhibitory regulation, trans-expression of CapuΔN and Capu-NT rescued fertility, actin mesh and cytoplasmic streaming phenotypes associated with expressing CapuΔN alone. We also found that the decrease in fertility is due to disruption in the late delivery of polarity factors due to the persistent mesh. Several classic polarity factors, such as *oskar, nanos,* and *bicoid* are improperly localized in the oocyte. Thus autoinhibition of Capu is critical to oogenesis and our ongoing work is elucidating the mechanisms underlying this observation.

The dissertation of Batbileg Bor is approved.

Emil Reisler

Frank A. Laski

Margot E. Quinlan, Committee Chair

University of California, Los Angeles

2014

Table of Contents

Acknowledgment

Although the following dissertation is an individual work, I could never have achieved full potential and scientific imagination without the help, support, guidance and efforts of a lot of people. First, I would like to thank my mentor Dr. Margot Quinlan for inspiring and teaching me to have qualities of being a good scientist and molecular biologist. Her unlimited wisdom and patience have been major driving forces through my graduate career at the University of California, Los Angeles. I want to thank my committee members Dr. Emil Reisler, Dr. Gregory Payne, Dr. Frank Laski and Dr. Robert Clubb for their support and guidance throughout the years. I would also like to thank past and present members of both Dr. Quinlan and Dr. Reisler lab for their constant feedback and support for my education and research. Especially, I want to thank Dr. Vizcarra for being there for me every little step of the way. She was a great trainer and mentor for my early career. I also want to thank Amy Rasson and Elizabeth Roth-Johnson for sharing with me the same lab space for more than five years and went through all the good and bad times together for our graduate careers. Their company late at night in the lab will never be forgotten.

A very special thank you to my friends Alok Joglaker, Rachel Resop and Ragini Bhargava for listening to my complains and guiding me to the right directions during hard times. You guys will be always in my life. I also want to thank my ACCESS class 15, who carried me through my first two years of graduate school. I always had shoulders to lean on during early days of my graduate work. I want to thank Dr. Justin Bois for teaching me how to analyze and critique data critically and his great understanding of the life sciences. I have to thank my mentor and adviser Dr. Kimberly Tanner and Angie Feather Bushi. Without their selfless support and contribution to my academia, I would not have attended graduate school and get my PhD. They will be always remembered as a hero to me.

Lastly, I want to thank my family. Although my mom and dad do not have PhDs, they are capable individuals with strong heart and will. Given the opportunity, they would have achieved

higher education and supported their communities. That is exactly what they did for me, providing great many opportunities in my life. Without their difficult decision to immigrate and search for better life and opportunities, I would not be here getting my PhD. I would like to give my greatest respect to them and their sacrifices that they made for me. I also like to thank my brother, sister and my uncle's family, who truly supported me throughout my graduate career and higher academic achievements.

Lastly, I want to thank a little boy who kept me busy every night. He always has a smile for me, whether I am angry or sad. When I am with him, I always turn into a little boy like him who is curios about world and science. I want to know more about how things work and why things work. Without knowingly, he helped me understand how exciting and interesting science is.

Vita

Education: B.S in Biochemistry, Graduated in Spring 2008 (SFSU, San Francisco CA),

Fellowships

2012 Whitcome fellowship (Molecular Biology Institute, UCLA)

Professional Experience

2013 Woods Hole, Physiology Course (Super Resolution Microscopy, Molecular Biology and Theoretical Modeling).

2010 Summer School on Actin Nucleators, University of Regensburg, Regensburg, Germany (Learning from the leaders in the field of actin nucleators and cytoskeleton using advanced techniques such as microinjection of cells, fluorescence imaging of cells by spinning disc confocal microscopy, and visualizing the single filament growth and regulation by TIRF microscopy)

2008 Summer intern at UCSF (Ciliogenesis and its affect on mouse ESC and differentiation, mentor Dr. Reiter)

2007 Summer intern at Genentech, ORDP in PROP rotational program and Quality Control Stability department (Automation of clot lysis Activase assay using Oasis, 96 well channel pipetter, manager Nithila Dozier)

2006 Undergraduate program, continuation of University of Montana (Research on nitrogen limited environment for yeast evolution by using chemostats and TECAN, mentor Dr. Frank)

2005 Special Project Lab on Organic Chemistry, chem 338 at SFSU, (Synthesis of Diarylureas for potential cancer therapeutics)

2005 Undergraduate program at University of Montana and Stanford University (Research on yeast evolution and mutagenesis by using chemostats, mentor Dr. Frank)

Meeting Presentations

2013 National Annual Meeting of American Society for Cell Biology, subsection *Molecular Control of Cytoskeletal Dynamics* (Talk)

2012 Annual lake Arrowhead retreat of Molecular Biology Institute at UCLA (Talk)

2012 Seaborg symposium presented by the Department of Chemistry and Biochemistry, Jonsson Comprehensive Cancer Center and David Gaffen School of Medicine at UCLA (Poster)

2011 Sigman symposium at UCLA (Poster)

2011, 2012 Annual lake Arrowhead retreat of Molecular Biology Institute at UCLA (Poster)

2011, 2012 National Annual Meeting of American Society for Cell Biology (Poster)

Publications

Bor, B., Vizcarra, C. L., Phillips, M.L., and Quinlan, M.E. (2012). Autoinhibition of the formin Cappuccino in the absence of canonical autoinhibitory domains. Mol Biol Cell 23, 3801-3813.

Honors and Awards

2013 ASCB graduate student travel award

2011, 2012 Poster award at Molecular Biology Institute retreat at UCLA

2011 Paul D. Boyer Outstanding Teaching Award given by Molecular Biology Institute at UCLA

Дуслыг Хураавал Далай

Дуулсныг Хураавал Эрдэм

Introduction: Formins

Formin domain structures and functions

Formins are a large family of proteins that regulate growth of the actin cytoskeleton. These proteins help build a variety of structures including, but not limited to, stress fibers, contractile rings and filopodia. Formins function as actin nucleators, elongation factors, bundlers, and in at least one case as a depolymerizing factor (Chhabra and Higgs, 2006; Goode and Eck, 2007). Formins are defined by their well-conserved Formin Homology 1 and 2 (FH1 and FH2) domains (Higgs and Peterson, 2005). The FH2 domain forms a donut-shaped homodimer that nucleates new filaments and remains associated with the barbed ends of growing filaments (Higashida et al., 2004; Otomo et al., 2005; Pruyne et al., 2002). Through its association with barbed ends, the FH2 domain can modulate the elongation rate and protect filaments from other barbed end binding proteins such as capping protein (Goode and Eck, 2007). The proline rich FH1 domain binds profilin-actin and perhaps some SH3-containing proteins (Ahern-Djamali, 1999; Paul et al., 2008). The FH1 and FH2 domains cooperate to accelerate filament elongation in many cases (Kovar et al., 2006; Neidt et al., 2009).

Formin N-terminal half and autoinhibitory regulation

Actin nucleators must be tightly regulated to control when and where new filaments are created. Actin assembly by formins is commonly inhibited by an intramolecular interaction between the N- and C-terminal halves of the protein (Figure 1). This autoinhibition was first described for diaphanous-related formins (DRFs), specifically mDia1 (Goode and Eck, 2007; Watanabe et al., 1999). Detailed analysis showed that actin nucleation activity is inhibited by a direct interaction between the C-terminal diaphanous autoregulatory domain (DAD) and the N-terminal diaphanous inhibitory domain (DID) (Figure 1, Alberts, 2001; Li and Higgs, 2003; Li and Higgs, 2005). Crystal structures of the DID/DAD complex show that the DAD domain forms a single α-helical peptide that binds in the concave surface formed by the five armadillo repeats of the DID domain (Lammers et al., 2005; Nezami et al., 2006). This interaction is commonly regulated by small GTPases, such as Rho, binding to a GTPase Binding Domain (GBD)

adjacent to and overlapping with the DID domain which results in release of the DAD domain (Lammers et al., 2005; Otomo et al., 2005; Rose et al., 2005). Recent studies confirmed these observations with full length mDia1, showing that it is an autoinhibited dimer that can be at least partially activated by RhoA (Maiti et al., 2012; Nezami et al., 2010; Otomo et al., 2010; Ramalingam et al., 2010).

Since the discovery of autoinhibition in mDia1, it has been shown that five of the seven metazoan groups of formins are regulated by autoinhibition, including Diaphanous (Dia), Formin HOmology Domain-containing protein (FHOD), Formin-Related gene in Leukocytes (FRL), Dishevelled-Associated Activator of Morphogenesis (DAAM) and INverted Formin (INF) (Figure 1, Schönichen and Geyer, 2010). Similar to mDia1, autoinhibition regulates *in vitro* polymerization activity of FRL1 (Seth et al., 2006) as well as thin stress fiber formation by FHOD1, FRL3 and DAAM1 (Liu et al., 2008; Schulte et al., 2008; Vaillant et al., 2008). INF2 is different from other formins, it has both polymerization and depolymerization activities (Chhabra and Higgs, 2006). Interestingly, INF2's DID domain inhibits the depolymerization but not the polymerization activity (Chhabra et al., 2009). All of the above formins, except INF2, have a GBD domain, which binds to Rho family GTPases to partially relieve autoinhibition. Yeast formins also have conserved DAD and DID domains (Higgs and Peterson, 2005). The Rho GTPase Cdc42 regulates fission yeast formin For3 and DAD mutants in this formin make more actin cables (Martin et al., 2007; Rincón et al., 2009).

Localization of both yeast and metazoan formins have also been shown to depend on the N-terminal half of formins. Cell membrane localization of mDia1, mDia2, FHOD1 and FRL1 depends on the N-terminal half and is regulated by the DID/DAD interaction (Gorelik et al., 2011; Schulte et al., 2008; Seth et al., 2006). mDia1 also needs its N-terminus to localize to the mitotic spindle in HeLa cells (Kato et al., 2001). Fission yeast Fus1, Cdc12 and For3 formins localize to the projection tip during cell mating, the contractile ring during cell division and the cell tip, respectively, using their N-termini (Martin et al., 2007; Petersen et al., 1998). Bni1 from

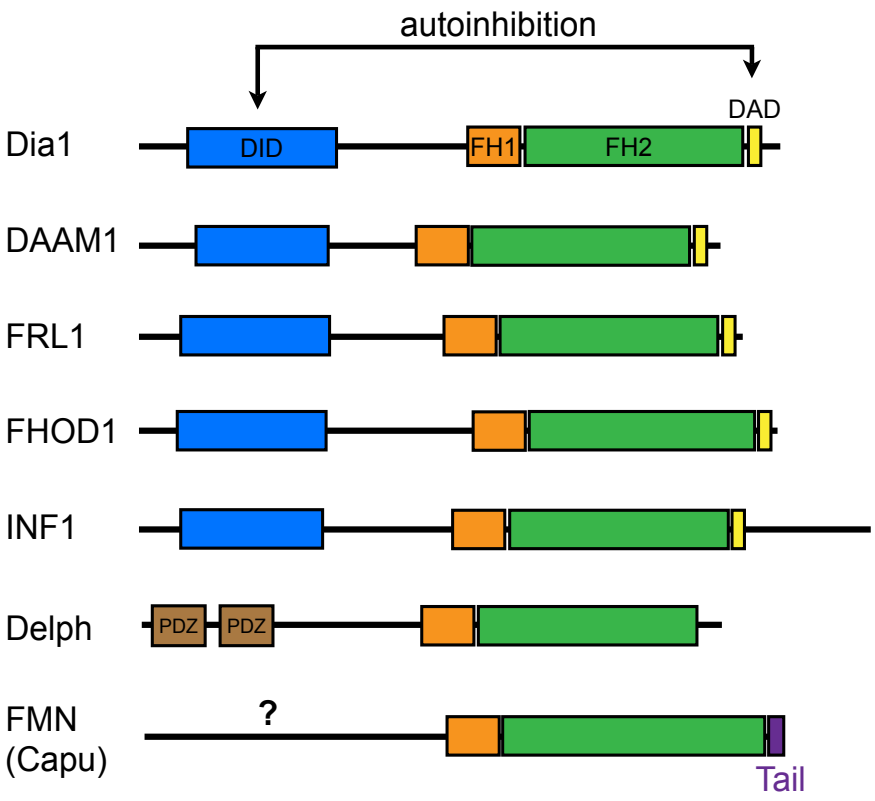

Figure 1. Domain organization of metazoan formins. Domains depicted are the Formin Homology 1 (FH1, orange), Formin Homology 2 (FH2, green), Diaphanous Inhibitory Domain (DID, blue), Diaphanous Autoregulatory Domain (DAD, yellow), Psd95/Dlg/Zo-1 domain (PDZ, brown) and Capu-Tail domain (Tail, purple). Autoregulatory domains DID and DAD interact to inhibit polymerization activity of the FH2 domain (shown by black arrows). The N-terminal half of FMN family of formins, including Capu, are uncharacterized (indicated by the question mark).

budding yeast also needs its N-terminus to localize to the bud tip and this process depends on Cdc42 (Ozaki-Kuroda et al., 2001). While the importance of autoinhibition has been shown for many formins, some formins are not autoregulated. For example, FRL2 has interacting DAD and DID domains, but it seems that this interaction is not necessary for regulating FRL2's activities such as actin polymerization and F-actin bundling (Vaillant et al., 2008). In fission yeast, mutating the putative DAD and DID domains in Cdc12 has no effect on its regulation (Yonetani et al., 2008).

The formin (FMN) group of formins does not have classical DID and DAD domains (Higgs and Peterson, 2005). Previously published data suggest that Capu, a member of the FMN group, is not autoregulated (Rosales-Nieves et al., 2006), consistent with the lack of sequence homology with DAD and DID domains. However, a mammalian ortholog of Capu, Formin-1, is autoinhibited (Kobielak et al., 2003), compelling us to re-examine the possibility that Capu's actin nucleation activity is autoinhibited. The actin nucleator Spire has the same phenotype as Capu and is known to regulate Capu's actin nucleation activity through an interaction between Spire-KIND and Capu-tail domains (Quinlan et al., 2007; Vizcarra et al., 2011). We are therefore interested in understanding the relationship between any potential autoinhibitory interactions within Capu and Capu's regulation by Spire.

***Drosophila* formin Cappuccino during oocyte development**

Capu was originally identified in a screen for maternal-effect genes important for pattern formation. Mutations in *capu* disrupt both anteroposterior (AP) and dorsoventral (DV) axis formation of the *Drosophila* embryo (Manseau and Schüpbach, 1989). In the AP axis, *capu* mutants exhibit reduced abdominal segmentation and loss of pole plasm. In the DV axis, *capu* mutants have fused dorsal appendages. These polarity defects eventually lead to female sterility (Manseau and Schupbach, 1989). The original study of *capu* resulted in the hypothesis that this gene, along with a second gene, *spire*, contributed to both major body axes by localizing and/or stabilizing other patterning factors.

Consistent with Capu's actin polymerization activity, recently Capu was linked to two actin structures in *Drosophila* oocytes: an isotropic mesh that traverses the oocyte and a network of filaments extending from the posterior cortex of the oocyte (Chang et al., 2011; Dahlgaard et al., 2007; Tanaka et al., 2011). The former structure is present throughout mid-oogenesis (stage 5-10), and disappears during stage 10B. In *capu* mutants the mesh is absent (Figure 2A). Capu is also needed to create and maintain the posterior network of actin filaments, which is important for anchoring posterior polarity determinants (Tanaka et al., 2011). In *capu* and *spire* mutants, these posterior actin filaments are completely missing.

A dramatic change in fluid dynamics coincides with disappearance of the actin mesh at stage 10B (Figure 2A). At early stages, the fluid within the oocyte flows in a slow, uncoordinated manner. After stage 10B, this fluid flow is ~15 times faster and coordinated (cytoplasmic streaming, Gutzeit and Koppa, 1982; Serbus et al., 2005). Cytoplasmic streaming requires both microtubules and kinesin heavy chain (Gutzeit, 1986; Palacios and St Johnston, 2002; Serbus et al., 2005). During stage 10B, microtubules reorganize from a biased random anterior-posterior polarity to parallel bundles along the oocyte cortex (Parton et al., 2011; Theurkauf et al., 1992). This change is thought to depend on cytoplasmic streaming. *capu* mutants exhibit premature onset of cytoplasmic streaming, suggesting that the Capu-dependent actin mesh regulates the timing of cytoplasmic streaming (Figure 2B, Dahlgaard et al., 2007; Theurkauf, 1994).

Establishment of the major body axes in *Drosophila* oocytes requires proper localization of polarity determinants such as *gurken* (*grk*), *oskar* (*osk*), *bicoid* (*bcd*) and *nanos* mRNAs (Frohnhöfer and Nüsslein-Volhard, 1986; Lehmann and Nüsslein-Volhard, 1986; Lehmann and Nüsslein-Volhard, 1991; Schüpbach, 1987; Wang and Lehmann, 1991). Localization of these polarity factors is largely dependent on microtubules and their associated motors, while both actin and microtubules are required for anchoring. Specific modes of localization vary with major rearrangements of the microtubules seen after stage 7 and again after stage 10. Early on

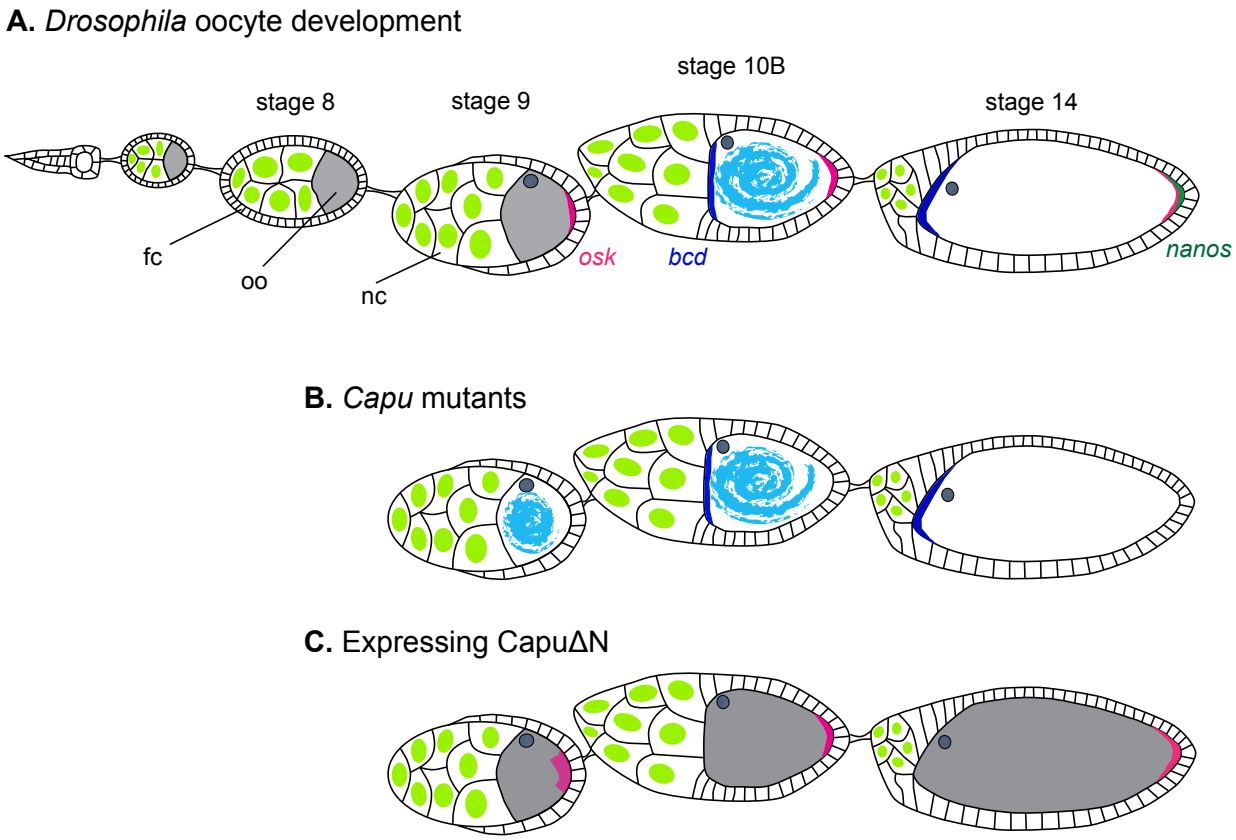

Figure 2. *Drosophila* oocyte development in normal, *capu* mutant and constitutively active Capu expressing oocytes. Posterior site of the oocytes are facing right and anterior is facing left. (A) Wild type oocytes (oo) are surrounded by follicle cells (fc) and have actin mesh structure from early stages to stage 9. During stage 10, the actin mesh disappears and an cytoplasmic streaming begins. Shortly after streaming begins, nurse cells (nc) dump all their content to the oocyte, resulting in expansion of oocytes during late stages. *Oskar* (*osk*, pink) mRNA localizes to the posterior region from early stages to stage 14. *Bicoid* (*bcd*, blue) mRNA localizes to the anterior region of the oocyte from late stage 10 to stage 14. *Nanos* (green) mRNA localizes to the posterior of the oocytes during late stages only. (B) In *capu* null mutants, the actin mesh is absent and cytoplasmic streaming begins prematurely. Due to these changes both *osk* and *nanos* localizations are disrupted in the mutant oocytes whereas *bcd* localization is normal. (C)

In contrast to *capu* mutants, expression of constitutively active Capu (CapuΔN) resulted in increased actin mesh at early stage and delayed mesh at stages 10-14 as well as inhibited cytoplasmic streaming during late stages. Due to these defects *osk* had diffuse localization at stage 9 but normal localization during late stages. Furthermore, both anterior localization of *bcd* and posterior localization of *nanos* were decreased or completely disrupted.

mRNAs that have been transcribed in nurse cells are transported by dynein into the oocyte along microtubules that are predominantly ordered with minus ends towards the posterior of the oocyte. Later, the posterior microtubule organizing center disappears and microtubules are rearranged to have biased random polarity with plus ends towards the posterior (stages 7-10) (Parton et al., 2011; Theurkauf et al., 1992). Thus, *osk*, which is enriched in the posterior after stage 7, is transported by kinesin (Brendza et al., 2000; Ephrussi et al., 1991; Kim-Ha et al., 1991) and bicoid, which is found at the anterior of the oocyte at this time, is transported by dynein (Figure 2A, Berleth et al., 1988; Schnorrer et al., 2000). The majority of *nanos* is localized to the posterior after stage 10 (Figure 2A, Wang et al., 1994), when the microtubules have been swept into bundles near the cortex of the oocyte (Theurkauf et al., 1992). *nanos* appears to be localized by a combination of advection due to cytoplasmic streaming and entrapment at the posterior as opposed to active transport by a motor (Forrest and Gavis, 2003). This is referred to as the late phase of polarity factor transport. *bcd* has a slightly different late phase localization mechanism as it depends more on microtubules and dynein and less on streaming (Weil et al., 2006).

grk, *osk* and *nanos*, but not *bcd*, localizations are disrupted in *capu* mutants (Figure 2B, Ephrussi et al., 1991; Manseau et al., 1996; Neuman-Silberberg and Schüpbach, 1993; Wang et al., 1994). Given that Capu is linked to two structures, the actin mesh and posterior extending filaments, we consider the roles of each in these phenotypes. The mesh is present during mid-oogenesis, linking it to the first phase of localization. Premature cytoplasmic streaming in *capu* mutants could mechanically disrupt the mRNA localization, or subsequent reorganization of the microtubule cytoskeleton may prevent the correct localization of mRNAs (Theurkauf, 1994). Given that these factors continue to accrue correctly after normal cytoplasmic streaming begins, it is not obvious why premature streaming is so detrimental. Perhaps establishment of “landing sites” is more delicate than later delivery of polarity factors. *Osk* at least has a positive feedback mechanism where the anchoring site at the posterior has to be established at early stages.

Once established, more *osk* is recruited during later stages (Sinsimer et al., 2011; Snee et al., 2007). How *capu* contributes to the second step of the mRNA localization is also unclear. It may be that Capu-dependent posterior filaments detected later in oogenesis are necessary for anchoring/entrapment during early and late phases of mRNA transport.

Formin family of formins in mammals

Capu isoforms in mammals also have been well studied. Knockout experiments show that one of the mammalian isoforms, Fmn2, is essential for an actin mesh in mouse oocytes as well (Azoury et al., 2008; Schuh and Ellenberg, 2008). The Spir/Fmn interaction is conserved in mammals (Quinlan et al., 2007; Pechlivanis et al., 2009) and Spir is essential to both the *Drosophila* and mammalian oocyte actin structures (Chang et al., 2011; Dahlgaard et al., 2007; Leader et al., 2002). These similarities make us question whether regulation of Fmn-family formins is, in fact, conserved as well.

Overview of the dissertation

We revisited the question of whether or not Capu is autoinhibited both *in vitro* (Chapter 1) and *in vivo* (Chapters 2 and 3). Here we present evidence that there is a direct and tight interaction between the N- (Capu-NT) and C-termini (Capu-CT) of Capu and that this interaction can, in fact, inhibit actin nucleation by the FH2 domain. Furthermore, using a TIRF microscopy assay, we showed that Capu-NT inhibits binding to the barbed end of elongating filaments by Capu-CT. We mapped the domains and performed hydrodynamic analysis on the N-terminal portion of Capu, which showed that Capu-NT is a dimer, similar to the N-termini of other formins. These data, combined with circular dichroism, suggest, however, that it is structurally distinct from the previously described formin DID domain. The dimerization domain is located between residues 222-321. Analogous to DID, we refer to the N-terminal autoregulatory domain as the Capu Inhibitory Domain (CID) and it was mapped to the first 222 residues of Capu. Interestingly, the CID binding site in the C-terminus of Capu mapped to the Capu-Tail (Capu1029-1059), a short sequence known to bind Spir-KIND (Vizcarra et al., 2011). Further

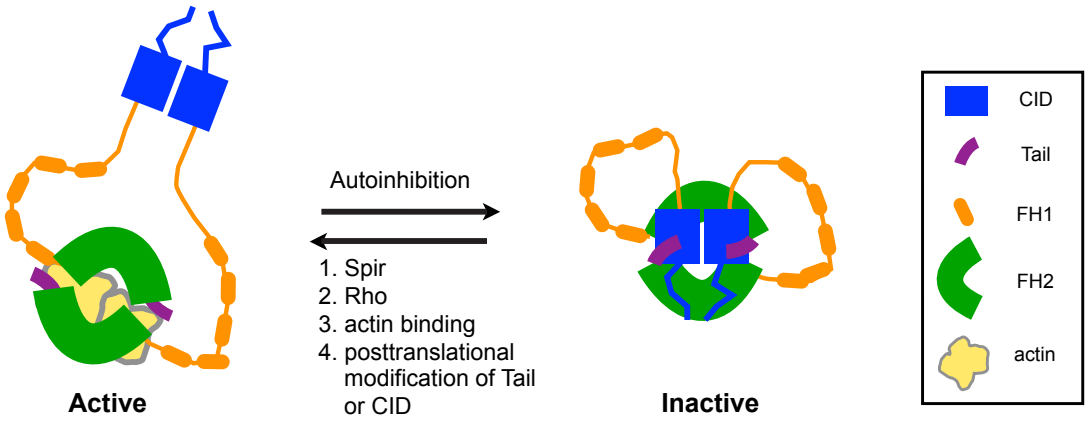

Figure 3. Despite the lack of conserved DID and DAD domains, Capu is autoinhibited. We think Capu exist in two different states, active and inactive. When Capu is autoinhibited, Capu's nucleation and elongation activities are inhibited. Capu may switch to the active state through different mechanisms such as binding to Spir, Rho GTPases or actin monomers. It is also possible that CID or Capu-Tail can be posttranslationally modified so that autoregulation is inhibited.

mutational analysis in the Capu-Tail domain suggested that Capu-NT and Spir-KIND binding sites overlap, but residues critical for Spir-KIND binding (L1048) did not have the same effect on Capu-NT binding. Despite testing many Capu-Tail mutations, we were not able to find point mutations that affect Capu-NT binding but not Spir-KIND. From these studies we conclude that the actin assembly activity of the *Drosophila* formin, Capu, is autoinhibited, despite the absence of canonical DID and DAD domains (Figure 3).

Capu autoinhibition has not been shown to regulate the physiological function of Capu in *Drosophila*. We employed two different *in vivo* systems to characterize Capu autoinhibition: *Drosophila* S2 cells (Chapter 3) and oocytes (Chapter 2). Study of other formins in mammalian cells showed that lack of autoinhibition results in thicker stress fibers, increased lamella actin and localization of formins to the cytoplasmic membrane (Alberts, 2001; Liu et al., 2008; Schulte et al., 2008; Seth et al., 2006; Vaillant et al., 2008; Watanabe et al., 1999). Therefore, we wanted to characterize the effect of Capu in *Drosophila* S2 cells. When we expressed Capu-CT in S2 cells, we saw uniform cytoplasmic localization of Capu-CT. More importantly we did not see actin cytoskeleton phenotypes similar to other formins. Expression of Capu-NT had very similar localization to Capu-CT and also had no affect on the actin cytoskeleton. From these results we could not distinguish whether Capu-CT is regulated in S2 cells or its activity is not strong enough to cause an actin phenotype. Furthermore we could not draw any conclusion about Capu autoinhibitiory regulation. To characterize the interaction between Capu-CT and Capu-NT, we coexpressed these proteins in S2 cells. Because their individual expression and localization was very similar, we targeted one of the proteins to the plasma membrane using either a CAAX or myristoylation tag. Compared to control expression, CAAX tagging and myristoylation localized Capu-CT or Capu-NT to the plasma membrane. However, cytoplasmic Capu-NT or Capu-CT, respectively, did not follow the tagged proteins to the plasma membrane, suggesting the two halves of the protein are not interacting or they are being regulated in S2 cells.

From the S2 cell experiments we could not conclude if Capu autoinhibition can regulate Capu's physiological functions. We therefore further characterized Capu autoinhibition during *Drosophila* oogenesis by expressing Capu that is lacking the CID domain (Chapter 2). Overexpression of this constitutively active Capu, compared to full-length Capu (FL), resulted in increased fertility defects due to disruption of oocyte polarity. Detailed analysis showed that the oocyte had increased actin mesh density at early stages and delayed actin mesh at late stages of development, and this late stage delay inhibited cytoplasmic streaming (Figure 2C). By co-expressing Capu-NT, we were able to rescue the fertility, actin mesh, and cytoplasmic streaming phenotypes, suggesting that Capu can be regulated by autoinhibition *in vivo*. Furthermore, interruption of the actin mesh and mis-timed cytoplasmic streaming resulted in diffuse localization of *osk* at early stages and decreased or no localization of *bcd* and *nanos* at late stages (Figure 2C). Therefore, we show not only that Capu is autoinhibited in *Drosophila* oocytes, but that the actin mesh and cytoplasmic streaming play a critical role in localization of polarity determinants.

In addition to regulating nucleation and elongation of actin filaments (F-actin), Capu can also bind the site of pre-existing F-actin and cross-link (bundle) them (Quinlan et al., 2007). In this study we further characterized Capu's F-actin binding and bundling activity (Chapter 4). We determined that Capu-Tail is necessary for Capu's F-actin binding and bundling activity, in addition to binding CID, Spir-KIND and microtubules (Bor et al., 2012; Quinlan et al., 2007; Roth-Johnson et al., 2014; Vizcarra et al., 2011). Truncated Capu-CT lacking Capu-Tail cannot bind F-actin, whereas GST tagged Capu-Tail was sufficient to bind F-actin. Consistent with our observation that Capu-Tail is required for F-actin binding, F-actin bundling activity also required Capu-Tail. Interestingly, GST-Capu-Tail was not able to bundle F-actin, suggesting that the FH2 domain is important for orienting Capu-Tail in such a way that it is able to cross-link two actin filaments. Capu bundling activity was tested using both a bulk bundling assay as well as TIRF microscopy. Whether Capu's F-actin side binding and therefore cross-linking activity is

important for regulating the actin cytoskeleton *in vivo* is still unknown. Future studies will be focused on finding point mutations that are required for F-actin binding but do not disrupt CID, Spir-KIND and microtubule binding.

Reference

Ahern-Djamali, S. M. (1999). Identification of profilin and src homology 3 domains as binding partners for Drosophila Enabled. *Proc. Natl. Acad. Sci.* **96**, 4977–4982.

Alberts, A. S. (2001). Identification of a carboxyl-terminal diaphanous-related formin homology protein autoregulatory domain. *J Biol Chem* **276**, 2824–30.

Azoury, J., Lee, K. W., Georget, V., Rassinier, P., Leader, B. and Verlhac, M.-H. (2008). Spindle positioning in mouse oocytes relies on a dynamic meshwork of actin filaments. *Curr Biol* **18**, 1514–9.

Berleth, T., Burri, M., Thoma, G., Bopp, D., Richstein, S., Frigerio, G., Noll, M. and Nüsslein-Volhard, C. (1988). The role of localization of bicoid RNA in organizing the anterior pattern of the Drosophila embryo. *EMBO J.* **7**, 1749–1756.

Bor, B., Vizcarra, C. L., Phillips, M. L. and Quinlan, M. E. (2012). Autoinhibition of the formin Cappuccino in the absence of canonical autoinhibitory domains. *Mol. Biol. Cell* **23**, 3801–3813.

Brendza, R. P., Serbus, L. R., Duffy, J. B. and Saxton, W. M. (2000). A function for kinesin I in the posterior transport of oskar mRNA and Staufen protein. *Science* **289**, 2120–2122.

Chang, C.-W., Nashchekin, D., Wheatley, L., Irion, U., Dahlgaard, K., Montague, T. G., Hall, J. and Johnston, D. S. (2011). Anterior-Posterior Axis Specification in Drosophila Oocytes: Identification of Novel bicoid and oskar mRNA Localization Factors. *Genetics* **188**, 883–896.

Chhabra, E. S. and Higgs, H. N. (2006). INF2 Is a WASP homology 2 motif-containing formin that severs actin filaments and accelerates both polymerization and depolymerization. *J Biol Chem* **281**, 26754–67.

Chhabra, E. S., Ramabhadran, V., Gerber, S. A. and Higgs, H. N. (2009). INF2 is an endoplasmic reticulum-associated formin protein. *J. Cell Sci.* **122**, 1430–1440.

Dahlgaard, K., Raposo, A. A. S. F., Niccoli, T. and Johnston, D. S. (2007). Capu and Spire assemble a cytoplasmic actin mesh that maintains microtubule organization in the Drosophila oocyte. *Dev Cell* **13**, 539–53.

Ephrussi, A., Dickinson, L. K. and Lehmann, R. (1991). Oskar organizes the germ plasm and directs localization of the posterior determinant nanos. *Cell* **66**, 37–50.

Forrest, K. M. and Gavis, E. R. (2003). Live imaging of endogenous RNA reveals a diffusion and entrapment mechanism for nanos mRNA localization in Drosophila. *Curr. Biol. CB* **13**, 1159–1168.

Frohnhöfer, H. G. and Nüsslein-Volhard, C. (1986). Organization of anterior pattern in the Drosophila embryo by the maternal gene bicoid. *Nature* **324**, 120–125.

Goode, B. L. and Eck, M. J. (2007). Mechanism and Function of Formins in the Control of Actin Assembly. *Annu Rev Biochem* **76**, 593–627.

Gorelik, R., Yang, C., Kameswaran, V., Dominguez, R. and Svitkina, T. (2011). Mechanisms of plasma membrane targeting of formin mDia2 through its amino terminal domains. *Mol Biol Cell* **22**, 189–201.

Gutzeit, H. (1986). The role of microtubules in the differentiation of ovarian follicles during vitellogenesis in Drosophila. **195**, 173–181.

Gutzeit, H. and Koppa, R. (1982). Time-lapse film analysis of cytoplasmic streaming during late oogenesis of Drosophila. *Development* **67**, 101–111.

Higashida, C., Miyoshi, T., Fujita, A., Oceguera-Yanez, F., Monypenny, J., Andou, Y., Narumiya, S. and Watanabe, N. (2004). Actin polymerization-driven molecular movement of mDia1 in living cells. *Science* **303**, 2007–2010.

Higgs, H. N. and Peterson, K. J. (2005). Phylogenetic analysis of the formin homology 2 domain. *Mol Biol Cell* **16**, 1–13.

Kato, T., Watanabe, N., Morishima, Y., Fujita, A., Ishizaki, T. and Narumiya, S. (2001). Localization of a mammalian homolog of diaphanous, mDia1, to the mitotic spindle in HeLa cells. *J. Cell Sci.* **114**, 775–84.

Kim-Ha, J., Smith, J. L. and Macdonald, P. M. (1991). oskar mRNA is localized to the posterior pole of the Drosophila oocyte. *Cell* **66**, 23–35.

Kobielak, A., Pasolli, H. A. and Fuchs, E. (2003). Mammalian formin-1 participates in adherens junctions and polymerization of linear actin cables. *Nat. Cell Biol.* **6**, 21–30.

Kovar, D. R., Harris, E. S., Mahaffy, R., Higgs, H. N. and Pollard, T. D. (2006). Control of the assembly of ATP- and ADP-actin by formins and profilin. *Cell* **124**, 423–435.

Lammers, M., Rose, R., Scrima, A. and Wittinghofer, A. (2005). The regulation of mDia1 by autoinhibition and its release by Rho*GTP. *EMBO J* **24**, 4176–87.

Leader, B., Lim, H., Carabatsos, M. J., Harrington, A., Ecsedy, J., Pellman, D., Maas, R. and Leder, P. (2002). Formin-2, polyploidy, hypofertility and positioning of the meiotic spindle in mouse oocytes. *Nat Cell Biol* **4**, 921–8.

Lehmann, R. and Nüsslein-Volhard, C. (1986). Abdominal segmentation, pole cell formation, and embryonic polarity require the localized activity of oskar, a maternal gene in Drosophila. *Cell* **47**, 141–152.

Lehmann, R. and Nüsslein-Volhard, C. (1991). The maternal gene nanos has a central role in posterior pattern formation of the Drosophila embryo. *Dev. Camb. Engl.* **112**, 679–691.

Li, F. and Higgs, H. N. (2003). The mouse Formin mDia1 is a potent actin nucleation factor regulated by autoinhibition. *Curr Biol* **13**, 1335–40.

Li, F. and Higgs, H. N. (2005). Dissecting requirements for auto-inhibition of actin nucleation by the formin, mDia1. *J Biol Chem* **280**, 6986–92.

Liu, W., Sato, A., Khadka, D., Bharti, R., Diaz, H., Runnels, L. W. and Habas, R. (2008). Mechanism of activation of the Formin protein Daam1. *Proc Natl Acad Sci USA* **105**, 210–5.

Maiti, S., Michelot, A., Gould, C., Blanchoin, L., Sokolova, O. and Goode, B. L. (2012). Structure and activity of full-length formin mDia1. *Cytoskelet. Hoboken NJ*.

Manseau, L. J. and Schüpbach, T. (1989). cappuccino and spire: two unique maternal-effect loci required for both the anteroposterior and dorsoventral patterns of the Drosophila embryo. *Genes Dev* **3**, 1437–52.

Manseau, L., Calley, J. and Phan, H. (1996). Profilin is required for posterior patterning of the Drosophila oocyte. *Development* **122**, 2109–16.

Martin, S. G., Rincón, S. A., Basu, R., Pérez, P. and Chang, F. (2007). Regulation of the formin for3p by cdc42p and bud6p. *Mol Biol Cell* **18**, 4155–67.

Neidt, E. M., Scott, B. J. and Kovar, D. R. (2009). Formin differentially utilizes profilin isoforms to rapidly assemble actin filaments. *J. Biol. Chem.* **284**, 673–684.

Neuman-Silberberg, F. S. and Schüpbach, T. (1993). The Drosophila dorsoventral patterning gene gurken produces a dorsally localized RNA and encodes a TGF alpha-like protein. *Cell* **75**, 165–174.

Nezami, A. G., Poy, F. and Eck, M. J. (2006). Structure of the autoinhibitory switch in formin mDia1. *Structure* **14**, 257–63.

Nezami, A., Poy, F., Toms, A., Zheng, W. and Eck, M. J. (2010). Crystal structure of a complex between amino and carboxy terminal fragments of mDia1: insights into autoinhibition of diaphanous-related formins. *PLoS ONE* **5**,.

Otomo, T., Tomchick, D. R., Otomo, C., Panchal, S. C., Machius, M. and Rosen, M. K. (2005). Structural basis of actin filament nucleation and processive capping by a formin homology 2 domain. *Nature* **433**, 488–494.

Otomo, T., Tomchick, D. R., Otomo, C., Machius, M. and Rosen, M. K. (2010). Crystal structure of the Formin mDia1 in autoinhibited conformation. *PLoS ONE* **5**,.

Ozaki-Kuroda, K., Yamamoto, Y., Nohara, H., Kinoshita, M., Fujiwara, T., Irie, K. and Takai, Y. (2001). Dynamic localization and function of Bni1p at the sites of directed growth in Saccharomyces cerevisiae. *Mol Cell Biol* **21**, 827–39.

Palacios, I. M. and St Johnston, D. (2002). Kinesin light chain-independent function of the Kinesin heavy chain in cytoplasmic streaming and posterior localisation in the Drosophila oocyte. *Dev. Camb. Engl.* **129**, 5473–5485.

Parton, R. M., Hamilton, R. S., Ball, G., Yang, L., Cullen, C. F., Lu, W., Ohkura, H. and Davis, I. (2011). A PAR-1-dependent orientation gradient of dynamic microtubules directs posterior cargo transport in the Drosophila oocyte. *J. Cell Biol.* **194**, 121–135.

Paul, A. S., Paul, A., Pollard, T. D. and Pollard, T. (2008). The role of the FH1 domain and profilin in formin-mediated actin-filament elongation and nucleation. *Curr. Biol. CB* **18**, 9–19.

Pechlivanis, M., Samol, A. and Kerkhoff, E. (2009). Identification of a short Spir interaction sequence at the C-terminal end of formin subgroup proteins. *J Biol Chem* **284**, 25324–33.

Petersen, J., Nielsen, O., Egel, R. and Hagan, I. M. (1998). FH3, a domain found in formins, targets the fission yeast formin Fus1 to the projection tip during conjugation. *J Cell Biol* **141**, 1217–28.

Pruyne, D., Evangelista, M., Yang, C., Bi, E., Zigmond, S., Bretscher, A. and Boone, C. (2002). Role of formins in actin assembly: nucleation and barbed-end association. *Science* **297**, 612–615.

Quinlan, M. E., Hilgert, S., Bedrossian, A., Mullins, R. D. and Kerkhoff, E. (2007). Regulatory interactions between two actin nucleators, Spire and Cappuccino. *J. Cell Biol.* **179**, 117–128.

Ramalingam, N., Zhao, H., Breitsprecher, D., Lappalainen, P., Faix, J. and Schleicher, M. (2010). Phospholipids regulate localization and activity of mDia1 formin. *Eur. J. Cell Biol.* **89**, 723–732.

Rincón, S. A., Ye, Y., Villar-Tajadura, M. A., Santos, B., Martin, S. G. and Pérez, P. (2009). Pob1 participates in the Cdc42 regulation of fission yeast actin cytoskeleton. *Mol Biol Cell* **20**, 4390–9.

Rosales-Nieves, A. E., Johndrow, J. E., Keller, L. C., Magie, C. R., Pinto-Santini, D. M. and Parkhurst, S. M. (2006). Coordination of microtubule and microfilament dynamics by Drosophila Rho1, Spire and Cappuccino. *Nat Cell Biol* **8**, 367–376.

Rose, R., Weyand, M., Lammers, M., Ishizaki, T., Ahmadian, M. R. and Wittinghofer, A. (2005). Structural and mechanistic insights into the interaction between Rho and mammalian Dia. *Nature* **435**, 513–8.

Roth-Johnson, E. A., Vizcarra, C. L., Bois, J. S. and Quinlan, M. E. (2014). Interaction between microtubules and the Drosophila formin Cappuccino and its effect on actin assembly. *J. Biol. Chem.* **289**, 4395–4404.

Schnorrer, F., Bohmann, K. and Nüsslein-Volhard, C. (2000). The molecular motor dynein is involved in targeting swallow and bicoid RNA to the anterior pole of Drosophila oocytes. *Nat. Cell Biol.* **2**, 185–190.

Schönichen, A. and Geyer, M. (2010). Fifteen formins for an actin filament: a molecular view on the regulation of human formins. *Biochim Biophys Acta* **1803**, 152–63.

Schuh, M. and Ellenberg, J. (2008). A new model for asymmetric spindle positioning in mouse oocytes. *Curr Biol* **18**, 1986–92.

Schulte, A., Stolp, B., Schönichen, A., Pylypenko, O., Rak, A., Fackler, O. T. and Geyer, M. (2008). The human formin FHOD1 contains a bipartite structure of FH3 and GTPase-binding domains required for activation. *Structure* **16**, 1313–23.

Schüpbach, T. (1987). Germ line and soma cooperate during oogenesis to establish the dorsoventral pattern of egg shell and embryo in Drosophila melanogaster. *Cell* **49**, 699–707.

Serbus, L. R., Cha, B.-J., Theurkauf, W. E. and Saxton, W. M. (2005). Dynein and the actin cytoskeleton control kinesin-driven cytoplasmic streaming in Drosophila oocytes. *Development* **132**, 3743–52.

Seth, A., Otomo, C. and Rosen, M. K. (2006). Autoinhibition regulates cellular localization and actin assembly activity of the diaphanous-related formins FRLalpha and mDia1. *J Cell Biol* **174**, 701–13.

Sinsimer, K. S., Jain, R. A., Chatterjee, S. and Gavis, E. R. (2011). A late phase of germ plasm accumulation during Drosophila oogenesis requires Lost and Rumpelstiltskin. *Development* **138**, 3431–3440.

Snee, M. J., Harrison, D., Yan, N. and Macdonald, P. M. (2007). A late phase of Oskar accumulation is crucial for posterior patterning of the Drosophila embryo, and is blocked by ectopic expression of Bruno. *Differ. Res. Biol. Divers.* **75**, 246–255.

Tanaka, T., Kato, Y., Matsuda, K., Hanyu-Nakamura, K. and Nakamura, A. (2011). Drosophila Mon2 couples Oskar-induced endocytosis with actin remodeling for cortical anchorage of the germ plasm. *Development* **138**, 2523–32.

Theurkauf, W. (1994). Premature microtubule-dependent cytoplasmic streaming in cappuccino and spire mutant oocytes. *Science* **265**, 2093–2096.

Theurkauf, W. E., Smiley, S., Wong, M. L. and Alberts, B. M. (1992). Reorganization of the cytoskeleton during Drosophila oogenesis: implications for axis specification and intercellular transport. *Dev. Camb. Engl.* **115**, 923–936.

Vaillant, D. C., Copeland, S. J., Davis, C., Thurston, S. F., Abdennur, N. and Copeland, J. W. (2008). Interaction of the N- and C-terminal autoregulatory domains of FRL2 does not inhibit FRL2 activity. *J Biol Chem* **283**, 33750–62.

Vizcarra, C. L., Kreutz, B., Rodal, A. A., Toms, A. V., Lu, J., Zheng, W., Quinlan, M. E. and Eck, M. J. (2011). Structure and function of the interacting domains of Spire and Fmn-family formins. *Proc. Natl. Acad. Sci. U. S. A.* **108**, 11884–9.

Wang, C. and Lehmann, R. (1991). Nanos is the localized posterior determinant in Drosophila. *Cell* **66**, 637–647.

Wang, C., Dickinson, L. K. and Lehmann, R. (1994). Genetics of nanos localization in Drosophila. *Dev. Dyn. Off. Publ. Am. Assoc. Anat.* **199**, 103–115.

Watanabe, N., Kato, T., Fujita, A., Ishizaki, T. and Narumiya, S. (1999). Cooperation between mDia1 and ROCK in Rho-induced actin reorganization. *Nat Cell Biol* **1**, 136–43.

Weil, T. T., Forrest, K. M. and Gavis, E. R. (2006). Localization of bicoid mRNA in late oocytes is maintained by continual active transport. *Dev. Cell* **11**, 251–262.

Yonetani, A., Lustig, R. J., Moseley, J. B., Takeda, T., Goode, B. L. and Chang, F. (2008). Regulation and targeting of the fission yeast formin cdc12p in cytokinesis. *Mol Biol Cell* **19**, 2208–19.

Chapter 1: Autoinhibition of the formin Cappuccino in the absence of canonical autoinhibitory domains

MBoC | ARTICLE

Autoinhibition of the formin Cappuccino in the absence of canonical autoinhibitory domains

Batbileg Bor[a], Christina L. Vizcarra[b], Martin L. Phillips[b], and Margot E. Quinlan[b,c]
[a]Molecular Biology Interdepartmental Program, [b]Department of Chemistry and Biochemistry, and [c]Molecular Biology Institute, University of California, Los Angeles, Los Angeles, CA 90095-1570

ABSTRACT **Formins are a conserved family of proteins known to enhance actin polymerization. Most formins are regulated by an intramolecular interaction. The *Drosophila* formin, Cappuccino (Capu), was believed to be an exception. Capu does not contain conserved autoinhibitory domains and can be regulated by a second protein, Spire. We report here that Capu is, in fact, autoinhibited. The N-terminal half of Capu (Capu-NT) potently inhibits nucleation and binding to the barbed end of elongating filaments by the C-terminal half of Capu (Capu-CT). Hydrodynamic analysis indicates that Capu-NT is a dimer, similar to the N-termini of other formins. These data, combined with those from circular dichroism, suggest, however, that it is structurally distinct from previously described formin inhibitory domains. Finally, we find that Capu-NT binds to a site within Capu-CT that overlaps with the Spire-binding site, the Capu-tail. We propose models for the interaction between Spire and Capu in light of the fact that Capu can be regulated by autoinhibition.**

Monitoring Editor
Thomas D. Pollard
Yale University

Received: Apr 12, 2012
Revised: Jul 17, 2012
Accepted: Jul 31, 2012

INTRODUCTION

Formins are a large family of proteins that regulate growth of the actin cytoskeleton. These proteins help build a variety of structures, including, but not limited to, stress fibers, contractile rings, and filopodia. Formins function as actin nucleators, elongation factors, bundlers, and, in at least one case, as a depolymerizing factor (Chhabra and Higgs, 2006; Goode and Eck, 2007). Formins are defined by their well-conserved formin homology 1 and 2 (FH1 and FH2) domains (Higgs and Peterson, 2005). The FH2 domain forms a donut-shaped homodimer that nucleates new filaments and remains associated with the barbed ends of growing filaments (Pruyne *et al.*, 2002; Higashida *et al.*, 2004; Otomo *et al.*, 2005). Through its association with barbed ends, the FH2 domain can modulate the elongation rate and protect filaments from other barbed end–binding proteins such as capping protein (Goode and Eck, 2007). The proline-rich FH1 domain binds profilin-actin and perhaps some SH3 domain–containing proteins (Ahern-Djamali, 1999; Paul *et al.*, 2008). The FH1 and FH2 domains cooperate to accelerate filament elongation in many cases (Kovar *et al.*, 2006; Neidt *et al.*, 2009).

Actin nucleators must be tightly regulated to control when and where new filaments are created. Actin assembly by formins is commonly inhibited by an intramolecular interaction between the N- and C-terminal halves of the protein. This autoinhibition was first described for diaphanous-related formins (DRFs), specifically mDia1 (Watanabe *et al.*, 1999; Goode and Eck, 2007). Detailed analysis showed that actin nucleation activity is inhibited by a direct interaction between the C-terminal diaphanous autoregulatory domain (DAD) and the N-terminal diaphanous inhibitory domain (DID; Alberts, 2001; Li and Higgs, 2003, 2005). The DID/DAD interaction also controls cellular localization of some formins (Seth *et al.*, 2006; Gorelik *et al.*, 2011). Crystal structures of the DID/DAD complex show that the DAD domain forms a single α-helical peptide that binds in the concave surface formed by the five armadillo repeats of the DID domain (Lammers *et al.*, 2005; Nezami *et al.*, 2006). This interaction is commonly regulated by small GTPases, such as Rho, binding to a GTPase-binding domain (GBD) adjacent to and overlapping with the DID domain, which results in release of the DAD domain (Lammers *et al.*, 2005; Otomo *et al.*, 2005; Rose *et al.*, 2005). Recent studies confirmed these observations with full-length mDia1, showing that it is an autoinhibited dimer that can be at least partially activated by RhoA (Ramalingam *et al.*, 2010; Maiti *et al.*, 2012).

This article was published online ahead of print in MBoC in Press (http://www.molbiolcell.org/cgi/doi/10.1091/mbc.E12-04-0288) on August 8, 2012.

Address correspondence to: Margot E. Quinlan (margot@chem.ucla.edu).

Abbreviations used: CID, Cappuccino inhibitory domain; CP, capping protein; DAD, diaphanous autoregulatory domain; DID, diaphanous inhibitory domain; Fmn, formin; GBD, GTPase-binding domain; KIND, kinase noncatalytic C-lobe domain.

The DID and DAD domains are readily identified in the amino acid sequences of five of the seven metazoan groups of formins (Schönichen and Geyer, 2010), as well as in fungal and amoeba formins (Higgs and Peterson, 2005). Furthermore, interaction between the N- and C-termini has been reported for six of the seven groups (Kobielak *et al.*, 2003; Li and Higgs, 2005; Liu *et al.*, 2008; Schulte *et al.*, 2008; Vaillant *et al.*, 2008; Chhabra *et al.*, 2009). The seventh group, delphilin-family formins, remains untested. In most cases, the DID/DAD interaction inhibits actin nucleation and elongation. There are, however, variations on this theme. For example, in the case of INF2, depolymerization but not polymerization is inhibited (Chhabra *et al.*, 2009). Intriguingly, no functional consequence of the FRL2 DID/DAD interaction has been identified (Vaillant *et al.*, 2008).

How members of the formin (Fmn) group of formins are regulated remains an open question, in part because the N-termini are not well conserved within this group. We and others originally predicted that Cappuccino (Capu), the only *Drosophila* Fmn-family formin, was not regulated by autoinhibition for two reasons: the canonical DID and DAD domains are absent (Higgs and Peterson, 2005), and an alternative means of regulating Capu's nucleation and elongation activity had been identified, namely the WH2-nucleator Spire (Spir; Quinlan *et al.*, 2007; Vizcarra *et al.*, 2011). Further evidence supporting this idea came from the report that the N- and C-termini of Capu interact in pull-down assays, but addition of the N-terminal half of Capu to its FH2 domain had no effect in pyrene-actin polymerization assays (Rosales-Nieves *et al.*, 2006). However, an autoinhibitory interaction was described for Fmn1, one of two mammalian Fmn isoforms (Kobielak *et al.*, 2003). One explanation for this difference is that Capu and Fmn1 are regulated by distinct mechanisms, an idea that is supported by the poor sequence conservation in the N-termini of Fmn-family formins.

Capu was originally identified in a genetic screen for developmental patterning genes (Manseau and Schüpbach, 1989). Loss of Capu results in premature cytoplasmic streaming during oogenesis, polarity defects in oocytes and embryos, and female sterility (Manseau and Schüpbach, 1989; Theurkauf, 1994; Emmons *et al.*, 1995). Recently it was linked to two actin structures in *Drosophila* oocytes: an isotropic mesh that traverses the oocyte and a network of filaments extending from the posterior cortex of the oocyte (Dahlgaard *et al.*, 2007; Chang *et al.*, 2011; Tanaka *et al.*, 2011). Knockout experiments show that one of the mammalian isoforms, Fmn2, is essential for an actin mesh in mouse oocytes as well (Azoury *et al.*, 2008; Schuh and Ellenberg, 2008). The Spir/Fmn interaction is conserved in mammals (Quinlan *et al.*, 2007; Pechlivanis *et al.*, 2009) and Spir is essential to both the *Drosophila* and mammalian oocyte actin structures (Dahlgaard *et al.*, 2007; Chang *et al.*, 2011; Pfender *et al.*, 2011). These similarities made us question whether regulation of Fmn-family formins is, in fact, conserved as well.

Recent in vivo studies provide insight into how Capu is regulated. Dahlgaard *et al.* (2007) created flies expressing a variant of Capu in which a putative Rho-binding site, residues 1–270, was deleted (green fluorescent protein [GFP]–CapuΔN). Expression of GFP-CapuΔN resulted in a denser ectopic actin mesh in the nurse cells relative to either wild-type or GFP-Capu–expressing flies, suggesting that CapuΔN is more active than full-length Capu. A complimentary observation showed that Capu's N-terminal 100 amino acids exert a dominant-negative effect on Capu's Oskar protein–anchoring activity, possibly by inhibiting formation of long arrays of actin filaments extending from the posterior cortex (Chang *et al.*, 2011). Thus the N-terminus of Capu is important for Capu's activity, and these findings suggested to us that an intramolecular interaction might be necessary. We therefore revisited the question of whether or not Capu is autoinhibited. Here we present evidence that there is a direct and tight interaction between the N- and C-termini of Capu and that this interaction can, in fact, inhibit actin nucleation by the FH2 domain. We mapped the domains and performed hydrodynamic analysis on the N-terminal portion, which we refer to as the Cappuccino inhibitory domain (CID). Of interest, the CID-binding site in the C-terminus of Capu maps to the Capu-tail, a short sequence known to bind Spir (Vizcarra *et al.*, 2011).

RESULTS

Polymerization activity of Capu is autoinhibited

To determine whether Capu is autoinhibited, we purified the N-terminal half of Capu (amino acids [aa] 1–466, Capu-NT; Figure 1, A and B) and tested its ability to inhibit the actin polymerization activity of Capu's C-terminal half (aa 467–1059, Capu-CT; Supplemental Figure S1A) in a pyrene-actin polymerization assay. Capu-NT alone had no effect on actin polymerization (green; Figure 1C). Capu-NT did inhibit Capu-CT's ability to stimulate actin polymerization in a dose-dependent manner, demonstrating that the polymerization activity of Capu can be regulated by autoinhibition (Figure 1C). We plotted the barbed-end concentration at half-maximal polymerization ($t_{1/2}$) for each concentration of Capu-NT (Figure 1D). These data were fitted with a quadratic binding curve. We chose to analyze our interaction data in terms of subunit concentrations, given that the dimers such as Capu-CT have two binding sites. Thus 20 nM Capu-CT here is equal to 10 nM of the nucleation competent dimer. The inhibition constant (K_i) calculated for inhibition of Capu-CT by Capu-NT is 10 nM, which suggests a tight interaction between the two halves of Capu. Calculation of the K_i based on the nucleation rate gave a similar result (K_i = 8 nM; Supplemental Figure S1, B and C).

Mapping the C-terminal binding domain

Most formins have a DAD domain C-terminal to the FH2 domain (Higgs and Peterson, 2005). Capu does not have a DAD domain, but we asked whether Capu-NT binds to the analogous region, where the previously described Capu-tail is located (Vizcarra *et al.*, 2011). Truncation of only 12 residues from the Capu-tail—Capu(467–1047)—dramatically reduced inhibition of actin assembly by Capu-NT as measured in the pyrene assay (Figure 2A). Capu-NT's inhibition activity continues to be reduced as Capu-CT is truncated further, with no activity remaining when residues 1036–1059 are removed. Because C-terminal truncations have a strong effect on Capu-CT's activity, as previously reported (Vizcarra *et al.*, 2011), we also used a competition assay to test for Capu-NT/Capu-tail interaction. We added increasing amounts of purified Capu-tail to a constant concentration of Capu-CT and Capu-NT. Unless otherwise indicated, Capu-tail experiments were performed with the monomeric peptide cleaved from a purified glutathione *S*-transferase (GST)–Capu-tail construct. Inhibition was relieved by addition of Capu-tail in a dose-dependent manner (Figure 2B). Capu-tail alone did not alter actin polymerization at concentrations as high as 12 μM, confirming that the effect was through interaction with Capu-NT (Supplemental Figure S2A).

By examining the barbed-end concentration at $t_{1/2}$ versus the Capu-tail concentration, we determined that the half-maximal effective concentration of Capu-tail (EC_{50}) is ~3 μM (Figure 2D). If we interpret this functional assay as a competition binding assay, then we can estimate the affinity of the Capu-tail for Capu-NT as described in Vinson *et al.* (1998; see *Materials and Methods*). An EC_{50} of 3 μM and a K_i of 10 nM for Capu-NT/Capu-CT predicts a K_d of 333 nM for the Capu-NT/Capu-tail interaction. This calculated

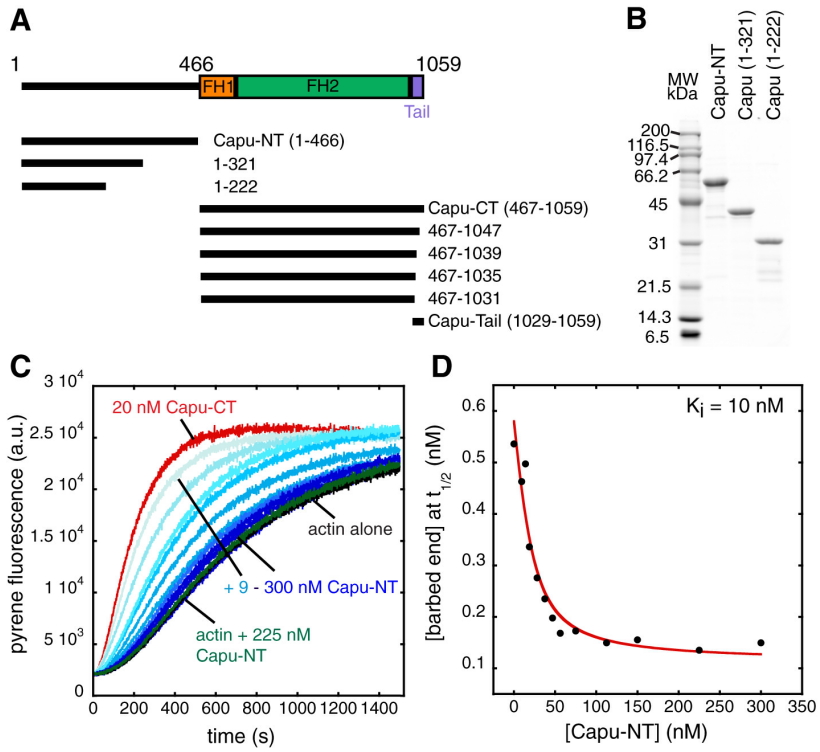

FIGURE 1: Capu-NT inhibits the polymerization activity of Capu-CT. (A) Domain organization of Capu along with diagrams of the constructs used in this study. Previously characterized domains are shown as boxes, including FH1 and FH2 domains (orange and green, respectively) and the Capu-tail (violet). (B) Purified Capu-NT and truncations visualized on a Coomassie-stained SDS–PAGE gel. (C) Pyrene-actin polymerization assays with Capu-CT and Capu-NT. Polymerization of 4 μM actin (5% pyrene labeled) was induced by adding Mg^{2+} and KCl (see *Materials and Methods*). Addition of 9–300 nM Capu-NT (shown with increasing shades of blue) to 20 nM Capu-CT (alone in red) before mixing with actin inhibited the polymerization activity of Capu-CT in a dose-dependent manner. Addition of 225 nM Capu-NT to actin (green) does not change polymerization kinetics (black). (D) From the pyrene assay in C, the barbed-end concentration at time until half-maximal polymerization ($t_{1/2}$) was calculated and plotted for each concentration of Capu-NT. Data were fitted with a quadratic binding equation, yielding an inhibition constant (K_i) of 10 nM.

affinity is much weaker than the K_i we measured for Capu-NT/Capu-CT. Because Capu-NT is a dimer (see later discussion), we reasoned that dimer (Capu-CT) to dimer (Capu-NT) binding might be tighter than monomer (Capu-tail) to dimer (Capu-NT) binding. To mimic the dimer/dimer interaction, we repeated the pyrene competition experiment with dimeric GST–Capu-tail under the same conditions (Figure 2C). On the basis of the GST crystal structure (Kursula *et al.*, 2005) and the length of the linker region, we expect GST–Capu-tail to be a reasonable spatial approximation for Capu-tail's position on the Capu-CT dimer. GST alone and GST–Capu-tail had no effect on actin polymerization (Supplemental Figure S2A), but GST–Capu-tail did relieve inhibition of Capu-CT by Capu-NT. The EC_{50} of GST–Capu-tail was ~1.5 μM (Figure 2D), and based on the Vinson analysis, the K_d was 167 nM, consistent with dimerization of Capu-tail modestly enhancing binding to Capu-NT. Of interest, competition with GST–Capu-tail resulted in complete recovery of Capu-CT's activity (Figure 2C). This was not so for monomeric Capu-tail or monomeric mDia-DAD in analogous experiments (Li and Higgs, 2005; Figure 2, B–D). Taken together, these results show that the Capu-tail is necessary for Capu-NT to regulate Capu-CT's polymerization activity. Although dimerization enhances the activity of Capu-tail, the difference in apparent affinities of Capu-NT for Capu-CT versus Capu-tail or GST-Capu-tail led us to conclude that the actual binding site is likely to extend beyond this short region.

Mapping the N-terminal binding domain

Neither phylogenetic analysis (Higgs and Peterson, 2005) nor a Pfam search (Punta *et al.*, 2012) predicted any domains or motifs in Capu-NT. In fact, the N-terminal halves of Fmn-family formins are poorly conserved. Thus it was difficult to predict what part of Capu-NT would bind to the Capu-tail. Initially we designed and characterized various truncated Capu-NT constructs, based on predicted secondary structure and previous biochemical studies (Rosales-Nieves *et al.*, 2006), in order to identify the Capu inhibitory domain (CID; Figure 3A and Supplemental Figure S3A). Inhibition activities were initially quantified by comparing the $t_{1/2}$ on a scale according to which Capu-CT alone is 0% and actin alone is 100% inhibited. Capu(1–321) was the shortest construct with inhibition activity similar to Capu-NT (Figure 3A and Supplemental Figure S3A). Two longer constructs had lower activity than Capu(1–321)—Capu(1–350) and Capu(1–402) (Supplemental Figure S3A). Perhaps these truncations fall in the middle of a domain, impairing activity due to its disruption. Capu(1–321) inhibits polymerization activity of Capu-CT in a dose-dependent manner (Figure 3B), with a K_i indistinguishable from that of Capu-NT (9 nM; Figure 3C). Calculation based on the nucleation rate gave a similar inhibition constant (12 nM; Supplemental Figure S4, A and B). Capu-tail also prevents inhibition of Capu-CT by Capu(1–321), with an EC_{50} of ~3 μM (Supplemental Figure S4, C and D). In sum, the activity of Capu(1–321) is indistinguishable from that of Capu-NT.

We also performed limited proteolysis of Capu-NT. Tryptic digest produced four different products over time (Figure 3D). Adding Capu-tail to this reaction slowed the proteolysis, suggesting that it stabilizes Capu-NT when bound (Figure 3D). Using N-terminal sequencing and matrix assisted laser desorption ionization (MALDI) mass spectrometry, we determined that the largest stable band could be either Capu(1–222) or Capu(1–257) (red arrows; Figure 3D and Supplemental Figure S3B). Capu(1–257) expressed poorly and was relatively insoluble, so we proceeded with only Capu(1–222). The inhibition activity of Capu(1–222) was ~40% that of Capu-NT at a concentration of 100 nM (Figure 3, A and E). The K_i determined (78 nM) overestimates the inhibitory effect because high concentrations of Capu(1–222) weakly inhibit polymerization of actin alone (Figure 3E and Supplemental Figure S4E).

Truncation of Capu constructs from the N-terminus generally reduced inhibition activity (Figure 3A and Supplemental Figure S3A).

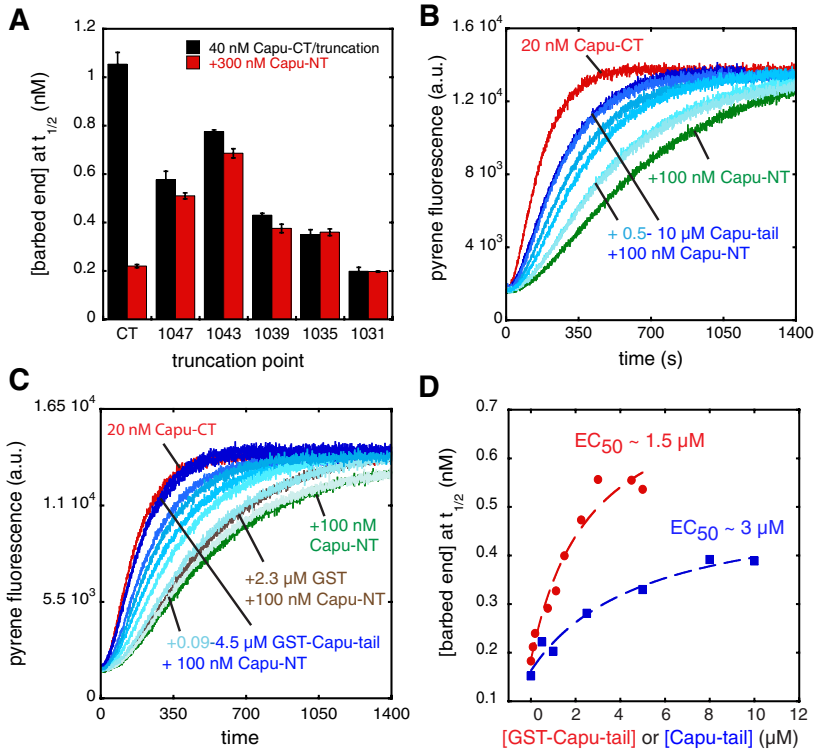

FIGURE 2: Capu-NT binds to the Capu-tail region. (A) Capu-NT does not inhibit C-terminally truncated Capu-CT. The bar graph shows the barbed-end concentrations at $t_{1/2}$ in the presence of 40 nM Capu-CT or truncations of the construct ending at the residues indicated, alone (black) or with 300 nM Capu-NT added (red). Each bar represents the average of three experiments (error bars, SD). (B) Capu-tail relieves inhibition by Capu-NT. Addition of 0.5–10 μM Capu-tail (shown with increasing shades of blue) to 20 nM Capu-CT plus 100 nM Capu-NT leads to recovery of Capu-CT polymerization activity in a dose-dependent manner. Capu-CT alone (20 nM, red) and with 100 nM Capu-NT (green) are shown. (C) GST–Capu-tail relieves inhibition by Capu-NT. The same experiment as in B but with increasing concentration (0.09–4.5 μM) of GST–Capu-tail. Adding 2.3 μM GST alone to the Capu-CT/Capu-NT mix had a weak effect on polymerization (brown). (D) From the pyrene assays in B and C, the barbed-end concentration at $t_{1/2}$ was calculated for each concentration of Capu-tail or GST–Capu-tail (concentration of the GST-tagged monomer is indicated) and graphed, yielding an estimated EC_{50} of ~3 μM for Capu-tail and ~1.5 μM for GST–Capu-tail. The dashed red and blue lines are drawn to guide the eye.

We conclude that the CID domain is situated near the N-terminus of Capu-NT, probably between residues 80 and 222, and its inhibition activity is enhanced by the flanking regions. Residues 1–105 greatly increase the activity of constructs ending at 321 or 466, although residual activity is present in both Capu(105–321) and Capu(105–466) (Figure 3A and Supplemental Figure S3A). Residues beyond 222 may act only by dimerizing the CID, as discussed later. A similar result was observed for mDia1: the affinity for the FH2-DAD construct is doubled by inclusion of the GBD in the DID construct (Nezami *et al.*, 2006), and the inhibitory activity of the N-terminus is enhanced 10-fold in longer constructs (+GBD = mDia1(1–548) vs. –GBD = mDia1(129–548); Li and Higgs, 2005). Likewise, truncation of the dimerization domain C-terminal to the core structural DID domain—mDia1(129–369)—decreased autoinhibitory activity another 10-fold (Li and Higgs, 2005).

We confirmed direct binding between the Capu-tail and three N-terminal Capu constructs—Capu-NT, Capu(1–321), and Capu(1–222)—using fluorescence anisotropy with Alexa Fluor 488–labeled Capu-tail (Figure 3F). Capu-NT and Capu(1–321) bind Capu-tail with the same affinity (K_d = 300 nM). Capu(1–222) binds with lower affinity (K_d = 4.8 μM). The dissociation constants for Capu-NT/Capu-tail and Capu(1–321)/Capu-tail are in excellent agreement with the affinities we calculated from functional competition assays (300 vs. 333 nM). The weaker affinity of Capu(1–222) compared with both Capu-NT and Capu(1–321) is consistent with its weaker inhibitory activity (Figure 3F). These data further support our conclusion that the C-terminal binding site extends beyond the Capu-tail.

Mutational analysis of the interaction between Capu-CT and Capu-NT

Capu-tail also binds to the Spir-kinase noncatalytic C-lobe domain (KIND; Figure 4A; Vizcarra *et al.*, 2011), leading us to ask whether Capu-NT and Spir-KIND bind to the same site within this small domain. To address this question, we asked whether Capu-NT can bind and inhibit Capu-CT with mutations in the Capu-tail domain. We first tested point mutations in residues that have been shown to abolish the Spir-KIND/Capu-tail interaction (L1048, K1049, R1051, M1052, R1055; Vizcarra *et al.*, 2011; Supplemental Figure S5A). Only mutations in R1051 had a notable effect on Capu-NT activity, but the baseline nucleation activity of Capu-CT was also compromised by this change. Thus we tested several more mutations. Based on the cocrystal structure of human Spir1-KIND bound to Fmn2 tail, residues 1048–1055 of the Capu-tail form an α-helix when Spir-KIND is bound (Figure 4A). We tested residues on the opposite face of this helix (L1053 and M1054) from the KIND-binding site, as well as residues N-terminal and C-terminal to the helix (Figure 4 and Supplemental Figure S5). Mutation of K1058, had a stronger effect than others, although it did not abolish the interaction (Figure 4B). When considered on a scale of 100% inhibition equal to Capu-NT inhibition of wild-type Capu-CT and 0% equal to Capu-CT alone (with each respective mutation), Capu-NT was able to inhibit R1051A and K1058A 70–80% as well as wild-type Capu-CT. The activity of Capu-NT was reduced ~50% when R1051 was mutated to D, which may reflect the effect of charge reversal. We could not carry out the same experiment with double or triple mutants because such changes greatly decreased Capu-CT's polymerization activity, complicating the interpretation of the data (e.g., K1039A/K1058A, Supplemental Figure S5B). In sum, residues critical for Spir-KIND binding do not have the same effect on Capu-NT binding, but the binding sites do overlap. We speculate that Capu-tail may take on a different structure when bound to Capu-NT since mutations likely to disrupt the α-helix are not as deleterious for Capu-NT binding as they are for Spir-KIND (e.g., R1051D or M1052D).

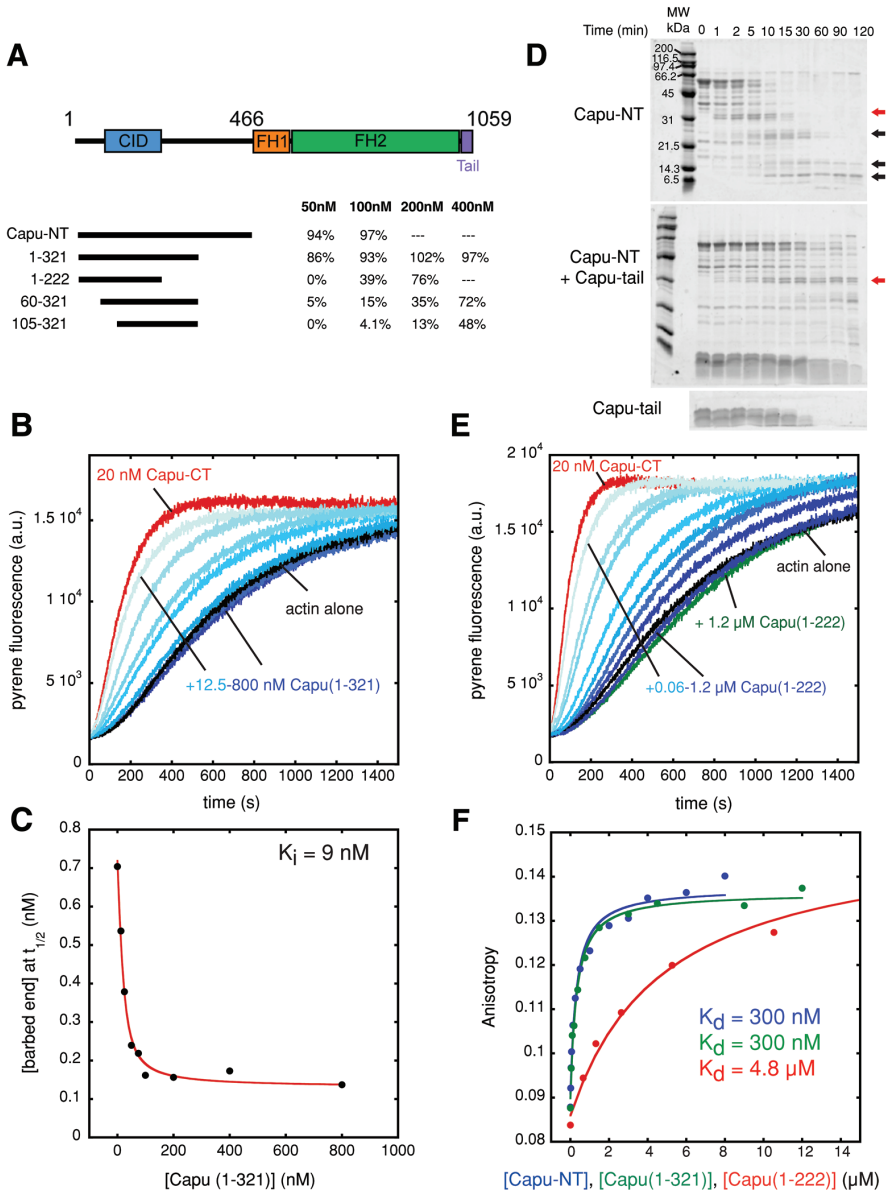

FIGURE 3: Mapping the CID. (A) Summary of the Capu-NT truncations that have inhibition activity against polymerization by Capu-CT. Four different concentrations (50, 100, 200, and 400 nM) were added to the pyrene assay containing 20 nM Capu-CT. Inhibition activities were quantified by comparing the $t_{1/2}$ where Capu-CT alone is 0% and actin alone is 100% inhibited. Conditions not tested are indicated by a dashed line (---). (B) Addition of 12.5–800 nM Capu(1–321) (shown with increasing shades of blue) to 10 nM Capu-CT before mixing with 4 µM actin inhibited Capu-CT polymerization activity in a dose-dependent manner. Capu-CT (20 nM) alone is shown in red, and 4 µM actin alone is in black. Capu(1–321) alone does not alter actin polymerization (Supplemental Figure S2B). (C) A K_i of 9 nM for Capu(1–321) was determined as described in Figure 1D. (D) Limited proteolysis of Capu-NT with or without Capu-tail. The proteolysis reaction containing 3 µM Capu-NT and 6 nM trypsin with or without 50 µM Capu-tail was incubated for up to 2 h. Red arrows indicate the band analyzed by N-terminal sequencing and MALDI, and black arrows indicate smaller, relatively stable digest products (see *Materials and Methods* and Supplemental Figure S3B). Bottom, proteolysis of 50 µM Capu-tail alone. (E) Addition of 0.06–1.2 µM Capu(1–222) (shown with increasing shades of blue) to 20 nM Capu-CT before mixing with 4 µM actin inhibited nucleation by Capu-CT in a dose-dependent manner. Capu-CT (20 nM) alone is in red, and 4 µM actin alone is in black. Adding 1.2 µM Capu(1–222) to actin alone weakly affected spontaneous polymerization of actin (green). (F) Polarization anisotropy of 20 nM Capu-tail–Alexa Flour 488 and increasing concentrations of Capu-NT in blue, Capu(1–321) in green, or Capu(1–222) in red. Capu-NT and Capu(1–321) had indistinguishable equilibrium dissociation constants (K_d = 300 nM). Capu(1–222) binds to Capu-tail–Alexa Fluor 488 less tightly (K_d = 4.8 µM).

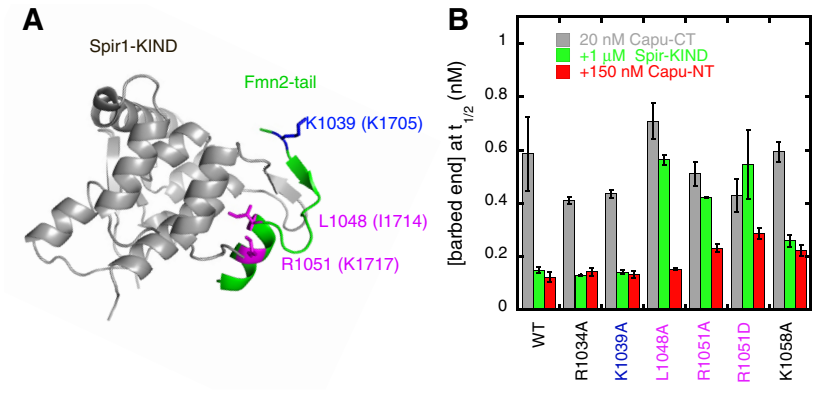

FIGURE 4: Mutational analysis of CID binding to the Capu-tail. (A) The structure of Spir1-KIND (gray) and Fmn2-tail (green; Vizcarra *et al.*, 2011). Numbering reflects Capu residues, with Fmn2 residues indicated in parentheses. (B) Barbed-end concentrations at $t_{1/2}$ in the presence of 20 nM Capu-CT or Capu-CT mutants (gray) plus 150 nM Capu-NT (red) or 1 μM Spir-KIND (green). Each bar represents the average of three experiments (error bars, SD). Residues shown in B are indicated in A. Pink are mutations tested in Vizcarra *et al.* (2011). Blue and black are new mutations. Residues equivalent to R1034 and K1058 were not visible in the crystal structure.

The effect of Capu-NT on nucleation and processive elongation by Capu-CT

Bulk pyrene-actin polymerization assays do not clearly distinguish between the effects that formins have on filament nucleation and elongation. There are several possible molecular mechanisms that could account for the activity of Capu-NT observed in Figure 1C. The Capu-CT/Capu-NT complex could be unable to nucleate new filaments. Alternatively, a Capu-CT/Capu-NT complex could nucleate normally but, when bound to filament barbed ends, slow or block elongation. To better understand the mechanism of inhibition by Capu-NT, we measured the elongation rate of individual actin filaments using total internal reflection fluorescence (TIRF) microscopy in the presence and absence of Capu-CT and Capu-NT.

Formins have been reported to accelerate barbed-end elongation in the presence of profilin (Kovar *et al.*, 2006; Neidt *et al.*, 2009). Capu-CT alone does not have a large effect on the barbed-end elongation rate but accelerates growth approximately fourfold in the presence of the *Drosophila* profilin, Chickadee (Chic; Figure 5, A and C). We did not originally observe enhanced elongation in bulk assays (Vizcarra *et al.*, 2011). Presumably, the acceleration was masked by the fact that profilin tends to bind unlabeled actin with higher affinity than actin labeled at Cys-374 (Vinson *et al.*, 1998). In TIRF assays, this bias results in dimmer filaments when Capu-CT and profilin are present. We used filament brightness and elongation rate to determine which filaments had Capu-CT bound and to ask how the Capu-CT/Capu-NT complex affects filament elongation. When we incubated Capu-CT with Capu-NT before adding them to profilin/actin monomers, only 2% of the filaments were dim and fast growing (n = 896 filaments), compared with 57% of the filaments in Capu-CT–alone samples (n = 756 filaments; Figure 5, A and B). In addition, slides with both Capu-CT and Capu-NT had fewer filaments than did those with Capu-CT alone. These results indicate that Capu-NT not only inhibits Capu-CT's nucleation activity but also prevents Capu-CT from binding to filament barbed ends.

Consistent with the TIRF assay, Capu-CT, in the presence of Capu(1–321), could not protect barbed ends from capping protein (CP) in bulk elongation assays (Figure 5C). Previously we found that Capu-CT alone can protect barbed ends from CP (Vizcarra *et al.*, 2011). When Capu(1–321) and Capu-CT were mixed before adding them to actin, barbed ends were no longer protected (Figure 5C and Supplemental Figure S6A). These results confirm that autoinhibited Capu-CT is unable to bind barbed ends. Spir-KIND can displace Capu-CT from growing barbed ends (Vizcarra *et al.*, 2011). To determine whether Capu(1–321) has the same effect, we added Capu(1–321) or Spir-KIND to the reaction after Capu-CT was already bound to growing filaments (Supplemental Figure S6B). Indeed, the addition of Capu(1–321) or Spir-KIND (in the presence of CP) slowed filament elongation to similar extents, demonstrating that Capu(1–321) can displace Capu-CT from growing barbed ends as well as Spir-KIND.

Physical properties of Capu-NT constructs

We characterized Capu-NT's physical properties using various solution-based assays. Circular dichroism (CD) showed that Capu-NT has substantial α-helix and random coil content and low β-sheet content (Figure 6A). Removing residues 322–466 reduced the α-helical content by ~12%, did not change β-sheet content, and increased the relative amount of random coil by ~10%. The CD spectra for Capu-NT plus Capu-tail and for Capu-NT alone were similar (Figure 6A). Overall, the CD data suggest that Capu-NT has a large amount of random structure. Proteolysis results with trypsin and proteinase K concur (Figure 3D and unpublished data). Although substructures were detectable within Capu-NT, overall it was rapidly digested, as would be expected for a protein with a substantial amount of random coil.

We used analytical ultracentrifugation and size-exclusion column (SEC) multiangle light scattering (MALS) to measure the sizes and shapes of Capu-NT, Capu(1–321), and Capu(1–222). If we fitted sedimentation equilibrium data for Capu-NT with a single-species model, the molecular mass measured was 83.5 kDa, suggesting that the molecule is a dimer (Figure 6B and Table 1). This result gives a 14% error from the expected mass of a dimer (97.2 kDa), so we also fitted the data with a monomer–dimer equilibrium model. The predicted K_d of 245 nM is consistent with the dominant species being a dimer at 2.4 μM of Capu-NT. In both cases there is small but systematic error in the residuals, which probably reflects the tendency of Capu-NT to aggregate over long periods of time. Capu(1–321) was not stable enough, and Capu(1–222) lacks tryptophan and tyrosine residues necessary to perform equilibrium sedimentation. We therefore obtained independent confirmation that the dominant Capu-NT species is a dimer and measured the molecular mass of Capu(1–321) and Capu(1–222) using SEC-MALS. The molecular mass of Capu-NT as measured with MALS was 102.9 kDa (Figure 6C). SEC-MALS shows that Capu(1–321) has a molecular mass of 64.9 kDa, similar to the predicted molecular weight for a dimer (66.6 kDa; Figure 6C and Table 1). Of interest, the molecular weight of Capu(1–222) is 22.9 kDa, consistent with the monomer weight of 22.3 kDa (Figure 6C and Table 1). This indicates that the dimerization domain of Capu-NT is located between residues 222 and 321. We also measured the sedimentation velocity coefficients of Capu-NT and Capu(1–321) (3.3 and 2.7 S, respectively; Supplemental Figure S7, A and B, and Table 1). Together our analytical ultracentrifugation and SEC-MALS data suggest that Capu-NT and Capu(1–321) are dimers with aspect ratios of ~17:1, assuming that they are

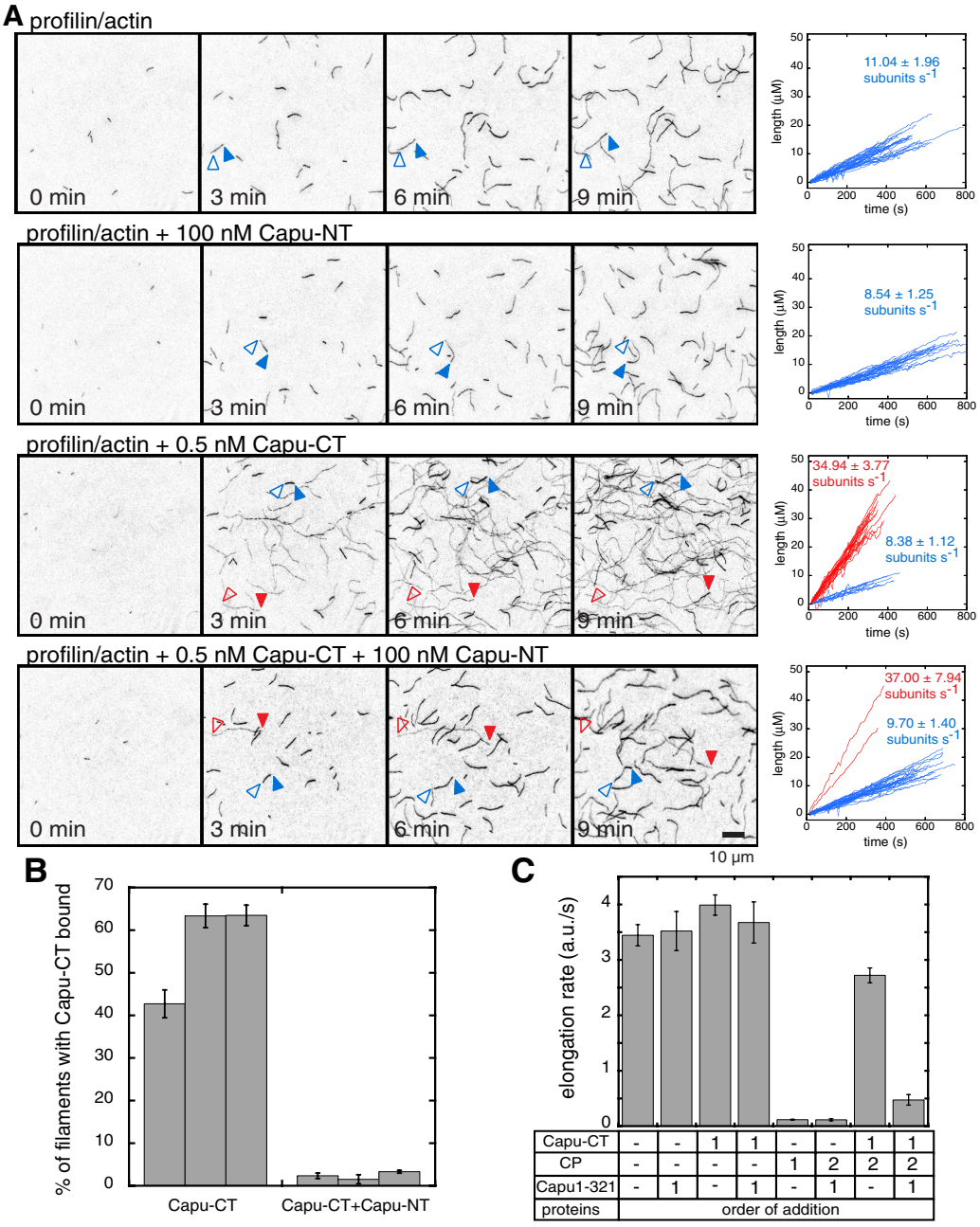

FIGURE 5: Capu-NT inhibits nucleation and competes with barbed- end binding by Capu-CT. (A) Direct observation of filament elongation in the presence of Capu-NT and/or Capu-CT by TIRF microscopy. For each condition, TIRF images are shown for 0, 3, 6, and 9 min, and elongation traces from three different slides, for each condition, are plotted to the right. The bright filaments are shown as blue traces and blue arrows, and the dim filaments, which grew approximately fourfold faster than the bright filaments, are shown as red traces and red arrows (open arrow, pointed end; closed arrow, barbed end). The average and SD of the rates, calculated by linear fits, are shown next to each set of traces. Conditions used are as follows: 1 µM actin (16% Oregon green), 5 µM profilin (Chic), 1 nM Capu-CT, and 100 nM Capu-NT. (B) Quantification of number of filaments bound to Capu-CT with and without Capu-NT from slides in A. For each condition, an average percentage bound is given for three different slides. Error bars are SEM for at least three fields of view from a given slide. Taken together, these data show that when Capu-CT is added alone, 57% ($n = 756$ filaments) of the filaments are dim and fast growing, that is, bound by Capu-CT. When Capu-CT is mixed with an excess of Capu-NT before addition to the actin, only 2% ($n = 896$ filaments) of filaments are dim and fast growing. (C) Capu(1–321) inhibits binding of Capu-CT to barbed ends when Capu(1–321) is incubated with Capu-CT before mixing with filament seeds. In this assay, 0.25 µM actin seeds were mixed with 0.5 µM actin monomers, 100 nM Capu-CT, 500 nM Capu(1–321), and 0.375 nM mouse capping protein (CP). The order of protein addition is indicated by a number (1 or 2). For both Capu-CT and Capu(1–321), 1 means that proteins were mixed together before they were added to the seeds. (Error bars, SD, $n = 3$.)

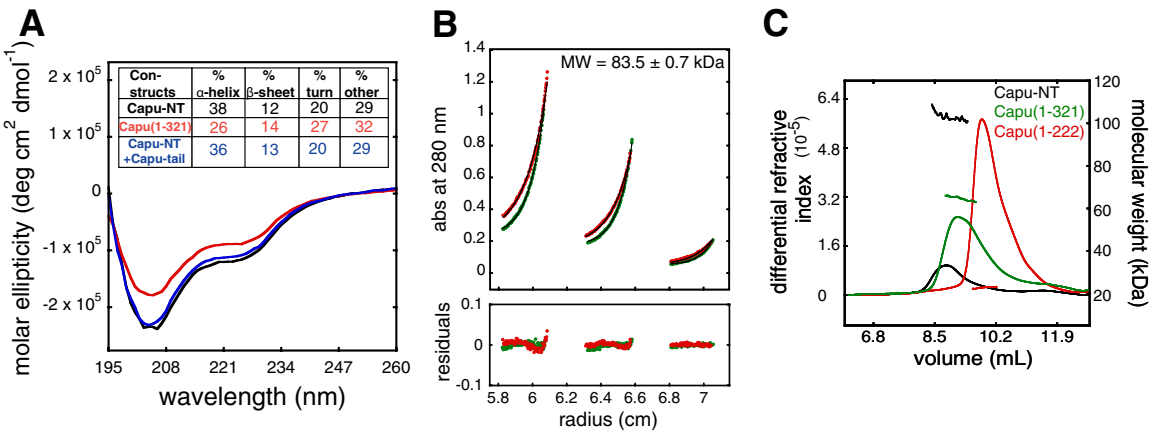

FIGURE 6: Capu-NT is a dimer. (A) Capu-NT (black; 2.9 μM), Capu(1–321) (red; 4.5 μM), and Capu-NT plus Capu-tail (blue; 3 μM of each) were analyzed by circular dichroism. Each was scanned three times and averaged for analysis. Inset table shows the calculated percentage secondary structure for each construct. (B) Equilibrium sedimentation showed that Capu-NT is a dimer in solution (monomer is 48.6 kDa). Capu-NT at varying concentrations (0.6, 1.8, and 2.8 μM) was spun to equilibrium at 11,000 rpm (red circles) and 13,000 rpm (green circles). Lines represent the best fit to a single-species model (molecular weight, 83.5 kDa). Residuals are shown below. When fitted to monomer–dimer model, the apparent dimer dissociation constant is 245 nM. (C) SEC-MALS data show that both Capu-NT (black) and Capu(1–321) (green) are dimers, with molecular weights of 102.9 and 64.9 kDa, respectively. Capu(1–222) (red) is a monomer with molecular weight of 22.9 kDa. The differential refractive index and calculated molecular weight of the proteins are plotted vs. retention volume. See Table 1 for a summary.

prolate ellipsoids. This ratio is extremely elongated and unlikely. We speculate that the low sedimentation coefficients reflect disordered loops at the surface of Capu-NT, in agreement with our CD data.

DISCUSSION

We found that the actin assembly activity of the *Drosophila* formin, Capu, is autoinhibited, despite the absence of canonical DID and DAD domains. This discovery agrees with data suggesting that the N-terminus of Capu plays an important physiological role (Dahlgaard *et al.*, 2007; Chang *et al.*, 2011; Tanaka *et al.*, 2011). In the original test of Capu autoinhibition, no effect of Capu-NT on nucleation by Capu-CT was observed (Rosales-Nieves *et al.*, 2006). In this case Capu(1–415) was used, which may be less potent than Capu(1–466) or Capu(1–321). Consistent with this idea, we find that Capu(1–402) has only minimal inhibitory activity. In addition, a 1:1 mixture of the two constructs was tested. We examined a range of concentrations and see a small effect at this ratio but very potent inhibition when the concentration of Capu-NT is increased. Because autoinhibition was observed for Fmn1 as well, we propose that this mode of regulation is conserved in Fmn-family formins. Whether Fmn2 is autoinhibited remains to be tested.

Comparison of autoinhibition by Capu with DRFs

Capu's autoinhibitory domains are positioned similarly to DID and DAD domains, on either side of the FH1-FH2 domains. Like the N-termini of other formins, Capu-NT is a dimer. However, the structural similarities seem to end there. The classic DAD domain is a well-described motif. DAD domains are contained within the sequence C-terminal to the FH2 domain, but the distance from the FH2 domain varies between formins. The Capu-tail is only ~30 residues long and highly basic. The Capu-tail is well conserved among Fmn-family formins, but the only similarity to DAD domains is a trivial similarity to the polybasic region at the end of the DAD motif. The classic DID domain consists of armadillo repeats, which are not apparent in the Capu sequence or those of other Fmn-family formins. Capu-NT and the shorter constructs we tested contain a high percentage of loops and random coil, which is very different from the tightly packed DID domain. We performed limited proteolytic digests and made a number of truncations in order to identify a minimal CID domain. Reaching this goal was more difficult than expected based on what we know about DID domains. We deduced that the core CID lies between residues 80 and 321 or even 80 and 222. Residues 1–80 could be contributing directly by binding to

Construct	Mass, calculated (kDa)	Mass, MALDI (kDa)	Mass, equilibrium AUC (kDa)[a]	Mass, MALS (kDa)[a]	$S_{20,W}$ collected at 20°C	$S_{20,W}$ collected at 4°C
Capu-NT	48.6	48.7	83.5 ± 0.7 (14%)[b]	102.9 ± 0.1 (6%)	3.3	3.3
Capu(1–321)	33.5	33.5	ND[c]	64.9 ± 0.1 (2%)	2.7	2.6
Capu(1–222)	22.3	22.3	ND	22.88 ± 0.07 (3%)	ND	ND

AUC, analytical ultracentrifugation; ND, not determined.
[a]Percentages indicate deviations from the predicted molecular weight.
[b]Monomer/dimer fit of the same data showed that Capu-NT has a dimerization K_d of 245 nM.
[c]We could not determine the mass of Capu(1–321) using equilibrium AUC due to protein instability..

TABLE 1: Size determination of Capu-NT constructs.

Capu-CT or indirectly by influencing the structure of the CID. In vivo data show that expression of Capu(1–100) has negative consequences but only in a sensitized background (Chang *et al.*, 2011). Perhaps the CID is not contained in one stable linear portion of Capu-NT but instead consists of multiple weak-binding sites within Capu-NT that together form the CID. Future studies, including high-resolution structural data, are needed for a clear understanding of the CID, how it interacts with Capu-CT, and how it compares to the DID.

Mechanism of autoinhibition

Ramalingam *et al.* (2010) and Maita *et al.* (2012) showed that purified full-length mDia1 is autoinhibited, confirming conclusions from many studies performed on formin subfragments similar to the work presented here. Structural insight into the mechanism of autoinhibition comes from two recent crystal structures of mDia1 N- and C-termini bound to each other (Nezami *et al.*, 2010; Otomo *et al.*, 2010). The crystal structures are complicated tetrameric complexes, which forced the authors to develop multiple models of autoinhibition. In most of the models presented, actin filaments are occluded at the FH2 domain by the DID/DAD interaction. Cryo–electron microscope reconstruction of mDia1 (Maita *et al.*, 2012) is consistent with the "trans model" presented by Nezami *et al.* (2010) and "Model 1" presented by Otomo *et al.* (2010). Based on the crystal structure, the autoinhibited complex could bind actin monomers but not in a productive manner. More than two monomers or a growing filament would be sterically blocked. Finally, regions close to the DAD domain have been shown to play a positive role in nucleation, and binding to the DID would prevent this activity (Gould *et al.*, 2011; Heimsath and Higgs, 2012).

How does this relate to Capu autoinhibition? Although Capu does not have a DAD domain, the Capu-tail is required for nucleation in a manner similar to that described for other formins (Gould *et al.*, 2011; Vizcarra *et al.*, 2011; Heimsath and Higgs, 2012). We believe that Capu-NT inhibits Capu's actin assembly activity by binding and effectively sequestering the Capu-tail as proposed for Spir-KIND (Vizcarra *et al.*, 2011); hence the ability of monomeric constructs, which might not occlude filament binding, to inhibit. We note a subtle but perhaps not insignificant difference between Capu-NT and Spir-KIND inhibition. Capu-NT completely inhibits actin assembly, whereas saturating concentrations of Spir-KIND do not. This may reflect the difference in binding sites we detect, and/or it could be due to dimer/dimer binding of Capu-CT and Capu-NT. We favor the former mechanism for two reasons. First, monomeric Capu(1–222) completely inhibits Capu-CT. Second, although GST-Capu-tail is sufficient to compete with Capu-CT for Capu-NT binding, the apparent affinities between Capu-NT and Capu-CT versus either tail construct differ by 10- to 50-fold. We interpret this as evidence that the actual Capu-NT binding site extends into the FH2 domain. This does not exclude a role of Capu-NT as steric inhibitor of polymerization. The combination of mechanisms would ensure that autoinhibition is highly effective.

Regulation of autoinhibition

How is the intramolecular interaction regulated? At least three of the DRFs are regulated by binding of small GTPases to a region adjacent to and overlapping with the DID. Rosales-Nieves *et al.* (2006) found a genetic and biochemical interaction between Capu and Rho1, making it a candidate for regulation of Capu autoinhibition. Capu(125–250) binds Rho1 with a preference for GTP- over GDP-Rho1. This fragment of Capu binds to Capu-CT in pull-down assays and overlaps with the constructs we identified in autoinhibition assays. However, our preliminary results indicate that constitutively active Rho1 does not relieve autoinhibition of actin assembly by Capu (unpublished data). Perhaps Rho1's interaction with Capu is similar to Rho1's interaction with DAAM: DAAM is epistatically downstream of Rho1 in a noncanonical Wnt-signaling pathway, but Rho1 does not significantly activate Daam1 (Liu *et al.*, 2008).

Regulation of Capu through autoinhibition and Spir

How does our finding that Capu is autoinhibited fit with data showing that Spir and Capu collaborate and that Spir inhibits Capu? One interpretation is that Capu can function independently of Spir, perhaps when expressed in cells lacking Spir (Supplemental Figure S8A). A clear role for a functional collaboration between Spir and Capu (and their mammalian homologues) has been established in oocytes, but much less is known about either protein in other cells (Dahlgaard *et al.*, 2007; Quinlan *et al.*, 2007; Pfender *et al.*, 2011). Outside of the oocyte, a role for Fmn1 in adherens junctions was described (Kobielak *et al.*, 2003). No role for Spir1 or Spir2 in adherens junctions has been observed, supporting the idea that Fmn-family formins may act independently at times. More work is required to address whether Fmn-family formins are expressed in the absence of Spir, a case in which autoinhibition would be the primary mechanism for regulation.

Autoinhibition may be part of the Spir/Capu regulatory cycle (Supplemental Figure S8B). A speculative model is as follows: 1, 2) Spir plays a positive role, in that when Spir and Capu are bound to each other, Spir nucleates; 2, 3) the new filament is handed off to Capu, and Spir is released; 4a) in time Capu autoinhibition displaces Capu-CT from barbed end and inhibits itself until (1) it binds Spir and is primed to nucleate again. Alternatively, Spir could function as a regulator of Capu elongation (4b), much like Bud14 (Chesarone *et al.*, 2009). The consequence of this mode of ending filament elongation is that Spir and Capu would then be bound to each other and primed to nucleate again upon termination of the previous nucleation/elongation cycle. On the basis of the fact that Spir-KIND and Capu-NT have similar affinities for Capu-CT and that Capu-NT acts in-*cis* as opposed to in-*trans*, we expect Capu-NT to outcompete Spir for binding to Capu-CT. Therefore we speculate that external factors, such as small GTPases and/or posttranslational modifications, play an important role in regulating the interaction between Capu and Spir and potentially selecting the paths outlined here.

MATERIALS AND METHODS

DNA constructs

Capu-NT (aa 1–466) and truncations of Capu-NT were generated by PCR amplification from a full-length Capu template (CG3399, Capu-PA). Capu-NT truncations were subcloned into pGEX-6P-2 (GE Healthcare, Piscataway, NJ) between the *Bam*HI and *Not*I sites. Point mutations were introduced into Capu-CT using QuikChange Site Directed Mutagenesis (Stratagene, Santa Clara, CA).

Protein expression and purification

Acanthamoeba castellani actin, Capu-tail, and Capu-CT constructs were purified according to published protocols (MacLean-Fletcher and Pollard, 1980; Vizcarra *et al.*, 2011). In brief, Capu-tail was expressed as a GST fusion and then cleaved away from the tag (unless otherwise indicated); Capu-CT was expressed as a histidine-tagged construct. We expressed Capu-NT::pGEX-6P-2 in Rosetta (DE3) pLysS-competent cells. Cells were grown in Terrific Broth at 37°C until they reached an optical density at 600 nm of 0.6–0.8, at which point the temperature was lowered to 20°C for 1 h. Then the cells were induced with 0.25 mM isopropyl-β-D-thiogalactoside and

harvested after 13–16 h. Cell pellets were flash frozen with liquid nitrogen and stored at –80°C.

Thawed cell pellets were resuspended in lysis buffer (50 mM Tris, pH 7, 150 mM NaCl, 0.2% Triton X-100, 1 mM dithiothreitol [DTT]) supplemented with 1.7 mM phenylmethanesulfonyl fluoride (PMSF) and 1 µg/ml DNaseI. All subsequent steps were carried out at 4°C or on ice. Cells were lysed by two passages through a microfluidizer (Microfluidics, Newton, MA). The lysate was centrifuged at 20,000 × *g* for 20 min, and the supernatant was nutated with 1.5 ml glutathione–Sepharose 4b beads (GE Healthcare) for 1 h. Capu-NT was cleaved from the bound GST by incubating with PreScission Protease (GE Healthcare) overnight at 4°C. The eluate was concentrated in an Amicon 10-kDa–molecular weight cutoff centrifugal filter unit and then gel filtered using a Superdex 200 10/300 GL column (GE Healthcare; column buffer: 20 mM Tris, pH 8, 100 mM NaCl, 0.5 M L-arginine, 1 mM DTT). Fractions were pooled based on SDS–PAGE analysis, dialyzed into storage buffer (10 mM Tris, pH 7, 1 mM DTT), and then placed in 1:1 glycerol:storage buffer overnight. Protein aliquots were flash frozen in liquid nitrogen and stored at –80°C. The resulting Capu-NT samples were >98% pure (Figure 1B).

While purifying Capu-NT, two problems arose: 1) protein breakdown, resulting in a doublet on gels, and 2) DnaK chaperone contamination. The former was remedied by using the lysis buffer described previously as opposed to the standard phosphate-buffered saline recommended for glutathione resin. Before protease cleavage, an additional wash step using lysis buffer supplemented with 5 mM ATP and 10 mM $MgCl_2$ removed most of the DnaK (Pastorino *et al.*, 2008). Truncations of Capu-NT were purified by the same method.

Concentrations of all proteins are reported in terms of their monomer (subunit) concentrations to simplify analysis of interactions. Thus 20 nM Capu-CT is equal to 10 nM of functional nucleation unit. Similarly, the new extinction coefficients reported here are in terms of monomer concentrations. To determine the extinction coefficient of Capu-NT (204,855 cm^{-1} M^{-1}), we measured the concentration of a purified sample by amino acid analysis (AAA) at the University of California at Los Angeles Biopolymer Laboratory. The extinction coefficient was calculated using Beer's law (Abs = c*ε*b), where c is the concentration of the protein measured by AAA, Abs is the absorbance at 280 nm measured for the sample analyzed by AAA, and b is path length (1 cm). The extinction coefficient of Capu(50–321) (41,758 cm^{-1} M^{-1}) was determined similarly. To determine the extinction coefficient of Capu(1–321) (99,582 cm^{-1} M^{-1}), we quantified bands from five different concentrations of Capu(1–321) on an SDS–PAGE gel stained with SyproRed (Invitrogen). Gels were imaged on a Pharos FX (Bio-Rad, Hercules, CA). The Capu(1–321) concentration was measured using Capu(50–321) as a standard. Because Capu(1–222) lacks tryptophan and tyrosine residues, we determined its concentration using quantitative SyproRed staining with Capu(1–321) as a standard.

Chickadee (*Drosophila* profilin) was expressed without an affinity tag in the pET17b plasmid in BL21 (DE3) pLysS-competent cells (overnight at 18°C). Cell pellets were resuspended in extraction buffer (10 mM Tris, pH 8, 1 mM EDTA, 1 mM DTT, 1 mM PMSF) and lysed with a microfluidizer. The lysate was centrifuged at 20,000 × *g* for 20 min, and the supernatant was incubated with DE52 resin for 30 min at 4°C. Both the flowthrough and an extraction buffer wash were collected. Ammonium sulfate was added to 35% saturation with stirring at 4°C for 15 min. The sample was centrifuged at 30,000 × *g* for 30 min. The supernatant was brought to 61% ammonium sulfate saturation and centrifuged again, and the pellet was dialyzed overnight with 5 mM potassium phosphate, pH 7.5, 1 mM DTT. The sample was filtered through a hydroxyapatite column (Bio-Rad) and then further purified by gel filtration on a HiLoad 26/60 Superdex 75 column (GE Healthcare) in 150 mM NaCl, 10 mM 4-(2-hydroxyethyl)-1-piperazineethanesulfonic acid (HEPES), pH 7, and 0.5 mM Tris(2-carboxyethyl)phosphine (TCEP). The purified protein was flash frozen in 50% glycerol, 50% 10 mM HEPES, pH 7, and 0.5 mM TCEP and stored at –80°C. The concentration of Chic was calculated by quantitative SyproRed staining using *Schizosaccharomyces pombe* profilin (1.63 OD/mg/ml) as a standard (Lu and Pollard, 2001).

Purified *Acanthamoeba castellani* actin was labeled with Oregon green 488 iodoacetamide (Life Technologies, Carlsbad, CA) on cysteine 374. Filamentous actin was dialyzed for 3–4 h with 100 mM KCl, 2 mM $MgCl_2$, 25 mM imidazole, pH 7.5, and 0.2 mM ATP to remove reducing reagents. The actin was rocked at 4°C overnight with a 5- to 10-fold molar excess of dye. The reaction was quenched with 10 mM DTT and spun at 195,000 × *g*. The pellet was resuspended in actin G buffer (2 mM Tris, 0.1 mM $CaCl_2$, 0.2 mM ATP, 0.5 mM TCEP, 0.04% sodium azide) and dialyzed for 3–4 d before gel filtration on a Superdex 200 10/300 GL column. Actin concentration and dye labeling percentage were calculated according to Kovar *et al.* (2003).

Pyrene-actin polymerization assays

Pyrene-actin assembly assays were carried out essentially as described (Zalevsky *et al.*, 2001). Briefly, 4 µM *A. castellani* actin (5% pyrene labeled) was incubated for 2 min at 25°C with ME buffer (final concentration, 200 µM ethylene glycol tetraacetic acid [EGTA] and 50 µM $MgCl_2$) to convert Ca-G-actin to Mg-G-actin. Polymerization was initiated by adding KMEH polymerization buffer (final concentration, 10 mM Na-HEPES, pH 7.0, 1 mM EGTA, 50 mM KCl, 1 mM $MgCl_2$) to the Mg-G-actin. Additional components, such as Capu-CT, Capu-tail, and Capu-NT, were combined in the polymerization buffer before addition to Mg-G-actin. Fluorescence was monitored in a spectrofluorometer (Photon Technology, Birmingham, NJ) or a TECAN F200 with $\lambda_{excitation}$ = 365 nm and $\lambda_{emission}$ = 407 nm.

Barbed-end concentrations at $t_{1/2}$ were calculated for the bulk pyrene assays using the following equation: [barbed end] = elongation rate/(k_+ × [actin monomers] – k_-), where k_+ = 11.6 μM^{-1} s^{-1} and k_- = 1.4 s^{-1} (Pollard, 1986). The elongation rate was determined by the slope of a best-fit line to the raw data at half-maximal polymerization. We assumed that the actin monomer concentration was 2 µM when analyzing the data near $t_{1/2}$. Calculation of the nucleation rates of Capu-CT in the presence of Capu-NT was done as described previously (Quinlan *et al.*, 2007). In brief, using a custom wavelet analysis–based algorithm, we smoothed the fluorescence intensity data. The data from the first 30 s were plotted versus time, and the slopes of these lines were taken as the rate of barbed-end formation (i.e., nucleation rate).

Competition pyrene polymerization experiments were analyzed using a competition binding model as described in Vinson *et al.* (1998). To calculate K_d for the Capu-tail/Capu-NT interaction, we used the following equation:

$$f = \frac{1}{K_d\left(\frac{L + K_{d2}}{K_{d2} R_0}\right) + 1}$$

where L = [Capu-tail], R_0 = [Capu-NT], K_d is the affinity of Capu-CT for Capu-NT, and K_{d2} is the affinity of Capu-tail for Capu-NT. At EC_{50} = 3 µM, f = 0.5 and L = 3 µM. Under these conditions and

when K_d is assumed to be 10 nM (K_i of Capu-CT/Capu-NT), K_{d2} is 333 nM.

Proteolysis

Capu-NT was dialyzed into 10 mM Tris, 50 mM KCl, and 1 mM DTT and diluted to a final concentration of 3 µM. At time 0 min, 6 nM trypsin was added to the Capu-NT. At time points 1, 2, 5, 10, 15, 30, 60, 90, and 120 min, samples were taken from the reaction and added to 4 mM PMSF to stop proteolysis. Samples were boiled and run on an SDS–PAGE gel for visualization. In the second condition, 50 µM Capu-tail was added to Capu-NT before adding trypsin.

To determine the boundaries of stable bands after tryptic digest, proteolyzed Capu-NT was run on an SDS–PAGE gel and transferred to Immobilon-P membrane (Millipore, Billerica, MA). The bands were visualized by Coomassie staining and cut out from the membrane. The Nevada Proteomics Center (Reno, NV) performed Edman protein sequencing to identify the N-terminus. To determine the molecular weights of the digested bands, both untreated and digested (5 min) Capu-NT were analyzed by MALDI mass spectrometry (Supplemental Figure S3B). Capu-NT (0.5 µl of 3.2 µM) was mixed with 0.5 µl of saturated sinapinic acid and analyzed on a Voyager-DE STR MALDI-TOF Mass Spectrometer (Applied Biosystems, Foster City, CA).

Fluorescence anisotropy

Fluorescence polarization anisotropy of 20 nM Capu-tail–Alexa Fluor 488 (40% labeled), with increasing amounts of Capu-NT, Capu(1–321), or Capu(1–222), was measured with a spectrofluorometer. All assays were carried out at 25°C in 10 mM HEPES, pH 7.0, 1 mM EGTA, 1 mM TCEP, 0.5 mM Thesit, 50 mM KCl, and 1 mM $MgCl_2$. The fluorophore was excited by plane-polarized light at 488 nm, and emission was measured at 520 nm at angles parallel and perpendicular to the angle of incidence. A bandpass filter at 520 ± 5 nm was placed in the emission path. Data were analyzed as previously described (Vizcarra *et al.*, 2011).

TIRF microscopy assays

Coverslips for TIRF elongation assays were prepared essentially as described (Hansen *et al.*, 2010). Briefly, coverslips were washed by sonication with ethanol, 1 M potassium hydroxide, and ethanol, washing with Milli-Q water after each step. The coverslips were then sonicated with isopropanol (15 min), followed by 5% 3-aminopropyltriethoxysilane (Sigma-Aldrich, St. Louis, MO) in isopropanol (30 min). Silanized coverslips were baked at 90°C and stored in 100% ethanol for up to 1 mo. Before PEGylation, coverslips were washed with Milli-Q water. A drop of 30 mg/ml *N*-hydroxylsuccinimide–functionalized polyethylene glycol (PEG-NHS; 97% methoxy-PEG-NHS and 3% biotin-PEG-NHS; JenKem Technology, Allen, TX) in *N*,*N*-dimethyl formamide was placed on half of the silanized coverslips. Another coverslip was placed over each drop to create a sandwich. The PEGylation reaction was carried out by incubating the sandwiches at 75°C for at least 2 h, followed by multiple washes with Milli-Q water. PEGylated coverslips were stored in a sealed container at 4°C for up to 1 mo before use.

Heavy meromyosin (HMM; a gift of the Reisler lab, University of California at Los Angeles) was biotinylated using maleimide-PEG_{11}-biotin (Thermo Scientific, Waltham, MA). HMM (0.5 mg/ml) was incubated with 0.5 mM TCEP for 30 min at room temperature. TCEP was removed using a PD10 column (GE Healthcare), and HMM was eluted in 50 mM sodium phosphate, pH 7, and 100 mM sodium chloride. A 40-fold molar excess of maleimide-PEG_{11}-biotin was incubated with the HMM for 2 h at room temperature, followed by dialysis with 25 mM Tris, pH 8, 30 mM KCl, and 1 mM DTT, and then the same buffer was mixed with equal volume of glycerol. The biotinylated-HMM was flash frozen and stored at −80°C. Streptavidin (VWR, Radnor, PA) was diluted to 30 µM tetramer in Milli-Q water, flash frozen, and stored at −80°C.

Flow cells with volumes of ~10–15 µl were assembled using double-stick tape. Immediately before imaging, 25 µl of 40 nM streptavidin was applied to the flow cell for 30 s, followed by a wash with 25 µl of 1× TIRF buffer (50 mM KCl, 1 mM $MgCl_2$, 1 mM EGTA, 10 mM HEPES, pH 7, 0.2 mM ATP, 50 mM DTT, 0.2% methylcellulose), 30 s of incubation with 25 µl of 20 nM biotinylated-HMM, and a wash with 25 µl of 1× TIRF buffer. Profilin/actin (final concentration, 1 µM actin, 16% Oregon green labeled, and 5 µM *Drosophila* profilin) was incubated with ME buffer for 2 min at room temperature. A solution containing 2× TIRF buffer, glucose oxidase (final concentration 0.25 mg/ml), catalase (final concentration 0.05 mg/ml), and any additional proteins (1 nM Capu-CT and/or 100 nM Capu(1–466) final concentrations) was mixed with the Mg-G-actin solution. Filament elongation was visualized on a DMI6000 TIRF microscope (Leica, Wetzlar, Germany) for at least 10 min, capturing images at 10-s intervals. Filament lengths and elongation rates were analyzed with JFilament incorporated in FIJI (Smith *et al.*, 2010).

Bulk elongation assay

Actin (5 µM) was polymerized in 1× KMEH buffer at 25°C for 1 h and aliquoted into 5-µl volumes of 5 µM 1 d before an experiment. To initiate polymerization at the barbed end, we added 20% labeled 0.5 µM Mg-G-actin to the seeds. Filament assembly was tracked for 700 s. Elongation rates were calculated from the slopes between 200 and 700 s. Final concentrations of proteins were 0.25 µM actin seeds, 0.5 µM Mg-G-actin, 100 nM Capu-CT, 500 nM Capu(1–321), and 0.375 nM recombinant mouse capping protein $\alpha1\beta2$. Capu-CT was mixed with buffer or Capu(1–321) and incubated for 60 s at 25°C. Subsequently, this mix was added to the seeds and incubated for another 30 s. At this time, Mg-G-actin was added to the ME buffer (see earlier description) and incubated for 2 min at 25°C. After 2 min, seeds, Mg-G-actin, and 1× KMEH buffer containing either buffer blank or CP were combined and analyzed in the fluorometer. To minimize filament shearing, cut pipette tips were used to transfer the polymerization reaction to the cuvette. For the "mid-assay" addition of protein, instead of adding Capu(1–321) or Spir-KIND in the beginning of the assay, we added one or the other after recording elongation for 200 s. Each condition was repeated three times.

Circular dichroism

Proteins were dialyzed into 50 mM potassium phosphate, 1 mM DTT (pH 7). Circular dichroism spectra were measured on a J-715 spectropolarimeter (Jasco, Tokyo, Japan) by averaging three wavelength scans from 195 to 280 nm. The data were analyzed using a previously described method within the Jasco and Sofsec1 software packages (Sreerama and Woody, 1993). The latter compares the input data with a database of spectra from proteins with known secondary structure.

Analytical ultracentrifugation

Sedimentation velocity analytical ultracentrifugation was performed on Capu-NT and Capu(1–321) essentially as described (Chen *et al.*, 2012). Both proteins were dialyzed into 10 mM Tris, 150 mM NaCl, and 0.5 mM TCEP (pH 7.5) and diluted to a final concentration of 2.4 µM Capu-NT or 5.0 µM Capu(1–321). Proteins were spun at 50,000 rpm at 4°C for 3 h in an Optima XL-A Analytical Ultracentrifugation system (Beckman Coulter, Brea, CA). Data were acquired

every 3 min for 50 scans. Data were analyzed with Beckman Origin-based software, version 3.01. Capu(1–321) was unstable over the course of an experiment at 20°C. This breakdown is apparent in the analysis (Supplemental Figure S6A), where we see a clear peak at 2.7S and then trailing shoulders from that peak. Data acquired at 4°C were corrected for the viscosity change.

Sedimentation equilibrium analytical ultracentrifugation was performed at two speeds (11,000 and 13,000 rpm) with three different concentrations of Capu-NT (0.6, 1.8, and 2.8 μM). Scans collected between 24 and 28 h after speed was attained were analyzed. The same buffer conditions, centrifuge, and analysis software were used as in the velocity sedimentation experiments.

Size-exclusion column with multiangle light scattering

To analyze Capu(1–222), Capu(1–321), and Capu-NT with SEC-MALS, the proteins were dialyzed into 10 mM Tris, 150 mM NaCl, and 0.5 mM TCEP overnight and spin concentrated using an Amicon 10-kDa–molecular weight cutoff centrifugal filter unit. An analytical size-exclusion column (5 μm, 300 Å, 7.8 × 300 mm; Wyatt Technology, Goleta, CA) was equilibrated with phosphate-buffered saline (140 mM NaCl, 2.7 mM KCl, 10 mM Na_2HPO_4, 1.8 mM KH_2PO_4). In each case a 100-μl sample was loaded: 43.5 μM Capu(1–222), 18.3 μM Capu(1–321), or 5.8 μM Capu-NT. The smaller the size of the protein, the more protein was needed to detect light scattering signals. During elution, light scattering was measured with a miniDAWN TREOS and the refractive index (*n*) was measured with an Optilab T-rEX system (Wyatt Technology). The data were analyzed by ASTRA 6 software to obtain average molecular weights (Table 1). The *dn*/*dc* (where *c* is concentration) for the calculation was set to 0.185 ml/g, a typical value for proteins.

ACKNOWLEDGMENTS

We thank Quinlan lab and Reisler lab members for invaluable discussion and feedback. We thank Elizabeth Roth and Andrey Shur for help purifying the Capu-tail mutants, Dan McNamara for help in using the MALS instrument, and R. Loo and J. Loo for help in analyzing the proteolyzed Capu-NT by MALDI. Last but not least, we thank O. Akin for his feedback and for providing software for pyrene assay analysis. This work was supported in part by grants from the National Institutes of Health (1R01GM096133-01), the Burroughs-Wellcome Fund (Career Award in the Biomedical Sciences), and March of Dimes Foundation Grant 5-FY10-81 (M.E.Q.) and National Institutes of Health National Research Service Award Postdoctoral Fellowship F32GM087857 (C.L.V.).

REFERENCES

Ahern-Djamali SM (1999). Identification of profilin and src homology 3 domains as binding partners for Drosophila Enabled. Proc Natl Acad Sci USA 96, 4977–4982.

Alberts AS (2001). Identification of a carboxyl-terminal diaphanous-related formin homology protein autoregulatory domain. J Biol Chem 276, 2824–2830.

Azoury J, Lee KW, Georget V, Rassinier P, Leader B, Verlhac M-H (2008). Spindle positioning in mouse oocytes relies on a dynamic meshwork of actin filaments. Curr Biol 18, 1514–1519.

Chang C-W, Nashchekin D, Wheatley L, Irion U, Dahlgaard K, Montague TG, Hall J, Johnston DS (2011). Anterior-posterior axis specification in *Drosophila* oocytes: identification of novel bicoid and oskar mRNA localization factors. Genetics 188, 883–896.

Chen CK, Sawaya MR, Phillips ML, Reisler E, Quinlan ME (2012). Multiple forms of Spire-actin complexes and their functional consequences. J Biol Chem 287, 10684–10692.

Chesarone M, Gould CJ, Moseley JB, Goode BL (2009). Displacement of formins from growing barbed ends by bud14 is critical for actin cable architecture and function. Dev Cell 16, 292–302.

Chhabra ES, Higgs HN (2006). INF2 Is a WASP homology 2 motif-containing formin that severs actin filaments and accelerates both polymerization and depolymerization. J Biol Chem 281, 26754–26767.

Chhabra ES, Ramabhadran V, Gerber SA, Higgs HN (2009). INF2 is an endoplasmic reticulum-associated formin protein. J Cell Sci 122, 1430–1440.

Dahlgaard K, Raposo AASF, Niccoli T, Johnston DS (2007). Capu and Spire assemble a cytoplasmic actin mesh that maintains microtubule organization in the *Drosophila* oocyte. Dev Cell 13, 539–553.

Emmons S, Phan H, Calley J, Chen W, James B, Manseau L (1995). Cappuccino, a *Drosophila* maternal effect gene required for polarity of the egg and embryo, is related to the vertebrate limb deformity locus. Genes Dev 9, 2482–2494.

Goode BL, Eck MJ (2007). Mechanism and function of formins in the control of actin assembly. Annu Rev Biochem 76, 593–627.

Gorelik R, Yang C, Kameswaran V, Dominguez R, Svitkina T (2011). Mechanisms of plasma membrane targeting of formin mDia2 through its amino terminal domains. Mol Biol Cell 22, 189–201.

Gould CJ, Maiti S, Michelot A, Graziano BR, Blanchoin L, Goode BL (2011). The formin DAD domain plays dual roles in autoinhibition and actin nucleation. Curr Biol 21, 384–390.

Hansen SD, Mullins RD (2010). VASP is a processive actin polymerase that requires monomeric actin for barbed end association. J Cell Biol 191, 571–584.

Heimsath EG Jr, Higgs HN (2012). The C terminus of formin FMNL3 accelerates actin polymerization and contains a WH2 domain-like sequence that binds both monomers and filament barbed ends. J Biol Chem 287, 3087–3098.

Higashida C, Miyoshi T, Fujita A, Oceguera-Yanez F, Monypenny J, Andou Y, Narumiya S, Watanabe N (2004). Actin polymerization-driven molecular movement of mDia1 in living cells. Science 303, 2007–2010.

Higgs HN, Peterson KJ (2005). Phylogenetic analysis of the formin homology 2 domain. Mol Biol Cell 16, 1–13.

Kobielak A, Pasolli HA, Fuchs E (2003). Mammalian formin-1 participates in adherens junctions and polymerization of linear actin cables. Nat Cell Biol 6, 21–30.

Kovar DR, Harris ES, Mahaffy R, Higgs HN, Pollard TD (2006). Control of the assembly of ATP- and ADP-actin by formins and profilin. Cell 124, 423–435.

Kovar DR, Kuhn JR, Tichy AL, Pollard TD (2003). The fission yeast cytokinesis formin Cdc12p is a barbed end actin filament capping protein gated by profilin. J Cell Biol 161, 875–887.

Kursula I, Heape AM, Kursula P (2005). Crystal structure of non-fused glutathione *S*-transferase from *Schistosoma japonicum* in complex with glutathione. Protein Pept Lett 12, 709–712.

Lammers M, Rose R, Scrima A, Wittinghofer A (2005). The regulation of mDia1 by autoinhibition and its release by Rho*GTP. EMBO J 24, 4176–4187.

Li F, Higgs HN (2003). The mouse formin mDia1 is a potent actin nucleation factor regulated by autoinhibition. Curr Biol 13, 1335–1340.

Li F, Higgs HN (2005). Dissecting requirements for auto-inhibition of actin nucleation by the formin, mDia1. J Biol Chem 280, 6986–6992.

Liu W, Sato A, Khadka D, Bharti R, Diaz H, Runnels LW, Habas R (2008). Mechanism of activation of the formin protein Daam1. Proc Natl Acad Sci USA 105, 210–215.

Lu J, Pollard TD (2001). Profilin binding to poly-L-proline and actin monomers along with ability to catalyze actin nucleotide exchange is required for viability of fission yeast. Mol Biol Cell 12, 1161–1175.

MacLean-Fletcher S, Pollard TD (1980). Identification of a factor in conventional muscle actin preparations which inhibits actin filament self-association. Biochem Biophys Res Commun 96, 18–27.

Maiti S, Michelot A, Gould C, Blanchoin L, Sokolova O, Goode BL (2012). Structure and activity of full-length formin mDia1. Cytoskeleton (Hoboken) 69, 393–405.

Manseau LJ, Schüpbach T (1989). Cappuccino and spire: two unique maternal-effect loci required for both the anteroposterior and dorsoventral patterns of the *Drosophila* embryo. Genes Dev 3, 1437–1452.

Neidt EM, Scott BJ, Kovar DR (2009). Formin differentially utilizes profilin isoforms to rapidly assemble actin filaments. J Biol Chem 284, 673–684.

Nezami A, Poy F, Toms A, Zheng W, Eck MJ (2010). Crystal structure of a complex between amino and carboxy terminal fragments of mDia1: insights into autoinhibition of diaphanous-related formins. PLoS One 5, e12992.

Nezami AG, Poy F, Eck MJ (2006). Structure of the autoinhibitory switch in formin mDia1. Structure 14, 257–263.

Otomo T, Tomchick DR, Otomo C, Machius M, Rosen MK (2010). Crystal structure of the formin mDia1 in autoinhibited conformation. PLoS One 5, e12896.
Otomo T, Tomchick DR, Otomo C, Panchal SC, Machius M, Rosen MK (2005). Structural basis of actin filament nucleation and processive capping by a formin homology 2 domain. Nature 433, 488–494.
Pastorino B, Rolland D, Peyrefitte CN, Wurtz N, Almeras L, Bessaud M, Tolou HJ (2008). Improvement of the purification of Saint Louis encephalitis virus NS2B-NS3 recombinant protease expressed in *Escherichia coli*. J Chromatogr B Analyt Technol Biomed Life Sci 868, 58–63.
Paul AS, Paul A, Pollard TD, Pollard T (2008). The role of the FH1 domain and profilin in formin-mediated actin-filament elongation and nucleation. Curr Biol 18, 9–19.
Pechlivanis M, Samol A, Kerkhoff E (2009). Identification of a short Spir interaction sequence at the C-terminal end of formin subgroup proteins. J Biol Chem 284, 25324–25333.
Pfender S, Kuznetsov V, Pleiser S, Kerkhoff E, Schuh M (2011). Spire-type actin nucleators cooperate with formin-2 to drive asymmetric oocyte division. Curr Biol 21, 955–960.
Pollard TD (1986). Rate constants for the reactions of ATP- and ADP-actin with the ends of actin filaments. J Cell Biol 103, 2747–2754.
Pruyne D, Evangelista M, Yang C, Bi E, Zigmond S, Bretscher A, Boone C (2002). Role of formins in actin assembly: nucleation and barbed-end association. Science 297, 612–615.
Punta M *et al*. (2012). The Pfam protein families database. Nucleic Acids Res 40, D290–D301.
Quinlan ME, Hilgert S, Bedrossian A, Mullins RD, Kerkhoff E (2007). Regulatory interactions between two actin nucleators, Spire and Cappuccino. J Cell Biol 179, 117–128.
Ramalingam N, Zhao H, Breitsprecher D, Lappalainen P, Faix J, Schleicher M (2010). Phospholipids regulate localization and activity of mDia1 formin. Eur J Cell Biol 89, 723–732.
Rosales-Nieves AE, Johndrow JE, Keller LC, Magie CR, Pinto-Santini DM, Parkhurst SM (2006). Coordination of microtubule and microfilament dynamics by *Drosophila* Rho1, Spire and Cappuccino. Nat Cell Biol 8, 367–376.
Rose R, Weyand M, Lammers M, Ishizaki T, Ahmadian MR, Wittinghofer A (2005). Structural and mechanistic insights into the interaction between Rho and mammalian Dia. Nature 435, 513–518.
Schönichen A, Geyer M (2010). Fifteen formins for an actin filament: A molecular view on the regulation of human formins. Biochim Biophys Acta 1803, 152–163.
Schuh M, Ellenberg J (2008). A new model for asymmetric spindle positioning in mouse oocytes. Curr Biol 18, 1986–1992.
Schulte A, Stolp B, Schönichen AS, Pylypenko O, Rak A, Fackler OT, Geyer M (2008). The human formin FHOD1 contains a bipartite structure of FH3 and GTPase-binding domains required for activation. Cell 16, 1313–1323.
Seth A, Otomo C, Rosen MK (2006). Autoinhibition regulates cellular localization and actin assembly activity of the diaphanous-related formins FRLalpha and mDia1. J Cell Biol 174, 701–713.
Smith MB, Li H, Shen T, Huang X, Yusuf E, Vavylonis D (2010). Segmentation and tracking of cytoskeletal filaments using open active contours. Cytoskeleton 67, 693–705.
Sreerama N, Woody RW (1993). A self-consistent method for the analysis of protein secondary structure from circular dichroism. Anal Biochem 209, 32–44.
Tanaka T, Kato Y, Matsuda K, Hanyu-Nakamura K, Nakamura A (2011). *Drosophila* Mon2 couples Oskar-induced endocytosis with actin remodeling for cortical anchorage of the germ plasm. Development 138, 2523–2532.
Theurkauf W (1994). Premature microtubule-dependent cytoplasmic streaming in cappuccino and spire mutant oocytes. Science 265, 2093–2096.
Vaillant DC, Copeland SJ, Davis C, Thurston SF, Abdennur N, Copeland JW (2008). Interaction of the N- and C-terminal autoregulatory domains of FRL2 does not inhibit FRL2 activity. J Biol Chem 283, 33750–33762.
Vinson VK, Cruz EMDL, Higgs HN, Pollard TD (1998). Interactions of *Acanthamoeba* profilin with actin and nucleotides bound to actin. Biochemistry 37, 10871–10880.
Vizcarra CL, Kreutz B, Rodal AA, Toms AV, Lu J, Zheng W, Quinlan ME, Eck MJ (2011). Structure and function of the interacting domains of Spire and Fmn-family formins. Proc Natl Acad Sci USA 108, 11884–11889.
Watanabe N, Kato T, Fujita A, Ishizaki T, Narumiya S (1999). Cooperation between mDia1 and ROCK in Rho-induced actin reorganization. Nat Cell Biol 1, 136–143.
Zalevsky J, Grigorova I, Mullins RD (2001). Activation of the Arp2/3 complex by the *Listeria* acta protein. Acta binds two actin monomers and three subunits of the Arp2/3 complex. J Biol Chem 276, 3468–3475.

Chapter 1 Appendix:

Supplementary Figures to:

Autoinhibition of the formin Cappuccino in the absence of canonical autoinhibitory domains

Batbileg Bor1, Christina L. Vizcarra2, Martin L. Phillips2 and Margot E. Quinlan2,3,*

1Molecular Biology Interdepartmental Program, University of California Los Angeles, Paul D. Boyer Hall, 611 Charles E. Young Drive East, Los Angeles, California 90095-1570, USA.

2Department of Chemistry and Biochemistry, University of California Los Angeles, 607 Charles E. Young Drive, Los Angeles, California 90095, USA.

3Molecular Biology Institute at UCLA, Paul D. Boyer Hall, 611 Charles E. Young Drive East, Box 951570, Los Angeles, California 90095-1570, USA.

*Correspondence should be addressed to M.E.Q. (margot@chem.ucla.edu).

Running title: Autoinhibition of Cappuccino

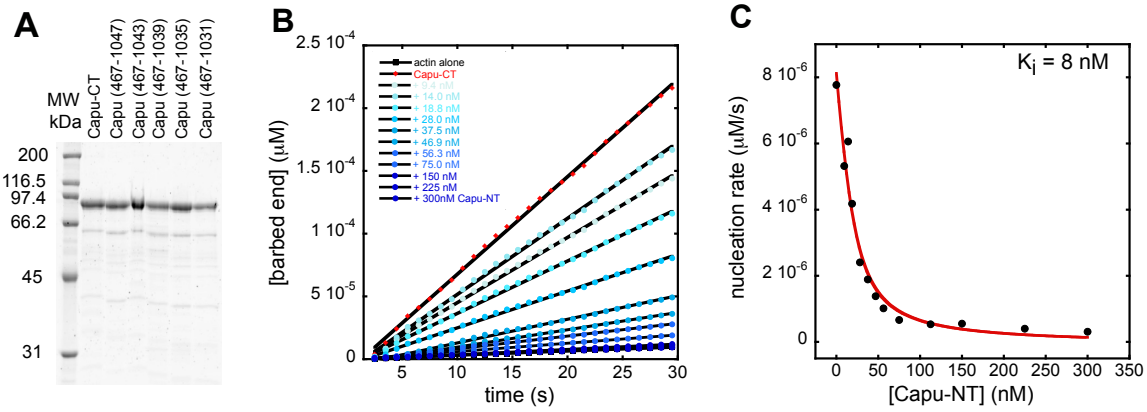

Figure S1. Capu-NT inhibits the nucleation activity of Capu-CT. (A) Purified Capu C-terminal truncations visualized on a Coomassie stained SDS-PAGE gel. (B) Analysis of Capu-CT's nucleation rate in the presence of Capu-NT. The concentration of barbed ends, calculated from the traces in Figure 1C, was plotted versus time for the initial 30 s, and the slopes of these lines were taken as the nucleation rate. (C) Nucleation rates are plotted as a function of Capu-NT concentration to determine the nucleation inhibition constant (K_i = 8 nM). This is very similar to the K_i calculated in Figure 1D.

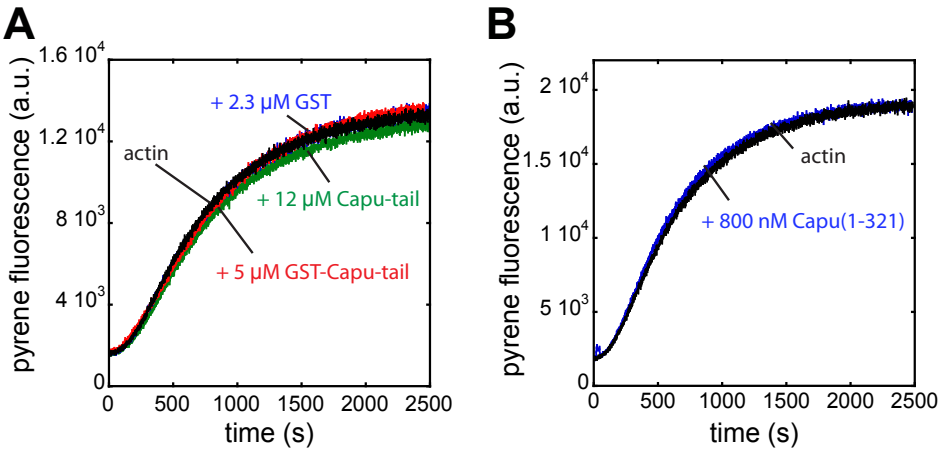

Figure S2. (A) Control experiments show that 12 µM Capu-tail (green), 2.3 µM GST (blue) or 5 µM GST-Capu-tail (red) had no effect on actin polymerization. (B) Control experiment shows that 800 nM Capu(1-321) had no effect on actin polymerization.

A

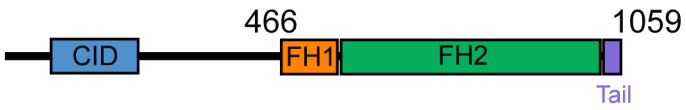

	50nM	100nM	150nM
Capu-NT	96%	---	---
50-466	76%	---	---
60-466	91%	---	---
80-466	74%	---	---
105-466	17%	52%	---
271-466	---	---	35%
318-466	---	---	11%
350-466	---	---	15%
380-466	---	---	13%
1-402	25%	---	---
1-350	45%	84%	---
1-321	80%	---	---
1-105	0%	17%	21%
25-185	23%	41%	52%
25-321	40%	---	---
50-321	0%	31%	---
60-321	---	---	61%
105-321	44%	---	---
80-350	0%	32%	47%
105-350	---	---	30%
197-350	---	---	7.2%
105-380	---	---	28%
197-380	---	---	13%

B

Pre-digest

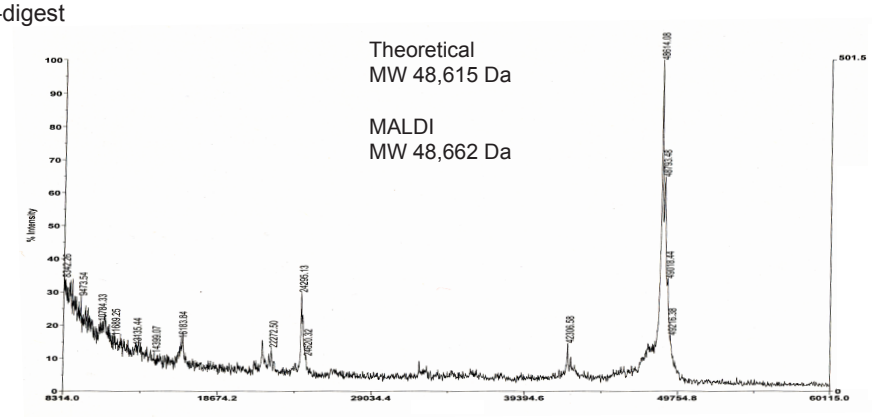

Post-digest

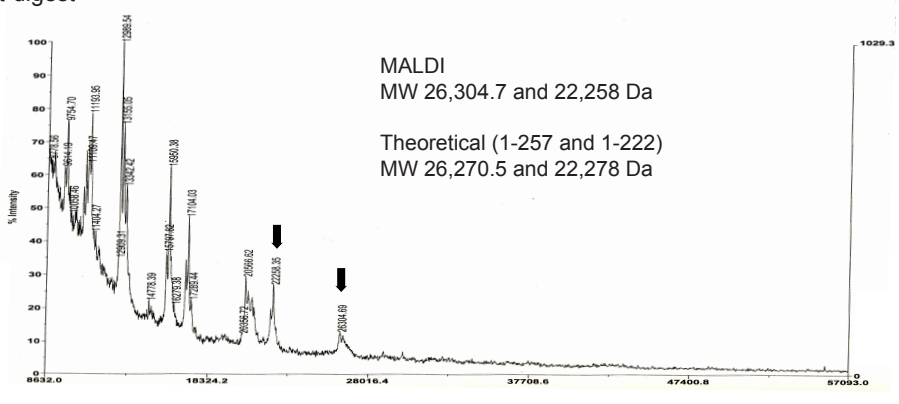

Figure S3. Mapping the CID domain. (A) Summary of the Capu-NT truncations and their Capu-CT inhibition activities. Three concentrations (50, 100, 150 nM) of various truncated Capu-NT constructs were added to the pyrene assay containing 20 nM Capu-CT. Inhibition activities were quantified by comparing the $t_{1/2}$ where Capu-CT alone is 0% and actin alone is 100% inhibited. Conditions not tested are indicated by '---'. Truncations from the N-terminus of Capu-NT quickly lost inhibition activity, suggesting the CID is near the beginning of Capu-NT. Truncations from the C-terminus of Capu-NT had varying effects. A few constructs break apparent trends. Notably Capu(50-466), Capu(1-402) and Capu(1-350). We propose that local structures are disrupted in these constructs causing their activity to be lower than expected. For this set of data, concentrations of all Capu-NT truncations were determined using a Bradford protein assay (Biorad). Concentrations for all other experiments described were determined as described in Methods. We reasoned that the comparison within this set of data is valid, although not directly comparable to the data in Figure 3A. (B) Mass spectra before and after tryptic digest. Pre- and post-digest samples of 3.2 μM Capu-NT were analyzed by MALDI. The pre-digested sample had one clear peak corresponding to Capu-NT at 48,662 Da (calculated MW is 48,614 Da). We also see a weaker peak at 24,295 Da, which is probably doubly charged Capu-NT. From the post-digest spectra, we were interested in the highest MW bands, which were two peaks at 26,305 and 22,258 Da (shown by arrows). N-terminal sequencing showed that the higher MW bands from the digest began at residue 1. Combining this information and the expected trypsin cut sites present in Capu-NT, we predicted that the highest band was Capu(1-257) (MW = 26,270 Da) or Capu(1-222) (MW = 22,278 Da).

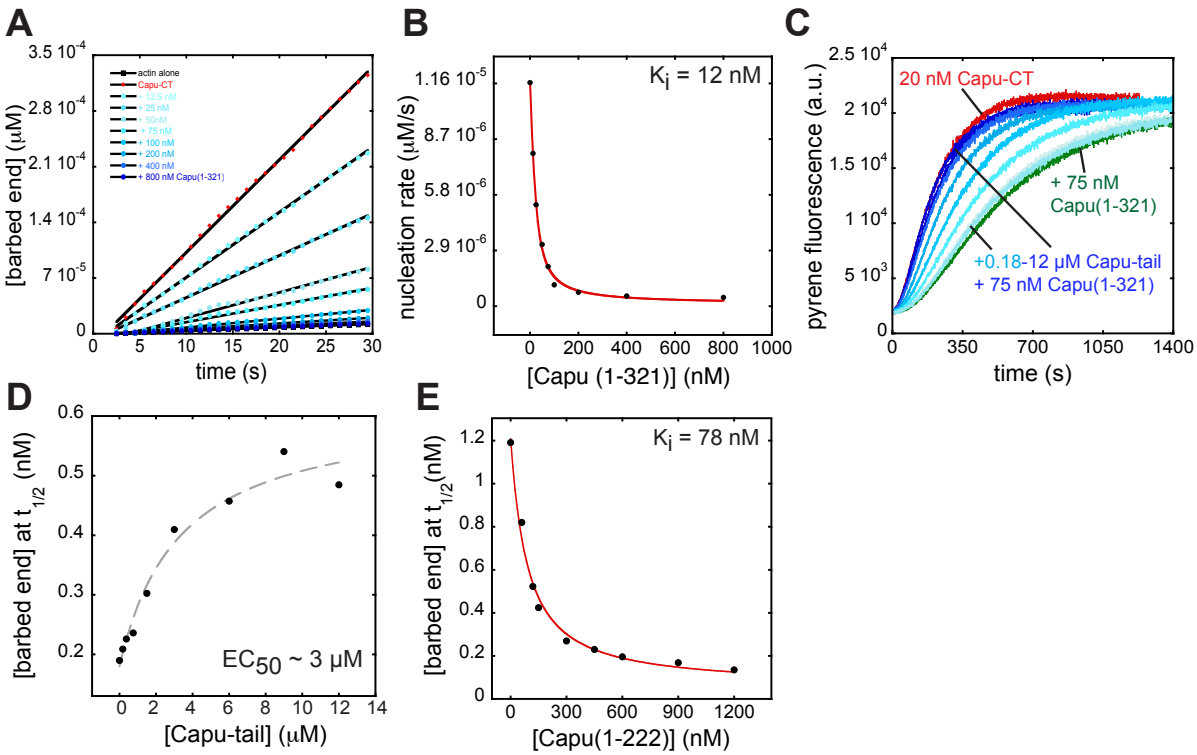

Figure S4. Analysis of the inhibitory activity of Capu(1-321) and Capu(1-222). (A-B) The data for the Capu(1-321) titration experiment in Figure 3B were fit as in Figure S1B–C. The analysis yielded a K_i of 12 nM based on nucleation rates. (C) Competition experiment with Capu(1-321), Capu-tail, and Capu-CT. Similar to Figure 2B, 0.18-12 μM Capu-tail (shown with increasing shades of blue) were added into 20 nM Capu-CT (alone in red) and 75 nM Capu(1-321) (alone in green). (D) Analysis of data from (C) was carried out as described in Figure 2C, showing EC_{50} ~3 μM. (E) The K_i of Capu(1-222) was determined as in Figure 1D, yielding a K_i of 78 nM. This is an overestimate of the affinity due to weak inhibition of actin polymerization by Capu(1-222).

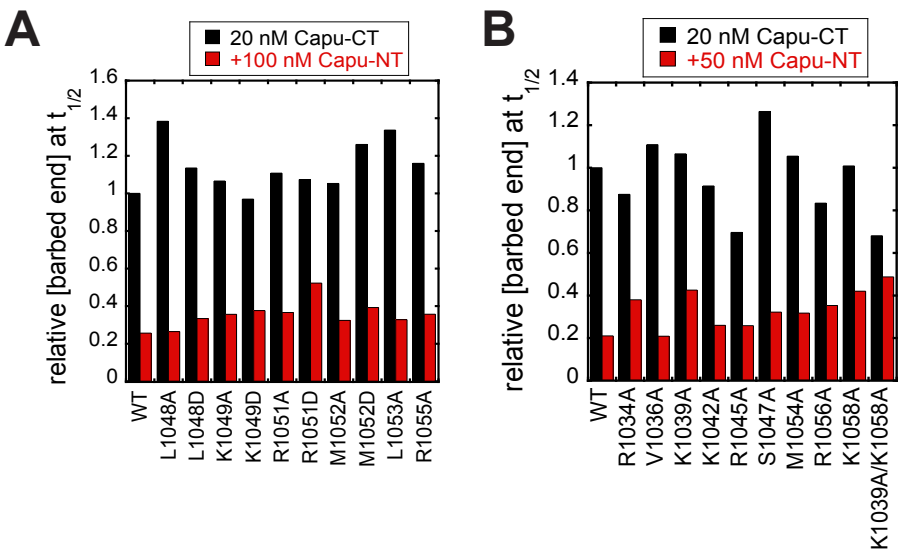

Figure S5. Mutational analysis of the Capu-CT/Capu-NT interaction. (A and B) Various mutations in the C-terminus of Capu-CT were tested for their effect on inhibition by Capu-NT. The two bar graphs show the summary of four experiments from four separate days. To compare the potency of Capu-NT inhibition from different days, wild type Capu-CT barbed end production was adjusted to an arbitrary value of 1, and the other traces were adjusted relative to the wild type data on the day they were measured. Black bars are wild type or mutant Capu-CT alone and red bars are with the indicated amount of Capu-NT.

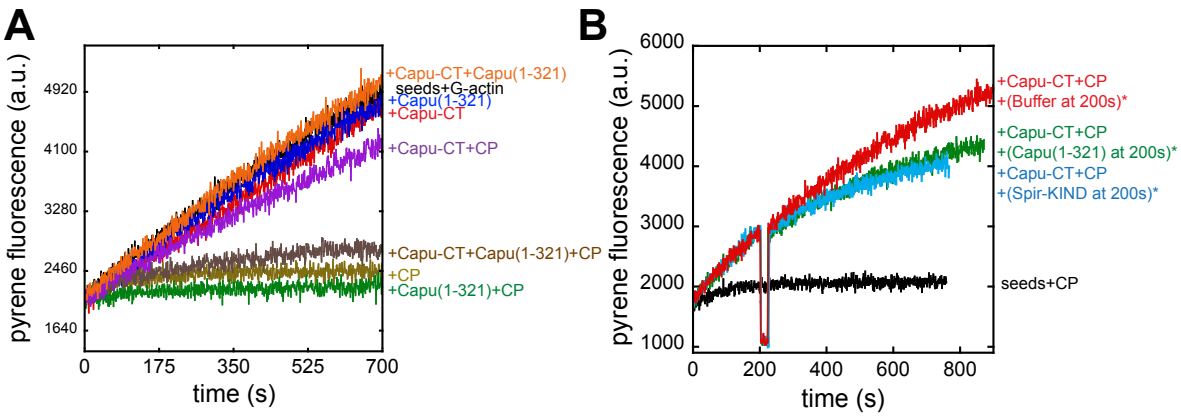

Figure S6. The effect of Capu(1-321) on processive elongation. (A) Example of pyrene fluorescence traces for each data set shown in Figure 5C. Data points between 200-700 s were fit with a line to obtain an elongation rate. (B) Essentially the same experiment as in (A) was carried out except that 2 μM Capu(1-321), 2 μM Spir-KIND or buffer were added 200 s after elongation was initiated (*). Adding a buffer control mid-assay had minimal effect on the barbed end protection by Capu-CT, but addition of either Capu(1-321) or Spir-KIND slowed elongation.

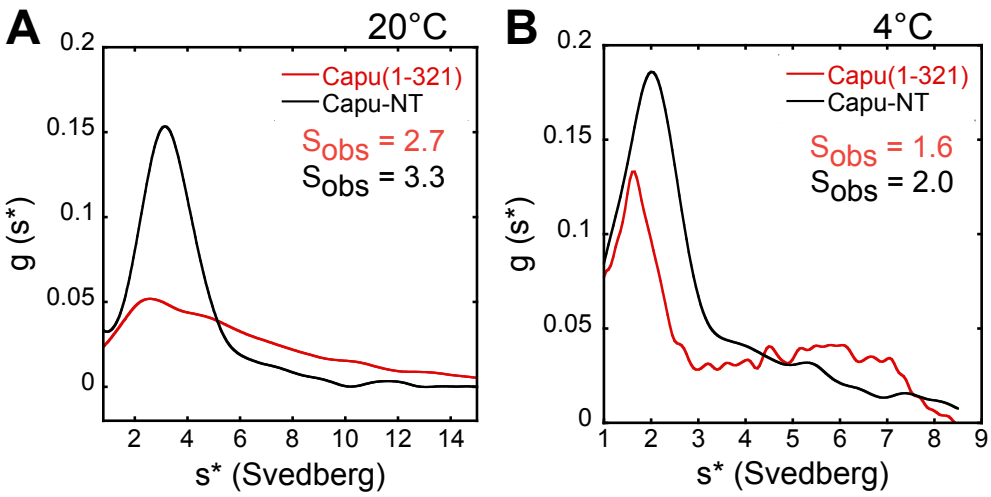

Figure S7. Capu-NT is an elongated dimer. (A) Velocity sedimentation at 20°C showed a single peak that corresponds to a sedimentation coefficient of 3.3 S for Capu-NT, indicating one dominant form of Capu-NT. The Capu(1-321) peak (2.7 S) had multiple faster sedimenting shoulders. SDS-PAGE analysis of the samples before and after centrifugation showed that Capu(1-321) degraded during the experiment (data not shown). (B) Because Capu(1-321) was not stable for the duration of the 20°C experiment, we repeated the experiment at 4°C. Both Capu-NT and Capu(1-321) had single peaks that corresponded to sedimentation coefficient of 3.3 S for Capu-NT and 2.6 S for Capu(1-321) after correction for the viscosity and density at 4°C (before correction, Capu-NT is 2.0 S and Capu(1-321) is 1.6 S), indicating one dominant form of Capu-NT or Capu(1-321). In both experiments, Capu-NT (2.4 μM) or Capu(1-321) (5 μM) were spun at 55,000 rpm for 3 hours.

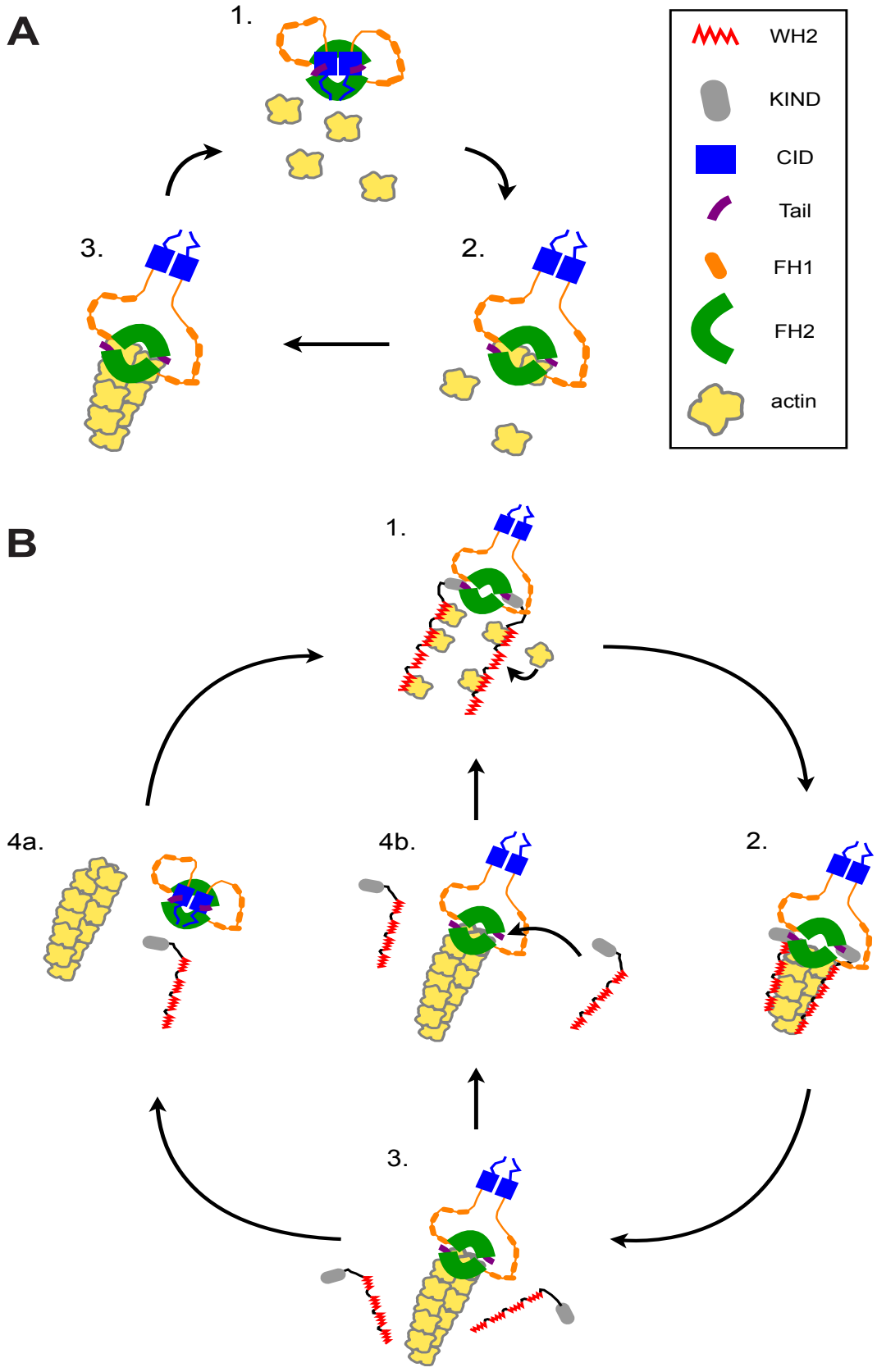
A
1.
2.
3.
WH2
KIND
CID
Tail
FH1
FH2
actin
B
1.
2.
3.
4a.
4b.

Figure S8. Models of Capu regulation. (A) In the absence of Spir, Capu is regulated by autoinhibition. In state 1, Capu is in its autoinhibited confirmation and does not nucleate or associate with barbed ends of filaments. In state 2, Capu is activated by some external signal and nucleates an actin filament. Once Capu nucleates actin filaments, it stays bound to the barbed end (state 3) until it dissociates either spontaneously or in response to an external cue. Once it dissociates, it could re-form the autoinhibited conformation (state 1) unless the autoinhibitory interaction is blocked by a regulatory protein that is bound to the N-terminus or by post-translational modification. (B) In the presence of Spir, there are several potential models of how actin filament assembly is regulated. We have illustrated two here. In state 1, Capu and Spir are bound to each other and recruit actin monomers to form a filament nucleus (state 2). Based on previous biochemical data, Spir and Capu do not form an elongation complex. Therefore, in order for the nascent filament to elongate with Capu-bound to the barbed end (state 3), their interaction must be broken, either by the filament or by an external cue. Eventually, Capu may dissociate from the barbed end spontaneously or as a result of another regulator that controls filament length (state 4a). This factor could be Spir (state 4b), acting as an elongation regulator similar to the Bud14/Bnr1 interaction in yeast (Chesarone et al., 2009). If Capu-CT dissociates from the barbed end without Spir binding, autoinhibition could keep Capu in an inactive form (state 4a) until Spir binds and re-forms the nucleation complex (state 1). Whether post-translational modifications or additional regulators control this cycle is currently unknown.

Chapter 2: Regulation of the formin Cappuccino during *Drosophila* oogenesis

Abstract

The *Drosophila* formin Cappuccino (Capu) is a key player in modulating the actin cytoskeleton during oocyte development. It creates an actin mesh-like structure that traverses the oocyte during mid-oogenesis to control the timing of fast cytoplasmic streaming during late-oogenesis. Normal cytoskeletal organization and cytoplasmic streaming is crucial for localization of polarity determinants such as *osk, grk, bcd* and *nanos* mRNAs. Capu mutants disrupt these events, leading to female sterility. Capu has been shown to be regulated by another nucleator, Spire, as well as by autoinhibition *in vitro*. Studies *in vivo* confirm that Spire modulates Capu's function in oocytes; however, how autoinhibition contributes is still unclear. To study the role of autoinhibition in flies, we expressed a Capu construct that is missing the Capu Inhibitory Domain, CapuΔN. Consistent with a gain of activity due to loss of autoinhibition, the actin mesh was denser in CapuΔN oocytes. Further, onset of cytoplasmic streaming was delayed and fertility levels decreased. We also observed fused dorsal appendages and disrupted abdominal segmentation in eggs and larvae, suggesting that polarity was disrupted. Consistent with this hypothesis, localization of *osk* mRNA in early stages, and *bcd* and *nanos* in late stages, were disrupted in CapuΔN-expressing oocytes. Finally, further evidence that these phenotypes were due to a loss of autoinhibition comes from co-expression of the N-terminal half of Capu with CapuΔN, which suppressed the defects in actin, cytoplasmic streaming and fertility. From these results, we conclude that Capu can be autoregulated during *Drosophila* oocyte development.

Introduction

Cappuccino (Capu) was originally identified in a screen for maternal-effect genes important for pattern formation. Mutations in *capu* disrupt both anteroposterior (AP) and dorsoventral (DV) axis formation of the *Drosophila* embryo, resulting in female sterility (Manseau and Schüpbach, 1989). The original study of *capu* led to the hypothesis that this gene, along with a second gene, *spire*, contributed to both major body axes by localizing and/or stabilizing other patterning factors by regulating the cytoskeleton (Emmons et al., 1995).

Detailed biochemical and genetic studies on Capu support this hypothesis and shed light on how Capu regulates polarity. Capu is a member of the formin family of actin nucleators. As such, it has well-conserved formin homology 1 and 2 (FH1 and FH2) domains in its C-terminal half (Higgs and Peterson, 2005). FH2 domains are crucial for actin filament nucleation and remains associated with the barbed ends of growing filaments to control elongation (Higashida et al., 2004; Otomo et al., 2005; Pruyne et al., 2002). FH1 domains bind to profilin-actin to facilitate fast delivery of actin monomers to the FH2 bound barbed ends (Paul et al., 2008). Consistent with Capu's actin polymerization activity, recently, Capu was linked to two actin structures in *Drosophila* oocytes: an isotropic mesh that traverses the oocyte and a network of long filaments extending from the posterior cortex of the oocyte (Chang et al., 2011; Dahlgaard et al., 2007; Tanaka et al., 2011). The long network of actin filaments is important for anchoring posterior polarity determinants (Tanaka et al., 2011). In *capu* mutants, these posterior actin filaments are missing. The former structure is present throughout mid-oogenesis (stage 5-10), and disappears during stage 10B. In *capu* mutants the mesh is absent (Dahlgaard et al., 2007).

A dramatic change in fluid dynamics coincides with disappearance of the actin mesh at stage 10B. At early stages, the fluid within the oocyte flows in a slow, uncoordinated manner. After stage 10B, this fluid flow is ~15 times faster and coordinated (Gutzeit and Koppa, 1982; Serbus et al., 2005). Cytoplasmic streaming requires both microtubules and kinesin heavy chain (Gutzeit, 1986; Palacios and St Johnston, 2002; Serbus et al., 2005). During stage 10B,

microtubules reorganize from a biased random anterior-posterior polarity to parallel bundles along the oocyte cortex (Parton et al., 2011; Theurkauf et al., 1992). This change is thought to depend on cytoplasmic streaming. *capu* mutants exhibit premature onset of cytoplasmic streaming (Theurkauf, 1994). Multiple studies link the Capu-dependent actin mesh to control of the timing of cytoplasmic streaming (Dahlgaard et al., 2007; Quinlan, 2013).

Establishment of the major body axes in *Drosophila* oocytes requires proper localization of polarity determinants such as *gurken* (*grk*), *oskar* (*osk*), *bicoid* (*bcd*) and *nanos* mRNAs (Frohnhöfer and Nüsslein-Volhard, 1986; Lehmann and Nüsslein-Volhard, 1986; Lehmann and Nüsslein-Volhard, 1991; Schüpbach, 1987; Wang and Lehmann, 1991). Localization of these polarity factors is largely dependent on microtubules and their associated motors, while both actin and microtubules are required for anchoring. Modes of transport and anchoring are specific to each polarity factor and the stage of development. For example, *osk*, which is enriched in the posterior after stage 7, is transported by kinesin along microtubules which are oriented with a slight bias towards the posterior at this time (Brendza et al., 2000; Ephrussi et al., 1991; Kim-Ha et al., 1991; Parton et al., 2011; Zimyanin et al., 2007). In contrast, the majority of *nanos* is localized to the posterior after stage 10 (Wang et al., 1994), when the microtubules have been swept in bundles towards the cortex of the oocyte (Theurkauf et al., 1992). It appears to be localized by a combination of advection due to cytoplasmic streaming and entrapment at the posterior, as opposed to active transport by a motor (Forrest and Gavis, 2003).

grk, *osk* and *nanos*, but not *bcd*, localizations are disrupted in *capu* mutants (Ephrussi et al., 1991; Manseau et al., 1996; Neuman-Silberberg and Schüpbach, 1993; Wang et al., 1994). Given that Capu is linked to two structures, the actin mesh and posterior extending filaments, we consider the roles of each in these phenotypes. The mesh is present during mid oogenesis, linking it to the first phase of localization. Premature cytoplasmic streaming in *capu* mutants could mechanically disrupt the mRNA localization, or subsequent reorganization of the

microtubule cytoskeleton may prevent the correct localization of mRNAs (Theurkauf, 1994). Given that these factors continue to accrue correctly after normal cytoplasmic streaming begins, it is not obvious why premature streaming is so detrimental. Perhaps establishment of "landing sites" is more delicate than later delivery of polarity factors. *Osk* at least has a positive feedback mechanism where the anchoring site at the posterior has to be established at early stages. Once established, more *osk* can be recruited during later stages (Sinsimer et al., 2011; Snee et al., 2007). How *capu* contributes to the second step of the mRNA localization is also unclear. It may be that Capu-dependent posterior filaments detected later in oogenesis are necessary for anchoring/entrapment during both early and late phases of mRNA transport.

To maintain proper timing of the actin mesh and cytoplasmic streaming, Capu needs to be regulated. Until recently, Spir was the sole candidate for modulating Capu's functions (Quinlan, 2013; Quinlan et al., 2007). However, we found that Capu can also be autoinhibited, like most other formins (Bor et al., 2012). We identified an N-terminal Capu Inhibitory Domain (CID; Capu1-222) that binds the C-terminal Capu-Tail domain to inhibit Capu's polymerization and elongation activities. This raises the question of how Capu is regulated during *Drosophila* oogenesis. Several lines of evidence support a role for Capu autoinhibition: Expression of Capu lacking the first 270 residues (green fluorescent protein [GFP]-CapuΔN) induced an actin mesh in the nurse cells and oocyte (Dahlgaard et al., 2007); A complimentary observation showed that Capu's N-terminal 100 amino acids exert a dominant-negative effect on Capu's oskar protein-anchoring activity, possibly by inhibiting formation of the actin filaments extending from the posterior cortex (Chang et al., 2011). Despite these observations, it is still unclear how Capu is regulated during oocyte development. We, therefore, further characterized Capu autoinhibition during *Drosophila* oogenesis by expressing the N-terminal half of Capu, which contains the CID domain (CapuNT), and truncated Capu that is lacking the CID domain (CapuΔN) in a wild type background. Overexpression of constitutively active Capu caused fertility defects. Detailed analysis showed that the oocytes had an increased actin mesh density

that persisited beyond stage 11 and inhibited cytoplasmic streaming. Furthermore, over production of the actin mesh and mis-timed cytoplasmic streaming resulted in diffuse localization of *osk* at early stages and decreased or no localization of *bcd* and *nanos* at late stages of oogenesis. By expressing Capu-NT, we were able to rescue the fertility, actin mesh, and cytoplasmic streaming phenotypes, suggesting that Capu is regulated by autoinhibition *in vivo*. Therefore, we show that not only is Capu autoinhibited in *Drosophila* oocytes, but properly regulated actin mesh and cytoplasmic streaming are critical for localization of polarity determinants and fertility.

Materials and Methods

Molecular Biology

GFP-Capu transgenes were generated by inserting a coding region corresponding to amino acids 1-466 or 1-103 between the BamHI and XbaI sites of pTIGER (Ferguson et al., 2012) with GFP inserted between the KpnI and SpeI sites. Primers were: forward, 5'-ctgttccaggggcccctggg- atccatggccttgcagctaggcaagaag-3'; reverse, 5'-tctactctagatcatttcgtcgaggattggccgca-3' (Capu1-466) and 5'-tctactctagatcaaacagttgattgcgtttccagcg-3' (Capu1-103). Untagged GFP protein was also inserted in the pTIGER vector.

Drosophila strains

We used the following transgenic fly lines: GFP-CapuFL and CapuFL (Quinlan, 2013), nos-GAL4-vp16 (#4937, Bloomington Stock Center, Van Doren et al., 1998), matα-GAL-vp16 (#7063, Bloomington Stock Center, Zimyanin et al., 2007) and hsp83-MCP-RFP (#9940, Bloomington Stock Center, Weil et al., 2006). GFP-CapuΔN was provided by Daniel St. Johnston (Dahlgaard et al., 2007). hsp83-MCP-mCherry, nos-$(ms2)_6$ and bcd-$(ms2)_6$ were provided by Elizabeth R. Gavis (Forrest and Gavis, 2003; Weil et al., 2006). grk-$(ms2)_{12}$ was provided by Trudi Schupbach (Jaramillo et al., 2008) and osk-$(ms2)_6$ was provided by Tze-Bin Chou (Lin et al., 2008). CantonS (CnS) was used as a wild type.

Fertility assays and abdominal segmentation

Fertility assays were performed as described previously (Quinlan, 2013). We crossed roughly 100 test females, expressing different Capu proteins in a wild type background, with 40 CantonS males. From these crosses, we quantified the number of hatched eggs as well as the number of eggs that contained fused dorsal appendages (Manseau and Schüpbach, 1989). Unhatched eggs were collected and prepared for cuticle analysis according to a standard protocol (Alexandre, 2008). Dark field images were taken using a Zeiss Imager Z.1 equipped with EC Plan-Neofluar 10x 0.3 M27 objective (Edward De Robertis lab, UCLA).

Actin mesh staining and measurement

The oocyte actin mesh was stained as described previously (Quinlan, 2013). In each experiment, ovaries from 3-4 WT and 6-8 GFP-Capu expressing flies were dissected and fixed together in 10% paraformaldehyde/PBS. Subsequently, we used 1 μM AlexaFluor647-phalloidin (Invitrogen) to stain actin so GFP could be used to distinguish WT from GFP-Capu expressing eggs. GFP and AlexaFluor647-phalloidin were excited with 488 and 635 nm lasers, respectively.

Single mid-section of oocytes were acquired with a Leica SPE I inverted confocal microscope equipped with an ACS APO 40x/1.15 oil CS immersion objective. Control and GFP-Capu expressing oocytes were imaged under identical conditions. Many times the cortical actin was saturated but we ensured that the cytoplasmic actin mesh was not saturated in our images. To quantify the density of the cytoplasmic actin mesh, the mean intensity of AlexaFluor647-phalloidin was measured in the cytoplasm of WT and GFP-Capu expressing oocytes using FIJI (Schindelin et al., 2012). To determine the change in actin mesh density, the mesh density of each GFP-Capu expressing oocyte was divided by the average density of 5 WT oocytes. This was performed independently for stage 9 and 11 oocytes.

Live imaging and cytoplasmic streaming

To trace the movement of the yolk granules (cytoplasmic streaming) or take the single mid-section images of mRNAs (red fluorescent protein [RFP] or mCherry), live oocytes were

dissected under halocarbon 700 oil and excited with 405 or 532 nm lasers, respectively, using a Leica SPE I inverted confocal microscope. Cytoplasmic streaming data were acquired and analyzed as described previously (Quinlan, 2013) with minor changes. Motion of autofluorescent of yolk granules was determined using particle image velocimetry (PIV) in movies collected every 5 seconds for 2.5 minutes. After the streaming velocities were determined, the speeds of all interrogation windows in a given movie were collated and the 95th percentile speed was determined to minimize the effect of potential outliers, including both yolk granules that were not moving and false reports of very fast moving objects. Sample maximum intensity projections were created in FIJI to show the relative movement of yolk granules (Schindelin et al., 2012).

Results

Constitutively active Capu decreases fertility

Previously, we demonstrated biochemically that Capu is autoinhibited (Bor et al., 2012). To test whether autoinhibition is important during Drosophila oogenesis, we expressed a constitutively active form of Capu, GFP-CapuΔN, in wild type background and assessed its affect on fertility (Figure 1A,B). We used two different germline specific drivers to express GFP-CapuΔN: the *nanos* promotor (nos-Gal4-VP16; nos) and the maternal α-tubulin promotor (matα-Gal4-VP16; matα). nos drives expression in the germarium, and again after stage 8 with low expression between stages 3-8 (Figure S1A, Hudson and Cooley, 2010). In contrast, matα is a strong driver throughout oogenesis (Figure S1B). For comparison, we also expressed full length Capu, GFP-CapuFL, and GFP alone. We measured fertility rates of these flies by crossing test females to wild type males, collecting eggs and counting the number that hatched within 24 hours. Only 48% of eggs hatched when laid by flies expressing GFP-CapuΔN driven by nos (nos:GFP-CapuΔN; Figure 1B). In contrast 89% of eggs hatched from flies expressing GFP-CapuFL (nos:GFP-CapuFL). When we used the matα driver, we saw stronger fertility defects for both GFP-CapuΔN (17%; matα:GFP-CapuΔN) and GFP-CapuFL (52%; matα:GFP-CapuFL)

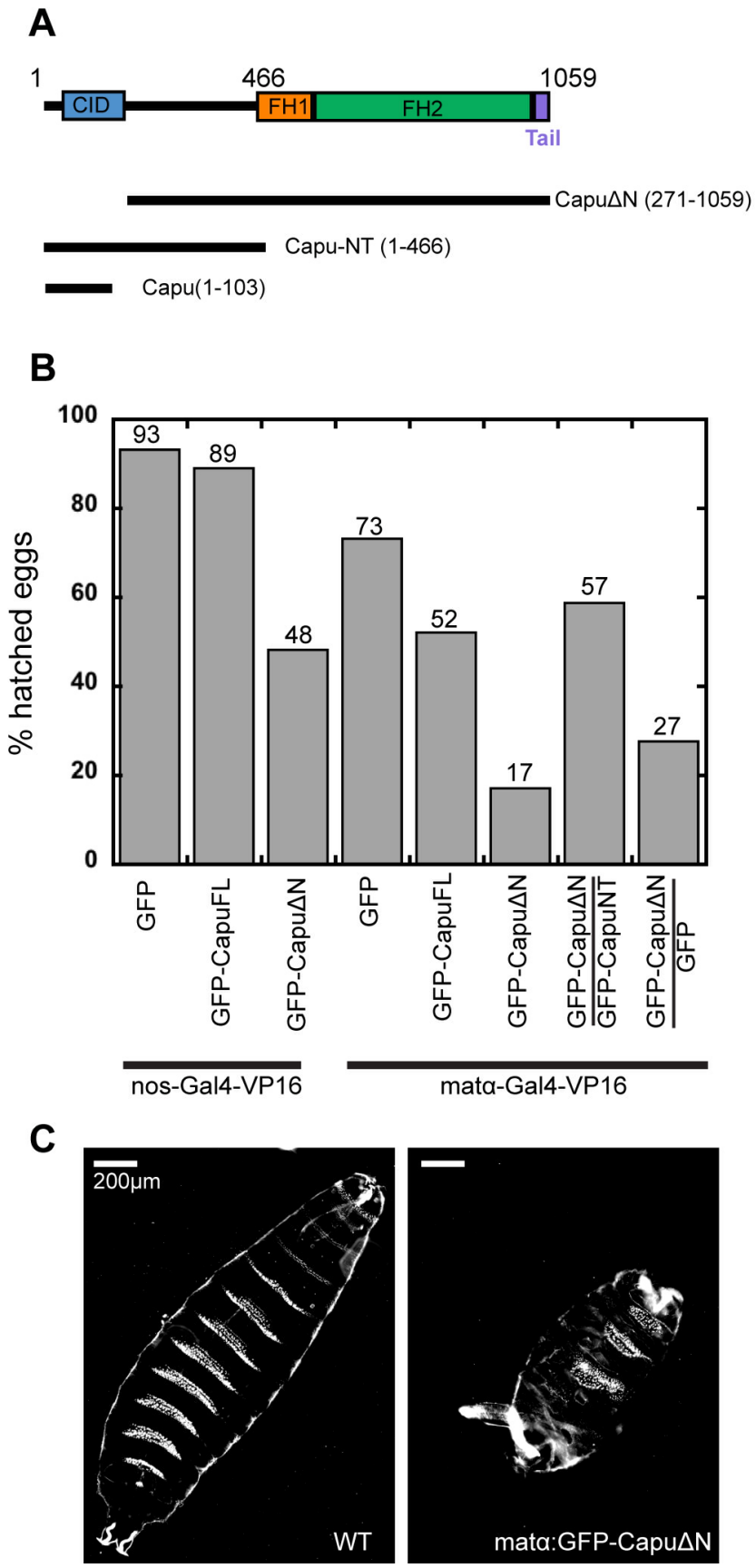
A
1
466
1059
CID
FH1
FH2
Tail
CapuΔN (271-1059)
Capu-NT (1-466)
Capu(1-103)
B
% hatched eggs
100
80
60
40
20
0
93
89
48
73
52
17
57
27
GFP
GFP-CapuFL
GFP-CapuΔN
GFP
GFP-CapuFL
GFP-CapuΔN
GFP-CapuΔN/GFP-CapuNT
GFP-CapuΔN/GFP
nos-Gal4-VP16
matα-Gal4-VP16
C
200μm
WT
matα:GFP-CapuΔN

Figure 1. **Constitutively active Capu decreases fertility.** (A) Domain organization of Capu: CID, Capu inhibitory domain (blue); FH1, formin homology 1 domain (orange); FH2, formin homolgy 2 domain (green); and Capu-Tail (violet). Black lines represent constructs used in this study. Specifically, we used transgenic flies containing UASp-GFP (green fluorescent protein)-tagged CapuFL (full-length), CapuΔN, Capu-NT and Capu(1-103). (B) Female fertility represented by % hatched eggs in flies expressing GFP, GFP-CapuFL, GFP-CapuΔN, GFP-Capu-NT or a combination of these proteins using either nanos-Gal4-VP16 (nos) or matα-Gal4-VP16 (matα) drivers. Each bar represents the average of three independent experiments with the total number of eggs shown in Table 1. (C) Cuticle preparation of first instar larvae derived from CantonS (wild type) or matα:GFP-CapuΔN females. Wild type larvae have 8 abdominal segments whereas GFP-CapuΔN expressing larvae have only 3 abdominal segments that have also lost their patterning.

(Figure 1B). To better understand why matα:GFP-CapuFL was so detrimental we tested the effect of expressing unlabeled CapuFL or GFP alone. Consistent with the difference in drivers, matα driven expression of GFP (matα:GFP) also had compromised fertility (73% hatched) as compared to the effect of nos driven expression (nos:GFP), which was negligible (93%) (Figure 1B and Table S1). We believe the loss in fertility is due to a combination of expressing large amounts of GFP as well as Gal4 since matα flies are generally sicker than wild type. CapuFL expression led to slightly increased fertility compared to GFP-CapuFL expression in both nos and matα flies (Table S1). This observation is consistent with the data from Dahlgard et al. (2007) indicating that the GFP tag increases Capu activity (Dahlgaard et al., 2007). By comparing data for GFP-CapuΔN and GFP-CapuFL (Figure 1B), we conclude that GFP-CapuΔN behaves like a constitutively active form of Capu and results in fertility defects.

Closer examination of the eggs laid in these experiments revealed that expression of GFP-CapuΔN caused polarity defects similar to those described for *capu* mutants. About 5% of matα:GFP-CapuΔN eggs had fused dorsal appendages (28/613) whereas matα:GFP-CapuFL had fewer such eggs (8/910). Fused dorsal appendages are a hallmark of defects in DV axis formation and appears in about 10% of strong *capu* alleles (Manseau and Schüpbach, 1989). In line with this idea, first instar larvae that did not hatch in matα:GFP-CapuΔN eggs had severely disrupted abdominal segmentation, which is a hallmark of defects in AP axis formation (Figure 1C). We draw two main conclusions from these experiments. First, an increase in Capu protein negatively impacts fertility and polarity. Secondly, truncating the CID domain (first 270 residues) enhances this negative effect. We believe that these negative effects are due to an increase in Capu activity. However, based on these observations alone, we cannot rule out the possibility that the truncation of first 270 residues affects fertility and polarity through another mechanism.

GFP-CapuΔN expression leads to increased actin mesh density

We studied the actin mesh in the oocyte as a measure of Capu activity. Spir and Capu cooperate to build this structure (Dahlgaard et al., 2007; Quinlan, 2013). In wild type oocytes,

the mesh is present until stage 10, and by stage 11, it disappears (Figure S2A). Therefore, we measured mesh density at stage 9, when the mesh is normally present, and stage 11, when the mesh is normally absent. Again, we used nos and matα drivers to express GFP, GFP-CapuFL, or GFP-CapuΔN and compared these oocytes to those from wild type flies. The actin mesh density increased at stage 9 of both nos:GFP-CapuFL (1.8-fold compared to control) and nos:GFP-CapuΔN (2.2-fold) oocytes (Figure 2B-D, Table 1). Stage 11 actin mesh also increased (Figure 2F-H) with a larger separation between nos:GFP-CapuFL (1.8-fold) and matα:GFP-CapuΔN (2.5-fold). Expression of GFP alone had no effect on the actin mesh, confirming that the change in density is due to Capu activity (Figure 2A,D,E,H, Table 1). The fact that nos:GFP-CapuFL causes an increase in actin mesh density at both stage 9 and 11 but has little affect on fertility suggests that the oocyte is resistant to an increase in mesh density to some extent. Increasing the mesh density beyond some threshold appears to negatively affect oocyte development because nos:GFP-CapuΔN had even higher mesh density both at stage 9 and 11 compared to nos:GFP-CapuFL, and this dense mesh corresponds to a dramatic decrease in fertility (Table 1).

Supporting the idea that an increase in actin mesh density negatively regulates fertility, matα-driven expression resulted in still denser average actin mesh. Stage 9 oocytes were 2.3- (matα:GFP-CapuFL) and 2.9-fold (matα:GFP-CapuΔN) denser than controls (Figure 3B-C,K and Table 1) and stage 11 oocytes were 3.3 and 3.8-fold denser, respectively (Figure 3G-H,L and Table 1). We note that the average stage 11 actin mesh density was similar to control stage 9 actin mesh. We cannot distinguish whether the fertility defects are due to an increase in actin mesh density at stage 9 or the presence of actin mesh at stage 11, or both. Regardless, these results indicate that there is a link between fertility phenotypes and an increase in Capu activity. Furthermore, GFP-CapuΔN is more active than GFP-CapuFL, probably due to loss of autoinhibition.

When the actin mesh density was increased by matα:GFP-CapuΔN, we also observed

Table 1. Change in actin mesh, cytoplasmic streaming and egg fertility.

driver	fly genotypes	% Hatched[a]	Stage 9, average fold increase in actin mesh	Stage 11, average fold increase in actin mesh	Stage 11, average cytoplasmic streaming (μm/s)
nos	GFP	93 (n=450)	1.0	1.1	0.29
	GFP-CapuFL	89 (493)	1.8	1.8	0.29
	GFP-CapuΔN	48 (772)	2.2	2.5	0.15
matα	GFP	73 (799)	1.4	0.9	0.31
	GFP-CapuFL	52 (910)	2.3	3.3	0.11
	GFP-CapuΔN	17 (613)	2.9	3.8	0.04
matα	GFP-CapuΔN / GFP-CapuNT	55 (600)	2.6	2.8	0.19
	GFP-CapuΔN / GFP	25 (600)	2.8	3.6	0.09

[a] percent hatched eggs from at least 3 independent experiments. n is total number of eggs analyzed from the 3 independent experiments.

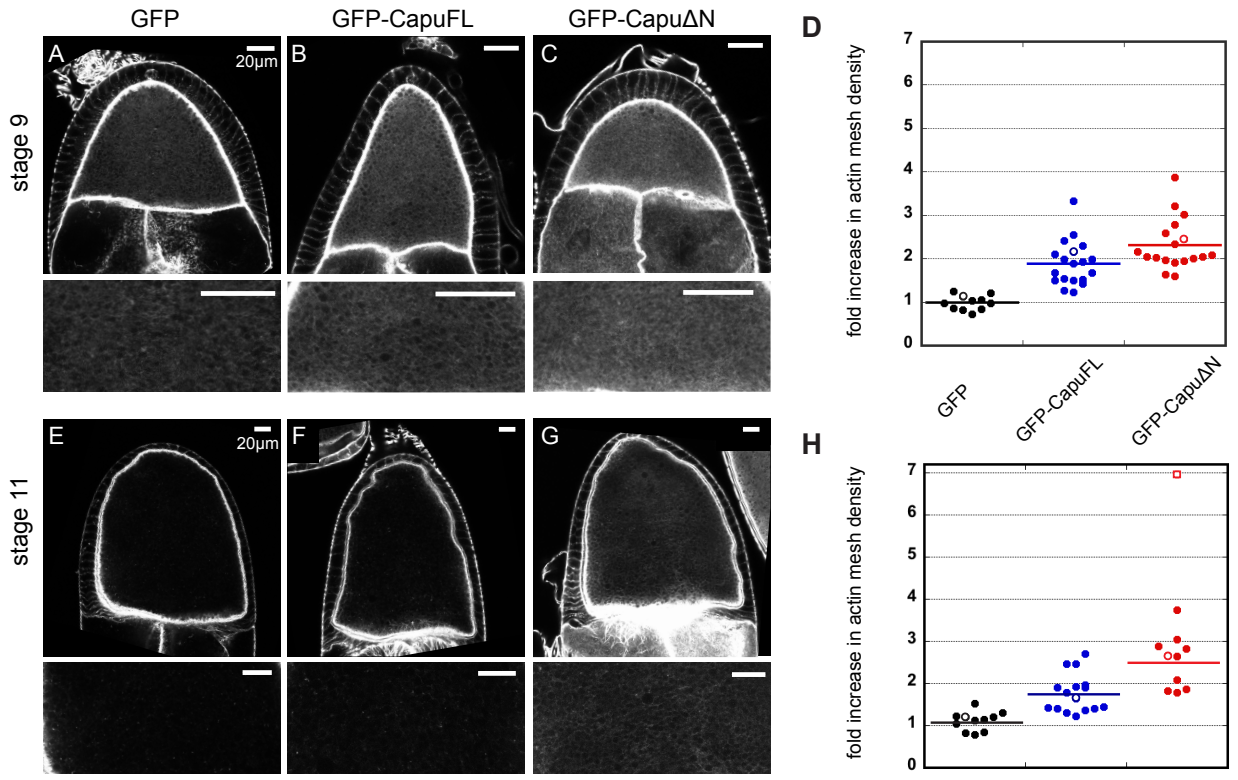

Figure 2. Increased actin mesh density caused by nos driven expression of Capu. Stage 9 (A, B, C) and 11 (E, F, G) egg chambers stained with 1μM AlexaFluor647-phalloidin to visualize the actin mesh density in nos:GFP, nos:GFP-CapuFL or nos:GFP-CapuΔN expressing eggs. The images are representative of more than 10 eggs and denoted by open circles in the graphs to the right (D and H). The lower images are 2-4x magnification of the actin mesh in the oocyte only. (D and H) Dot plots show oocyte actin mesh density in stage 9 (D) or 11 (H) oocytes relative to control oocytes. Controls were heterozygous for nos (**Figure S2A**, see methods). We analyzed more than 10 eggs for each experiment. The line represents the mean increase of actin mesh density. All egg chambers in this figure as well as in subsequent figures are oriented with the oocyte posterior facing up and anterior facing down. One outlier point in the nos:GFP-CapuΔN stage 11 oocytes is shown (open square in H) but was not included when calculating the average actin mesh density.

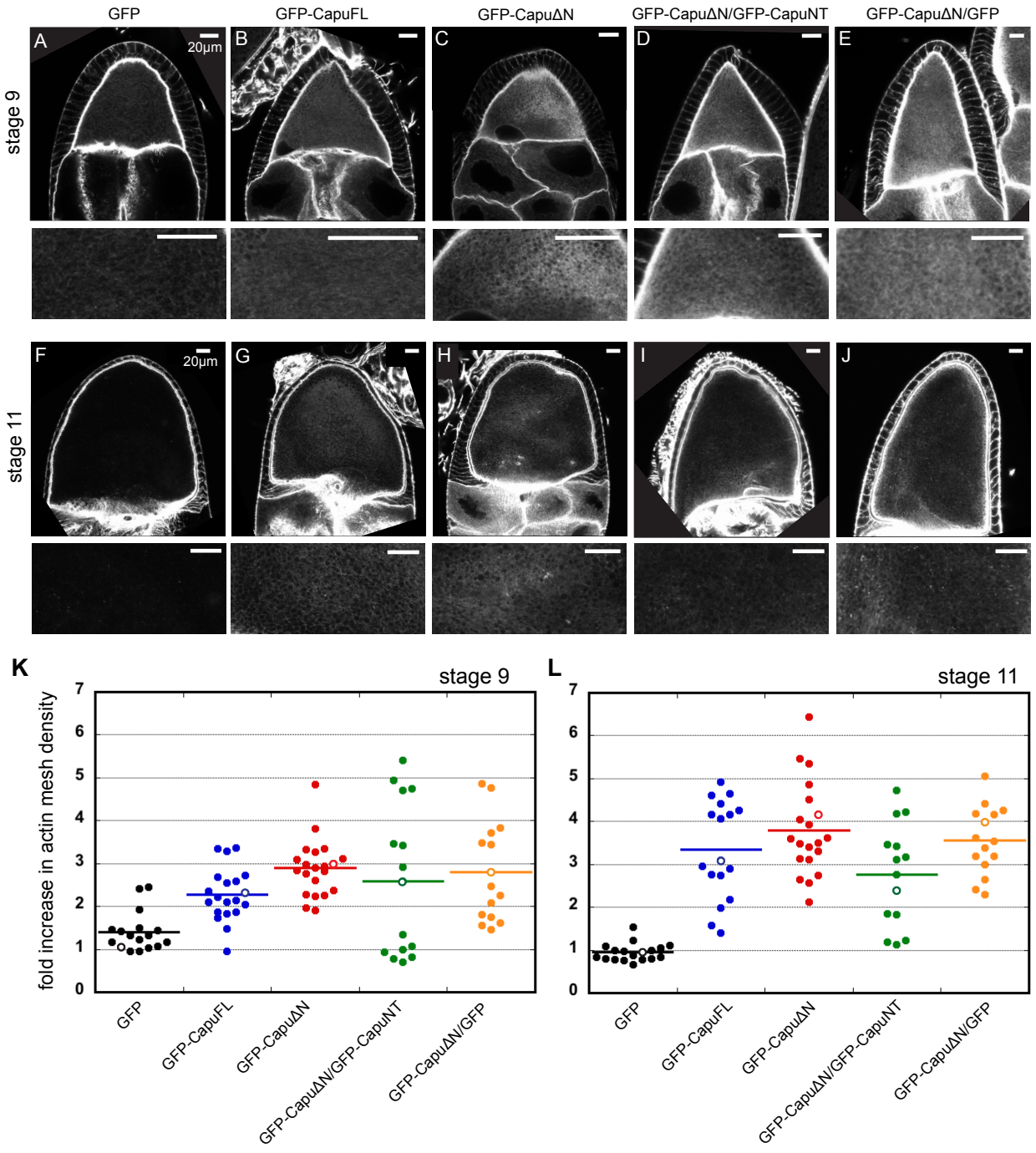

Figure 3. Increased actin mesh density caused by matα driven expression of Capu. Stage 9 (A, B, C, D, E) and 11 (F, G, H, I, J) egg chambers stained with 1 μM AlexaFluor647-phalloidin. Oocytes expressing GFP, GFP-CapuFL, GFP-CapuΔN, GFP-Capu-NT or a combination of these proteins using the matα driver are compared. (K, L) The images were

analyzed as described for Figure 2. The representative images shown in A-J is indicated by the open circles in K and L.

other actin phenotypes. Similar to what was reported by Dahlgaard *et al*., stage 9 and 11 nursecells had actin mesh-like structures in the nurse cell cytoplasm (Figure 3C,H). Therefore, we asked whether Capu activity affected additional aspects of oocyte development. The oocyte nucleus translates to the anterior-dorsal corner at stage 6-7. An increase in the oocyte actin mesh did not disrupt this localization (Figure S2B,D), suggesting that the mesh dynamics are not altered despite the increase in Capu's activity. We observed no change in border cell migration; border cells were found at the anterior of oocytes by stage 9 (Figure S2B,C). Nurse cell dumping relies on an actomyosin contraction. While an ectopic actin mesh in the nurse cells could disrupt this process by a number of mechanisms, dumping was apparently normal in GFP-CapuΔN and GFP-CapuFL flies. However, because fast streaming was prevented by the persistent actin mesh, we often saw that the oocyte content does not mix with the nurse cell content, forming two layers of cytoplasm as reported for expression of GFP-SpirD or loss of *khc* activity (Figure S2D; Dahlgaard et al., 2007; Serbus et al., 2005). Therefore, we hypothesize that the increase in oocyte actin mesh density is the major cause of infertility.

Increased actin mesh density prevents late stage cytoplasmic streaming

In wild type oocytes, fluid flows are relatively slow while the actin mesh is present. Coinciding with the disappearance of the mesh at stage 10B, cytoplasmic streaming begins and by stage 11, this streaming is fast and coordinated. The cytoplasmic flow is readily visualized by imaging the autofluoresent yolk granules. Using Particle Image Velocimetry (see methods for more details), we quantified the velocity of cytoplasmic streaming in oocytes expressing GFP, GFP-CapuFL or GFP-CapuΔN at stages 9 and 11. Interestingly, despite the increase in actin mesh density, whether we used the nos or matα driver, expressing these proteins had no measurable effect on the slow fluid flows of stage 9 oocytes (Figure 4A-D, I-K, S). In contrast, the rate of cytoplasmic streaming at stage 11 was dramatically affected (Figure 4). nos:GFP-CapuFL (0.29 ± 0.12 μm/s) resulted in oocytes with the same velocity on average as nos:GFP (0.29 ± 0.07 μm/s) but the range of velocities was much broader, as reflected in the standard

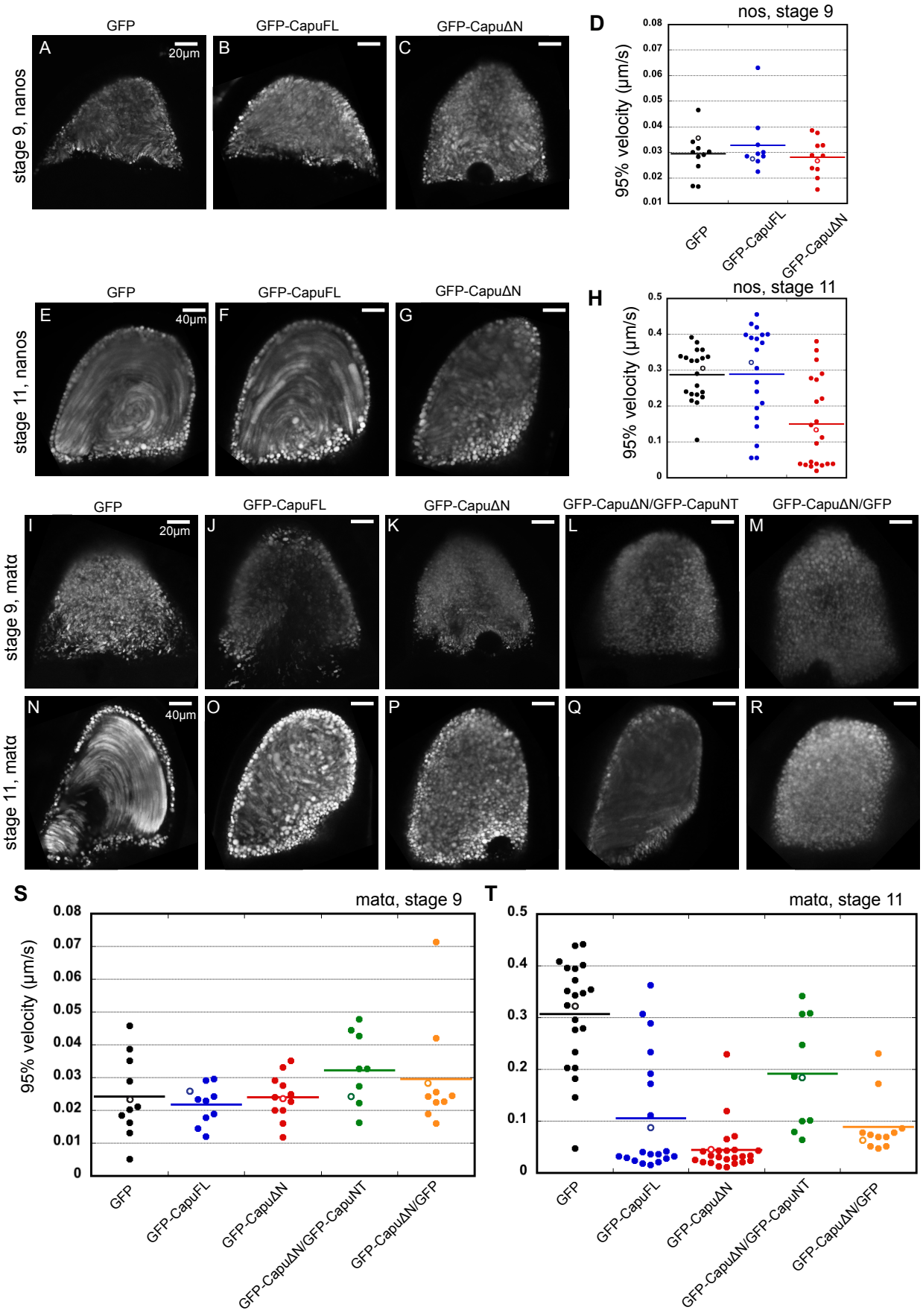
GFP
GFP-CapuFL
GFP-CapuΔN
stage 9, nanos
A
20μm
B
C
D
nos, stage 9
95% velocity (μm/s)
0.08
0.07
0.06
0.05
0.04
0.03
0.02
0.01
GFP
GFP-CapuFL
GFP-CapuΔN
stage 11, nanos
E
40μm
F
G
H
nos, stage 11
95% velocity (μm/s)
0.5
0.4
0.3
0.2
0.1
0
GFP
GFP-CapuFL
GFP-CapuΔN
GFP-CapuΔN/GFP-CapuNT
GFP-CapuΔN/GFP
stage 9, matα
I
20μm
J
K
L
M
stage 11, matα
N
40μm
O
P
Q
R
S
matα, stage 9
95% velocity (μm/s)
0.08
0.07
0.06
0.05
0.04
0.03
0.02
0.01
0
GFP
GFP-CapuFL
GFP-CapuΔN
GFP-CapuΔN/GFP-CapuNT
GFP-CapuΔN/GFP
T
matα, stage 11
0.5
0.4
0.3
0.2
0.1
0
GFP
GFP-CapuFL
GFP-CapuΔN
GFP-CapuΔN/GFP-CapuNT
GFP-CapuΔN/GFP

Figure 4. Increased actin mesh density prevents late stage cytoplasmic streaming. Maximum intensity projections of autofluorescent yolk granules over 2.5 minutes for stage 9 (A-C, I-M) and 11 (E-G, N-R) oocytes expressing proteins as indicated. Each image is representative (shown in open circles in D, H, S and T) of the 10 or more egg chambers examined. (D, H, S, T) Quantification of cytoplasmic streaming movement using Particle Image Velocimetry (see methods). Dot plots show the 95th percentile of velocities detected.

deviations (Figure 4E,F,H). Streaming was strongly inhibited in most of the nos:GFP-CapuΔN oocytes (0.15 μm/s) (Figure 4G,H). We do not report a standard deviation in this case because the data are not normally distributed. We attribute the breadth of velocities to variable expression levels. We see a similar breadth of mesh intensities, especially with matα-driven expression at stage 11 (Figure 3L). The effect of the matα driver on streaming is more severe, consistent with this being a stronger driver overall. The average streaming velocity was low for matα:GFP-CapuFL (0.11 μm/s) and reduced to a rate similar to stage 9 for matα:GFP-CapuΔN (0.04 μm/s) (Figure 4N-P, T). These data correlate with the increase in actin mesh described above. Thus, we believe that an increase in Capu activity, due to increased protein level and/or truncating the CID domain, results in decreased cytoplasmic streaming during late stages reflecting the increased actin mesh density. These results are consistent with the hypothesis that Capu and the actin mesh affect fertility and polarity by controlling the timing of cytoplasmic streaming.

Capu-NT localizes to the nurse cell cortex and inhibits GFP-CapuΔN

To test whether the effect of GFP-CapuΔN is due to loss of Capu autoinhibition, as opposed to another mechanism such as loss of a binding partner or proper localization of Capu, we expressed GFP-Capu-NT (Figure 1A). First we examined GFP-Capu-NT's localization in the egg chambers. Previous studies showed that GFP-CapuFL is enriched at the nurse cell cortex (Dahlgaard et al., 2007; Quinlan, 2013), whereas GFP-CapuΔN lacks this localization (Figure 5A-C,E-G; Dahlgaard, 2007). Therefore, we asked whether the N-terminal half of Capu is sufficient to localize Capu by comparing GFP-Capu-NT to GFP-CapuFL. Indeed, they appear similar in the egg chamber, enriched at the nurse cell cortex and diffuse in both the nurse cells and the oocyte (Figure 5D,H). Thus the loss of proper localization could contribute to misregulation of Capu and the phenotypes we observe. However, we note that the difference is in the nurse cells and no difference in localization is apparent in the oocyte.

We also asked whether we could inhibit endogenous Capu in trans. We tested two

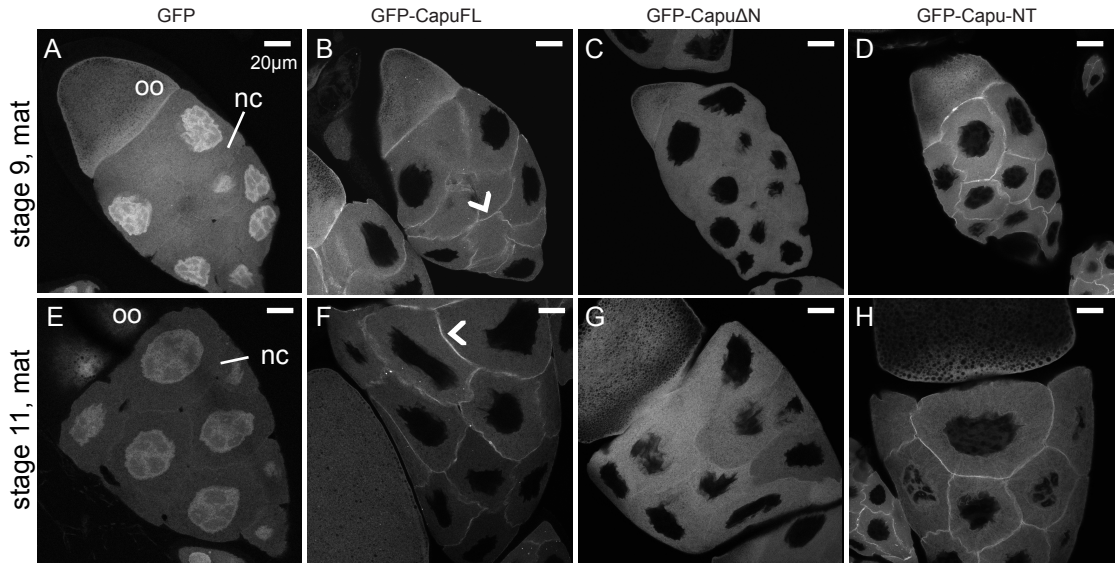

Figure 5. Capu's N-terminus localizes Capu. (B, F) Visualization of GFP in fixed oocytes shows that GFP-CapuFL localizes to the nurse cell cortex (chevrons) whereas GFP alone (A, E) localizes to the nucleus as well as diffusely in the nurse cells. (C, G) In contrast to full-length Capu, GFP-CapuΔN is not enriched at the nurse cell cortex. It is diffuse throughout these cells. (D, H) The N-terminal half of Capu (Capu-NT) is sufficient for localization to the nurse cell cortex. nc, nurse cells; oo; oocytes.

proteins, GFP-Capu1-103 (Chang et al., 2011) and GFP-Capu-NT, for their ability to inhibit Capu *in vivo*. To our surprise, neither had an effect on fertility (Table S1). The fact that these constructs asdfk do not act as dominant negatives suggests that Capu's regulation is more complicated than a single autoregulatory cycle. This is consistent with the fact that Spire and Capu-NT bind to the same site within Capu, the Capu-Tail (Bor et al., 2012; Vizcarra et al., 2011). Next, we coexpressed GFP-Capu-NT and GFP-CapuΔN in a wild type background. Fertility increased from 17% for matα:GFP-CapuΔN to 57% when coexpressing GFP-Capu-NT and GFP-CapuΔN using the matα driver (Figure 1B). To control for expression strength we also coexpressed GFP with GFP-CapuΔN. This pair resulted in only 25% fertility. Thus GFP-Capu-NT can inhibit GFP-CapuΔN in trans, consistent with autoinhibition being a bona fide mode of regulating Capu *in vivo*. We also examined mesh density and cytoplasmic streaming in flies coexpressing GFP-Capu-NT and GFP-CapuΔN. Actin mesh density decreased on average in both stage 9 (2.6-fold) and 11 (2.8-fold) egg chambers compare to when GFP-CapuΔN was expressed alone (see previous section) or in combination with GFP (stage 9, 2.8-fold; stage 11, 3.6-fold) (Figure 3D, E, I, J, K and L). While the range was broad at stage 9, about half of the flies had mesh densities similar to matα:GFP. The average mesh density did not recover to wild type levels at stage 11 either, consistent with fertility levels. As expected based on the change in actin mesh, cytoplasmic streaming velocity at stage 11 increased substantially for matα:GFP-Capu-ΔN/GFP-Capu-NT oocytes (0.19 μm/s) compared to matα:GFP-Capu-ΔN/GFP oocytes (0.09 μm/s) (Figure 4Q,R,T). Stage 9 slow streaming had no observable change (Figure 4L,M,S). Overall, about half of matα:GFP-Capu-ΔN/GFP-Capu-NT oocytes had mesh densities and streaming velocities close to wild type, consistent with the fertility rate we measured (57%). Therefore, we conclude that GFP-CapuΔN is more active than GFP-CapuFL because autoinhibition is absent.

Capu impacts mRNA localization during mid-oogenesis

We asked whether unregulated Capu activity disrupts localization of classic polarity factors. To visualize the localization of polarity determinants, we used previously developed live imaging techniques (Becalska and Gavis, 2009). We coexpressed two transgenes: mRNAs carrying 6-12 copies of the stem-loop binding site for bacteriophage MS2 coat protein (MCP) and MCP protein fused with red fluorescent protein (RFP) or mCherry. MCP binding to the MS2 stem-loop labels the mRNAs in the oocyte. Using this tool, we asked whether the increased density of actin mesh at stage 9 or prevention of cytoplasmic streaming at stage 11 due to the persistent actin mesh affected localization of polarity determinants such as *grk, osk, bcd* and *nanos*. We visualized these mRNAs while expressing GFP-CapuFL or GFP-CapuΔN using only the matα driver because it gives a more pronounced phenotype compared to the nos driver.

Early localization of polarity determinants is disrupted by increased Capu activity (Figure 6). Normally, *osk* localizes in a tight band (within 2-3 μm) at the posterior of the ooctye during stages 7-9 (Ephrussi et al., 1991). We observed diffuse posterior localization of *osk* mRNA (as far as 25 μm away from the posterior) at stage 9 of matα:GFP-CapuΔN and matα:GFP-CapuFL oocytes. By stage 10B, *osk* was more restricted to the posterior for matα:GFP-CapuFL but not matα:GFP-CapuΔN (Figure 6A-F). It is difficult to distinguish between transport and anchoring defects in this case. The increased actin mesh density could delay delivery of the *osk* particles. Indeed, the timing correlates with the level of Capu activity, and it follows mesh density given that the GFP-CapuFL is less severe. If anchoring is contributing, we do not think this is due to loss of posterior anchoring filaments because these oocytes contain endogeneous Capu. Instead the phenotype could reflect an aberrant excess of the anchoring structure. However, we were not able to test this hypothesis due to masking of fine actin structures by the dense and persistent mesh.

In wild type oocytes, *grk* mRNA localizes to the posterior region during stages 6-7 and then moves to the anterodorsal corner near the nucleus during stages 9-10 (Jarmillo et al., 2008

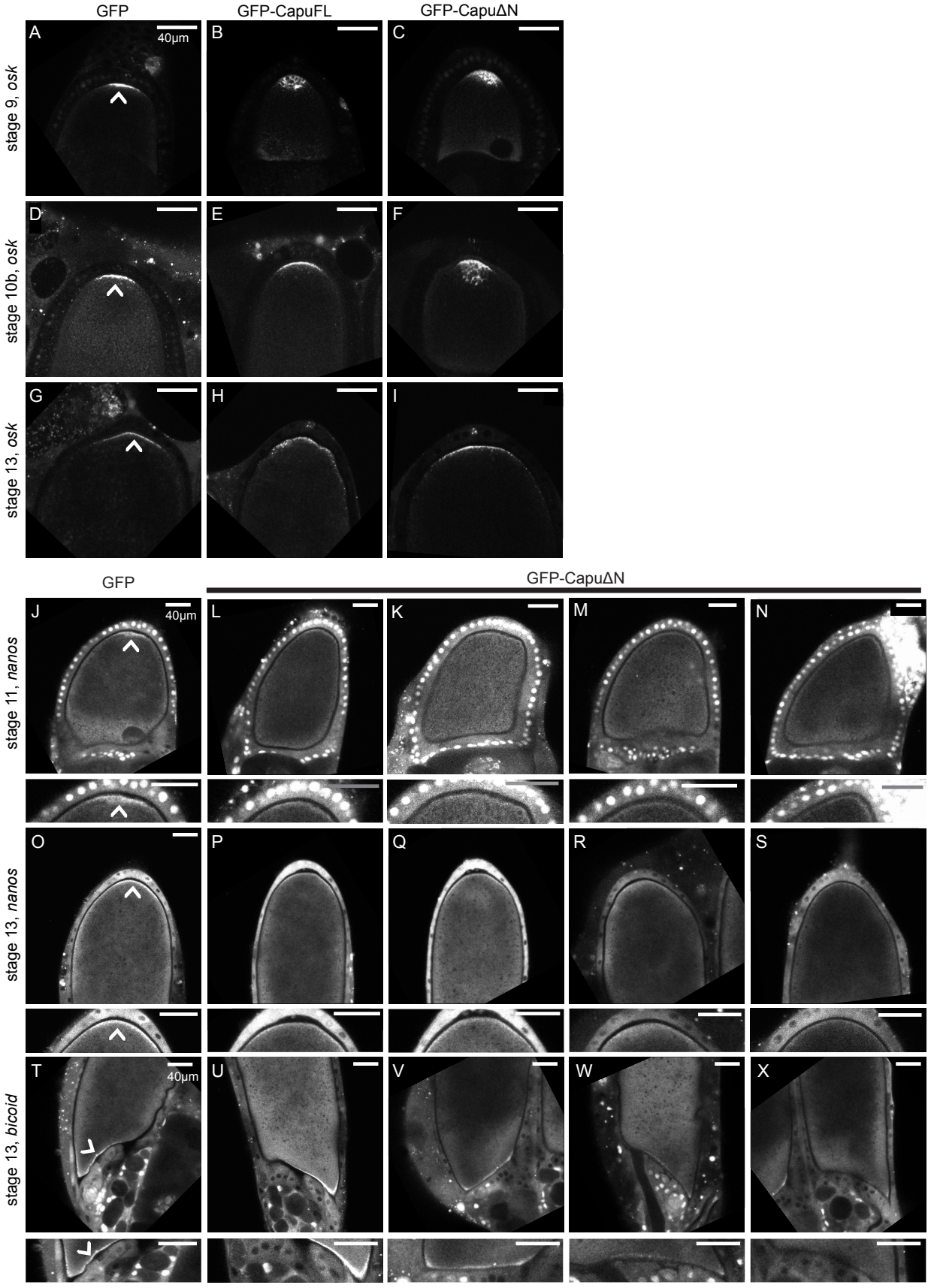
GFP
GFP-CapuFL
GFP-CapuΔN
A
40μm
B
C
stage 9, osk
D
E
F
stage 10b, osk
G
H
I
stage 13, osk
GFP
GFP-CapuΔN
J
40μm
L
K
M
N
stage 11, nanos
O
P
Q
R
S
stage 13, nanos
T
40μm
U
V
W
X
stage 13, bicoid

Figure 6. Capu impacts mRNA localization (A-I) Egg chambers at indicated stages expressing *osk*-$(ms2)_6$ mRNA and MCP-RFP in combination with matα:GFP, matα:GFP-CapuFL or matα:GFP-CapuΔN. *osk* accumulates at the posterior forming very narrow band at all stages in controls (A, D, G, chevrons). In contrast, *osk* has a diffuse posterior localization in stage 9 matα:GFP-CapuFL and matα:GFP-CapuΔN oocytes (B, C). By stage 10B localization is more restricted in matα:GFP-CapuFL but not matα:GFP-CapuΔN oocytes (E, F). By stage 13, *osk* is restricted to a tight band in the posterior; experimental flies are indistinguishable from control flies (G-I). (J-X) Egg chambers expressing MCP-mCherry and *nanos*-$(ms2)_{18}$ (J-S) or *bcd*-$(ms2)_6$ (T-X) in combination with either matα:GFP or matα:GFP-CapuΔN. The lower images are 5-7x magnifications of the posterior for *nanos* and anterior for *bcd*. *nanos* (in stage 11 and 13) and *bcd* (stage 13 only) localized to the posterior and anterior similar to wild type *osk* mRNA in GFP expressing oocytes (J, O, T, open arrows). Multiple images showing the high to low (from left to right) expression pattern of the *nanos* (L-N, P-S) or *bcd* (U-X) are shown for the matα:GFP-CapuΔN oocytes. Both MCP-RFP and MCP-mCherry are expressed with the hsp83 promoter whereas mRNAs are expressed only in the nurse cells. A nuclear localization sequence drives excess MCP-mCherry to the nucleus.

; Neuman-Silberberg and Schüpbach, 1993). When we examined *grk*-ms2/MCP-mCherry localization in matα:GFP-CapuΔN oocytes during stage 9, we found that most *grk* mRNA localized normally to the anterodorsal corner. However, 3 of 15 oocytes had either substantiallydecreased or undetectable levels of *grk* (Figure S3A). In contrast, *grk* was correctly localized in matα:GFP oocytes (12/12). Mislocalization of *grk* leads to disruption of DV axis formation and thereby results in fused dorsal appendages, which we observed in fertility assays (Figure 1; Neuman-Silberberg and Schüpbach, 1993; Schüpbach, 1987). The low number of dorsalized eggs we observed is consistent with the small fraction of oocytes with mislocalized *grk* mRNA. This low frequency of *grk* mis-localization suggests that perhaps only the highest density of actin mesh at early stages can inhibit the correct localization of *grk*. Even so, the observation is intriguing given that *grk* localization and anchoring are both thought to be solely microtubule dependent.

Both *bcd* and *nanos* localize to the anterior of the oocyte during stages 7-9 (Forrest and Gavis, 2003; Weil et al., 2006). Their localizations at stage 9 were indistinguishable from wild type in our experiments (Figure S3B, C). Thus despite the fact that fluid dynamics are seemingly unaffected by the denser actin mesh at stage 9 (Figure 4A-D, I-K, S), Capu activity has an impact on the early stage of polarity establishment. This affect is not uniform for all mRNAs as *bcd* and *nanos* localization were not affected whereas *osk* and *grk* were.

Capu impacts late phase mRNA localization

Next we examined late stage posterior localization of *nanos* and late stage accumulation of *osk* and *bcd*. Posterior localization of *osk* was normal at stage 13 for both matα:GFP-CapuFL and matα:GFP-CapuΔN oocytes, indicating that the second phase of *osk* localization is not affected by either the early stage disruption of *osk* localization or the persistence of actin mesh and inhibition of cytoplasmic streaming (Figure 6G-I). Late stage recovery of *osk* localization was surprising given that normally, late stage transport of *osk* is thought to be driven by cytoplasmic streaming (Glotzer et al., 1997; Sinsimer et al. 2011).

In comparison, *nanos* localization to the posterior was low at stage 11 (Figure 6J-N) and continued to be disrupted in stage 13 oocytes (Figure 6O-S). *nanos* localization depends on the correct prior localization of *osk* mRNA and formation of pole plasm (Ephrussi et al., 1991). Although stage 13 *osk* localized normally, we saw decreased *nanos* localization in all stage 11 ooctyes (7/ 7) and most stage 13 oocytes (13/19) expressing matα:GFP-CapuΔN (Figure 6J-S). In contrast matα:GFP had no effect on the *nanos* localization at either stage 11 (6/6) or stage 13 (10/10). We cannot determine whether the failed *nanos* localization is a secondary effect of the diffuse posterior localization of *osk,* which delayed pole plasm formation or a direct effect of inhibiting cytoplasmic streaming.

Previously, it was shown that *bcd* localization is normal in *capu* mutants (Manseau et al., 1996). Interestingly, *bcd* localization to the anterior at late stages of oogenesis was disrupted when Capu activity was increased. Nine of 17 matα:GFP-CapuΔN oocytes had no (Figure 6X) or decreased amounts (Figure 6U-W) of *bcd* at the oocyte anterior. In contrast, GFP expressing oocytes (10/10) had normal localization of *bcd* (Figure 6T). These results suggest that an increase in actin mesh density and prevention of cytoplasmic streaming selectively inhibits the second phase of *nanos* and *bcd* mRNA localization but, intriguingly, not that of *osk*. It follows that disruption of both *nanos* and *bcd* localization is responsible for the abdominal segmentation phenotype we observed in the fertility assay.

Discussion

The role of autoinhibition in regulating Capu

Capu builds an actin mesh in the oocyte during mid-oogenesis (stages 5-10a) in cooperation with Spir (Dahlgaard et al., 2007; Quinlan, 2013). The two proteins must interact but also spend time apart based on partial-overlapping localization and rescue experiments (Quinlan, 2013). Thus it seemed likely that Capu would be regulated by autoinhibition when not associated with Spir. This simple model led us to expect Capu-NT to act as a dominant negative. The fact that it did not behave so suggests that regulation of Capu is more

complicated. In fact, Capu-NT and Spir bind to the same region of Capu, Capu-tail, and with similar affinities (Bor et al., 2012; Vizcarra et al., 2011). It follows that competition between the two interactions, in the context of full length Capu, would lead to autoinhibition dominating. Because the Spir-Capu interaction is necessary, we expect that the oocyte has developed a means of blocking autoinhibition during oogenesis, presumably by reversibly modifying the Capu-Tail or the CID. In this case, even excess Capu-NT would not have a phenotype. Furthermore, it is possible that localization of GFP-Capu-NT confounds its ability to inhibit endogeneous function. GFP-Capu-NT was enriched at the nurse cell cortex, whereas GFP-CapuΔN was diffuse and GFP-CapuFL is found at the cortex and diffuse throughout the egg chamber. We do not know where Capu is most active but if it is not at the membrane, most of the GFP-Capu-NT would not be in the right place to act.

We reasoned that GFP-CapuΔN functions free of regulation by Spir after stage 10B because both endogenous Spir and Capu protein levels decrease dramatically at this time (Quinlan, 2013). Dahlgaard et al. found that, oocytes expressing exogenous Capu (full-length or CapuΔN) but lacking Spir have an actin mesh (Dahlgaard et al., 2007). This is consistent with ectopic expression of GFP-CapuFL and GFP-CapuΔN resulting in persistent actin mesh at stage 11. Demonstrating that an autoinhibitory interaction can take place in the ooctye, co-expression of GFP-Capu-NT with GFP-CapuΔN led to decreased activity of GFP-CapuΔN at stage 11. Furthermore, this result indicates that the defects due to GFP-CapuΔN expression are largely due to loss of autoinhibition as opposed to loss of another interaction or proper localization.

We conclude that Capu can be autoinhibited in the oocyte and that Capu lacking autoinhibition is deleterious to oocyte development. However, our results suggest that Capu autoinhibition is a secondary mechanism to regulation by Spir during mid-oogenesis and decreasing Capu protein level during late oogenesis. Perhaps, Capu functions independently of

Spir elsewhere in *Drosophila*, and Capu autoinhibition plays a more important role in that situation.

Oocyte actin mesh and its role in regulating cytoplasmic streaming

Our data are consistent with the idea that the actin mesh in the oocyte regulates cytoplasmic streaming. Previously, premature streaming had been observed in the absence of actin mesh (Dahlgaard et al., 2007; Theurkauf, 1994). Complementary to this, we show that a mesh that persists beyond stage 10B is sufficient to inhibit fast streaming. Two outstanding and possibly related questions about the mesh are: What determines mesh density? and How is the mesh removed? Dahlgaard et al. presented evidence that Capu activity level controls mesh density and our data are consistent. We observe that expression of constituitively active Capu increases actin mesh density at both stages 9 and 11 and increases the mesh more than CapuFL (Figures 2 and 3). We note that the mesh is less dense at stage 11 than 9 but we do not know what is limiting the actin mesh density at stage 11. This could reflect to the loss of endogenous Spir and Capu (Quinlan, 2013); limiting amounts of other (unknown) mesh components; the large size of the ooctye at this stage; or the onset of mechanisms to remove the mesh. This brings us to the issue of mesh removal. If the mesh is dynamic, loss of its nucleators (Spir and Capu) could be sufficient for mesh removal. An increase in net motor activity and onset of fast streaming (e.g. inhibition of dynein as described in Serbus et al., 2005) could accelerate the process but is not necessary, as Dahlgaard et al. (2007) showed that the mesh disappears in *khc* nulls.

Regardless of how the mesh density is normally regulated, it can exist at various levels of density and streaming velocity loosely correlates with that density (Figure 4). Under wild type conditions, cytoplasmic flows are approximately 30 nm/s during stage 9 and about 10 times faster during stage 11. We note that a two-fold increase in mesh density at stage 11 had minimal effect on streaming, suggesting that streaming can still take place up until some threshold of mesh density. Beyond that, the range of densities and range of streaming velocities

we observe suggest that there is a correlation between the two. In contrast, we were intrigued that a three-fold (on average) increase in mesh density had no apparent affect on slow streaming at stage 9. We do not know if mesh dynamics are altered by increased Capu activity but normal migration of the nucleus under these conditions suggests that the mesh is not overly stable. If mesh dynamics are on the order of the slow fluid flows at stage 9, this would explain why the increased density had no impact.

mRNA transport and localization

Sinsimer et al. (2011) hypothesized that late stage mRNA delivery amplifies the patterns generated earlier in oogenesis. In previous studies of late phase mRNA transport, cytoplasmic streaming was inhibited by depolymerizing the microtubules (Forrest and Gavis, 2003; Glotzer et al., 1997; Weil et al., 2006). We inhibited cytoplasmic streaming by increasing the actin mesh, leaving intact microtubules, enabling us to separate the effects of microtubules and cytoplasmic streaming in late stage transport. Advection based localization is thought to be responsible for *osk* and *nanos* localization to the posterior during late stages; cytoplasmic streaming provides the advective forces (Forrest and Gavis, 2003; Glotzer et al., 1997; Sinsimer et al., 2011; Snee et al., 2007). *bcd* also continues to be transported in the late phase but by a mechanism distinct from *osk* and *nanos*. It requires continual active transport mediated by dynein and intact microtubules nucleated from the anterior, and depends less on streaming (Weil et al., 2006). Thus we were surprised to find that *bcd* localization was low or undetectable in about 50% of the egg chambers we examined. Because transport and anchoring of *bcd* depend on microtubules, the role of streaming could not be separated by colcemid treatment in the original studies of late phase *bcd* localization. The simplest explanation of our results is that streaming plays a greater role than expected. Ooplasmic *bcd* mRNA is dynamic at the anterior. It needs to be continually loaded back on to the microtubules. Perhaps streaming is important for this step, facilitating microtubule/dynein capture events or returning *bcd* that diffused too far away to be captured. Alternatively, Weil et al. (2006) found that the specific subset of microtubules

necessary to anchor *bcd* depends on the actin cytoskeleton. Increased Capu activity could alter this arrangement, though we do not favor this explanation, in part because *bcd* localization in *capu* null mutants is normal (Manseau et al., 1996).

Localization of *osk* during early stages (7-10) of oocyte development depends on kinesin and a slightly biased organization of microtubules. Continued accumulation of *osk* to the posterior during late stages (11-14) was hypothesized to depend on nurse cell dumping and cytoplasmic streaming, with the latter acting as a transport mechanism (Glotzer et al., 1997; Sinsimer et al., 2011). We found that inhibiting cytoplasmic streaming by creating a persistent actin mesh does not block transport of *osk* during the second phase of accumulation. One could interpret this as evidence that streaming is not the transport mechanism. Instead we favor the idea that *osk* (and perhaps multiple mRNAs) are adapted to utilize more than one transport pathway (Sinsimer et al., 2011). In this case, it is likely that *osk* mRNA is still associated with kinesin during late stages and in the absence of cytoplasmic streaming, *osk* is able to use microtubules, which remain oriented by the persistent mesh as in earlier stages, to localize to the posterior. We note that earlier localization of *osk* (stage 9-10B) was not wild type in a manner that corresponded to Capu activity. Instead of a tight strip of posterior localization, we saw partially diffuse *osk* localization at the posterior. The altered localization could be due to defects in the transportation and/or anchoring. Perhaps increased Capu activity causes the posterior landing zone to expand, at least temporarily.

The strongest mRNA defect we observed was of late stage *nanos* localization to the posterior. At stage 11, none of the egg chambers had wild type levels of *nanos* and by stage 13, when *osk* was apparently normally localized, only 6 of 19 egg chambers had wild type levels of *nanos.* While the defect could be secondary, due to the delayed normal *osk* localization, we believe that inhibiting cytoplasmic streaming is the main cause for the defect we observed. Our data are consistent with those of Forrest and Gavis (2004), who showed that inhibition of cytoplasmic streaming by depolymerization of microtubules results in strongly reduced *nanos*

localization. These results together suggest that the main mechanism for *nanos* localization to the posterior is through the advective forces of cytoplasmic streaming.

Finally, we ask, why does fast cytoplasmic streaming occur? It is counterintuitive to have so much motion in a cell after establishing the localization patterns of crucial polarity factors. Two ideas, which are not mutually exclusive are: 1) streaming accomplishes long distance transport in a large cell (diameter of ~100 um) and 2) streaming is important for mixing the nurse cell cytoplasm with the ooplasm upon dumping. If streaming were the only means of moving mRNAs across the large oocyte, *osk* would not reach the posterior in our experiments or experiments in which the microtubules are depolymerized. However, *osk* appears to reach the posterior unimpeded by the lack of streaming, demonstrating that streaming is not necessary for long distance transport. Perhaps streaming is a more efficient mode of transport. The modeling and experiments required to test this hypothesis are important future aims. We do not consider *nanos* in this part of the discussion because we cannot distinguish with confidence whether the low posterior localization of *nanos* is due to lack of cytoplasmic streaming or a secondary effect of late *osk* delivery and subsequent poor entrapment of *nanos*. In considering the second idea, we note that lack of mixing between the nurse cell cytoplasm and ooplasm has been observed under conditions that block streaming, e.g. kinesin mutants and increased mesh (Dahlgaard et al., 2007; Palacios and St Johnston, 2002; Serbus et al., 2005; this study). Why would it be important to mix the cytoplasm if long distance transport were not the reason? Here we can only speculate. We know that gradients of nanos and bicoid are essential during embryogenesis. We propose that starting with a “clean slate” is a good way to ensure a uniform gradient. Streaming could create a mechanically and chemically clean slate.

Acknowledgements

We thank the Gavis, Schupbach and St. Johnston labs for generously sharing various fly lines used in our experiments. We thank the De Robertis’ lab for use of their dark field microscope and the Courey lab for reagents and help with methods. I thank my parents (Bor Batsuuri and

Altanchimeg Mishig) for bringing me to this world and to this country. This work was supported by several funding sources: Whitcome fellowship (UCLA; B.B.); National Institutes of Health (1R01GM096133-01), the Burroughs-Welcome Fund (Career Award in the Biomedical Sciences), and March of Dimes Foundation (#5-FY10-81) (M.E.Q.)

Competing interests statement

The authors declare no competing financial interests.

References

Alexandre, C. (2008). Cuticle preparation of Drosophila embryos and larvae. *Methods Mol. Biol. Clifton NJ* **420**, 197–205.

Becalska, A. N. and Gavis, E. R. (2009). Lighting up mRNA localization in Drosophila oogenesis. *Development* **136**, 2493–2503.

Bor, B., Vizcarra, C. L., Phillips, M. L. and Quinlan, M. E. (2012). Autoinhibition of the formin Cappuccino in the absence of canonical autoinhibitory domains. *Mol. Biol. Cell* **23**, 3801–3813.

Brendza, R. P., Serbus, L. R., Duffy, J. B. and Saxton, W. M. (2000). A function for kinesin I in the posterior transport of oskar mRNA and Staufen protein. *Science* **289**, 2120–2122.

Chang, C.-W., Nashchekin, D., Wheatley, L., Irion, U., Dahlgaard, K., Montague, T. G., Hall, J. and Johnston, D. S. (2011). Anterior-Posterior Axis Specification in Drosophila Oocytes: Identification of Novel bicoid and oskar mRNA Localization Factors. *Genetics* **188**, 883–896.

Dahlgaard, K., Raposo, A. A. S. F., Niccoli, T. and Johnston, D. S. (2007). Capu and Spire assemble a cytoplasmic actin mesh that maintains microtubule organization in the Drosophila oocyte. *Dev Cell* **13**, 539–53.

Emmons, S., Phan, H., Calley, J., Chen, W., James, B. and Manseau, L. (1995). Cappuccino, a Drosophila maternal effect gene required for polarity of the egg and embryo, is related to the vertebrate limb deformity locus. *Genes Dev* **9**, 2482–94.

Ephrussi, A., Dickinson, L. K. and Lehmann, R. (1991). Oskar organizes the germ plasm and directs localization of the posterior determinant nanos. *Cell* **66**, 37–50.

Ferguson, S. B., Blundon, M. A., Klovstad, M. S. and Schüpbach, T. (2012). Modulation of gurken translation by insulin and TOR signaling in Drosophila. *J. Cell Sci.* **125**, 1407–1419.

Forrest, K. M. and Gavis, E. R. (2003). Live imaging of endogenous RNA reveals a diffusion and entrapment mechanism for nanos mRNA localization in Drosophila. *Curr. Biol. CB* **13**, 1159–1168.

Frohnhöfer, H. G. and Nüsslein-Volhard, C. (1986). Organization of anterior pattern in the Drosophila embryo by the maternal gene bicoid. *Nature* **324**, 120–125.

Glotzer, J. B., Saffrich, R., Glotzer, M. and Ephrussi, A. (1997). Cytoplasmic flows localize injected oskar RNA in Drosophila oocytes. *Curr. Biol. CB* **7**, 326–337.

Gutzeit, H. (1986). The role of microtubules in the differentiation of ovarian follicles during vitellogenesis in Drosophila. **195**, 173–181.

Gutzeit, H. and Koppa, R. (1982). Time-lapse film analysis of cytoplasmic streaming during late oogenesis of Drosophila. *Development* **67**, 101–111.

Higashida, C., Miyoshi, T., Fujita, A., Oceguera-Yanez, F., Monypenny, J., Andou, Y., Narumiya, S. and Watanabe, N. (2004). Actin polymerization-driven molecular movement of mDia1 in living cells. *Science* **303**, 2007–2010.

Higgs, H. N. and Peterson, K. J. (2005). Phylogenetic analysis of the formin homology 2 domain. *Mol Biol Cell* **16**, 1–13.

Hudson, A. M. and Cooley, L. (2010). Drosophila Kelch functions with Cullin-3 to organize the ring canal actin cytoskeleton. *J. Cell Biol.* **188**, 29–37.

Jaramillo, A. M., Weil, T. T., Goodhouse, J., Gavis, E. R. and Schupbach, T. (2008). The dynamics of fluorescently labeled endogenous gurken mRNA in Drosophila. *J. Cell Sci.* **121**, 887–894.

Kim-Ha, J., Smith, J. L. and Macdonald, P. M. (1991). oskar mRNA is localized to the posterior pole of the Drosophila oocyte. *Cell* **66**, 23–35.

Lehmann, R. and Nüsslein-Volhard, C. (1986). Abdominal segmentation, pole cell formation, and embryonic polarity require the localized activity of oskar, a maternal gene in Drosophila. *Cell* **47**, 141–152.

Lehmann, R. and Nüsslein-Volhard, C. (1991). The maternal gene nanos has a central role in posterior pattern formation of the Drosophila embryo. *Dev. Camb. Engl.* **112**, 679–691.

Lin, M.-D., Jiao, X., Grima, D., Newbury, S. F., Kiledjian, M. and Chou, T.-B. (2008). Drosophila processing bodies in oogenesis. *Dev. Biol.* **322**, 276–288.

Manseau, L. J. and Schüpbach, T. (1989). cappuccino and spire: two unique maternal-effect loci required for both the anteroposterior and dorsoventral patterns of the Drosophila embryo. *Genes Dev* **3**, 1437–52.

Manseau, L., Calley, J. and Phan, H. (1996). Profilin is required for posterior patterning of the Drosophila oocyte. *Development* **122**, 2109–16.

Neuman-Silberberg, F. S. and Schüpbach, T. (1993). The Drosophila dorsoventral patterning gene gurken produces a dorsally localized RNA and encodes a TGF alpha-like protein. *Cell* **75**, 165–174.

Otomo, T., Tomchick, D. R., Otomo, C., Panchal, S. C., Machius, M. and Rosen, M. K. (2005). Structural basis of actin filament nucleation and processive capping by a formin homology 2 domain. *Nature* **433**, 488–494.

Palacios, I. M. and St Johnston, D. (2002). Kinesin light chain-independent function of the Kinesin heavy chain in cytoplasmic streaming and posterior localisation in the Drosophila oocyte. *Dev. Camb. Engl.* **129**, 5473–5485.

Parton, R. M., Hamilton, R. S., Ball, G., Yang, L., Cullen, C. F., Lu, W., Ohkura, H. and Davis, I. (2011). A PAR-1-dependent orientation gradient of dynamic microtubules directs posterior cargo transport in the Drosophila oocyte. *J. Cell Biol.* **194**, 121–135.

Paul, A. S., Paul, A., Pollard, T. D. and Pollard, T. (2008). The role of the FH1 domain and profilin in formin-mediated actin-filament elongation and nucleation. *Curr. Biol. CB* **18**, 9–19.

Pruyne, D., Evangelista, M., Yang, C., Bi, E., Zigmond, S., Bretscher, A. and Boone, C. (2002). Role of formins in actin assembly: nucleation and barbed-end association. *Science* **297**, 612–615.

Quinlan, M. E. (2013). Direct interaction between two actin nucleators is required in Drosophila oogenesis. *Dev. Camb. Engl.* **140**, 4417–4425.

Quinlan, M. E., Hilgert, S., Bedrossian, A., Mullins, R. D. and Kerkhoff, E. (2007). Regulatory interactions between two actin nucleators, Spire and Cappuccino. *J. Cell Biol.* **179**, 117–128.

Schindelin, J., Arganda-Carreras, I., Frise, E., Kaynig, V., Longair, M., Pietzsch, T., Preibisch, S., Rueden, C., Saalfeld, S., Schmid, B., et al. (2012). Fiji: an open-source platform for biological-image analysis. *Nat. Methods* **9**, 676–682.

Schüpbach, T. (1987). Germ line and soma cooperate during oogenesis to establish the dorsoventral pattern of egg shell and embryo in Drosophila melanogaster. *Cell* **49**, 699–707.

Serbus, L. R., Cha, B.-J., Theurkauf, W. E. and Saxton, W. M. (2005). Dynein and the actin cytoskeleton control kinesin-driven cytoplasmic streaming in Drosophila oocytes. *Development* **132**, 3743–52.

Sinsimer, K. S., Jain, R. A., Chatterjee, S. and Gavis, E. R. (2011). A late phase of germ plasm accumulation during Drosophila oogenesis requires Lost and Rumpelstiltskin. *Development* **138**, 3431–3440.

Snee, M. J., Harrison, D., Yan, N. and Macdonald, P. M. (2007). A late phase of Oskar accumulation is crucial for posterior patterning of the Drosophila embryo, and is blocked by ectopic expression of Bruno. *Differ. Res. Biol. Divers.* **75**, 246–255.

Tanaka, T., Kato, Y., Matsuda, K., Hanyu-Nakamura, K. and Nakamura, A. (2011). Drosophila Mon2 couples Oskar-induced endocytosis with actin remodeling for cortical anchorage of the germ plasm. *Development* **138**, 2523–32.

Theurkauf, W. (1994). Premature microtubule-dependent cytoplasmic streaming in cappuccino and spire mutant oocytes. *Science* **265**, 2093–2096.

Theurkauf, W. E., Smiley, S., Wong, M. L. and Alberts, B. M. (1992). Reorganization of the cytoskeleton during Drosophila oogenesis: implications for axis specification and intercellular transport. *Dev. Camb. Engl.* **115**, 923–936.

Van Doren, M., Williamson, A. L. and Lehmann, R. (1998). Regulation of zygotic gene expression in Drosophila primordial germ cells. *Curr. Biol. CB* **8**, 243–246.

Vizcarra, C. L., Kreutz, B., Rodal, A. A., Toms, A. V., Lu, J., Zheng, W., Quinlan, M. E. and Eck, M. J. (2011). Structure and function of the interacting domains of Spire and Fmn-family formins. *Proc. Natl. Acad. Sci.* **108**, 11884–11889.

Wang, C. and Lehmann, R. (1991). Nanos is the localized posterior determinant in Drosophila. *Cell* **66**, 637–647.

Wang, C., Dickinson, L. K. and Lehmann, R. (1994). Genetics of nanos localization in Drosophila. *Dev. Dyn. Off. Publ. Am. Assoc. Anat.* **199**, 103–115.

Weil, T. T., Forrest, K. M. and Gavis, E. R. (2006). Localization of bicoid mRNA in late oocytes is maintained by continual active transport. *Dev. Cell* **11**, 251–262.

Zimyanin, V., Lowe, N. and St Johnston, D. (2007). An oskar-dependent positive feedback loop maintains the polarity of the Drosophila oocyte. *Curr. Biol. CB* **17**, 353–359.

Chapter 2 Appendix:

Supplementary materials: Autoinhibitory regulation of the formin Cappuccino during *Drosophila* oogenesis

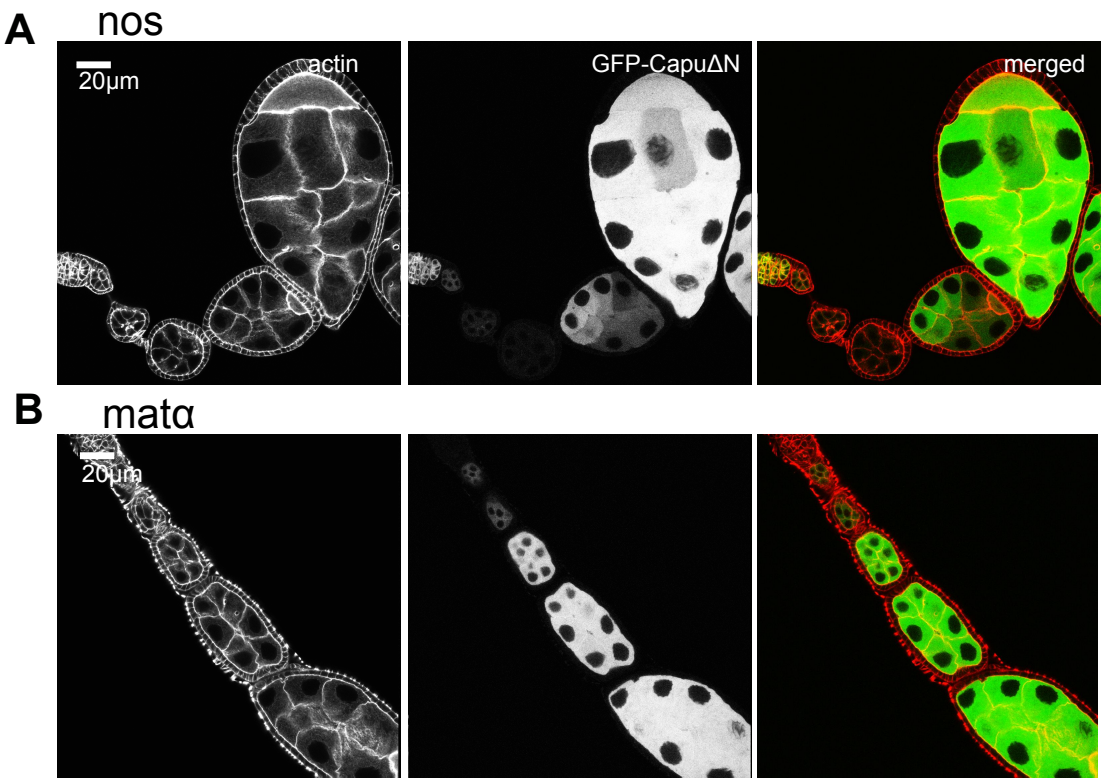

Figure S1. Expression profile of germline specific nos and matα drivers during oocyte development . (A, B) Fixed images showing the actin cytoskeleton (red in merged images) and GFP-CapuΔN (green) using nos or matα drivers. Actin was visualized by AlexaFluor647-phalloidin staining. (A) nos driver expresses in the early germarium and then decreases during stages 3-8. During stage 8-9, nos expression increases again. This has been documented before (Hudson and Cooley, 2010). (B) matα driver starts to express during early stages of oocyte development and stays uniformly high throughout the rest of oogenesis. Only expression during the early stages are shown.

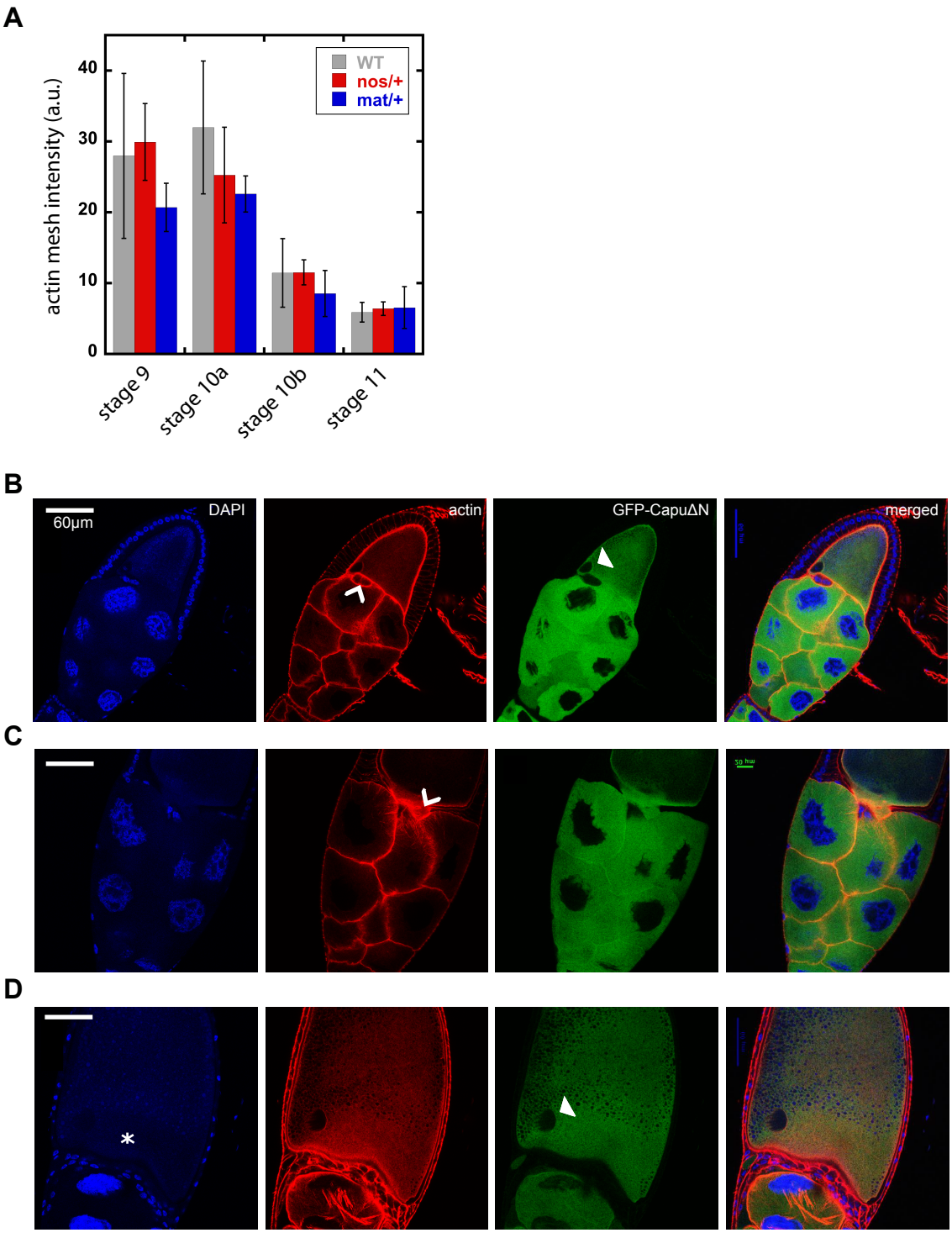

Figure S2. Characterization of actin mesh and its effect on border cell migration, oocyte nuclear localization and nurse cell dumping. (A) Oocytes from CantonS (wild type, gray) flies compared to those heterozygous for nos (nos/+, red) or matα (mat/+, blue) were stained with

AlexaFluor647-phalloidin and mesh density was quantified (see methods) at stages 9, 10A, 10B and 11. Consistent with previous findings, the actin mesh disappeared after stage 10a, during stage 10B and is gone by stage 11 (Dahlgaard et al., 2007). These controls had similar actin mesh densities at various stages. We used them as an internal controls for our quantification of actin mesh density (see methods). (B, C and D) Fixed oocytes expressing matα:GFP-CapuΔN stained for DNA (DAPI) and actin. In these oocytes border cell migration (chevrons; B, C), oocyte nuclear localization (closed arrowheads; B, D) as well as nurse cell dumping (asterisk; D) were all normal. (D) Because the oocyte contained increased actin mesh and no cytoplasmic streaming during nurse cell dumping, the ooplasm did not mix with the nurse cell content. As a result, the oocyte showed layering; the posterior half of the oocyte contained yolk granules whereas the anterior half contained nurse cell content (asterisk).

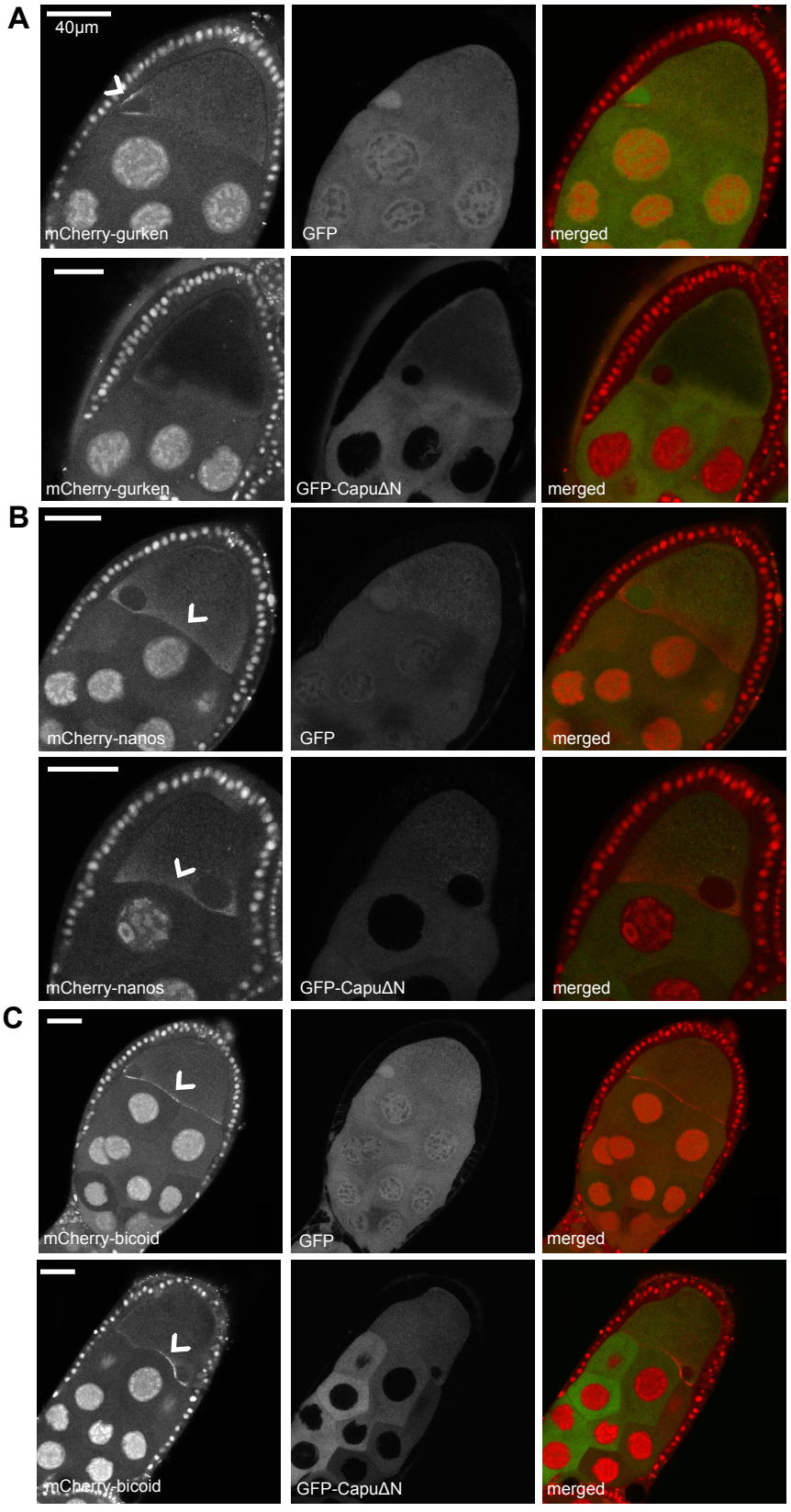
A
40μm
mCherry-gurken
GFP
merged
mCherry-gurken
GFP-CapuΔN
merged
B
mCherry-nanos
GFP
merged
mCherry-nanos
GFP-CapuΔN
merged
C
mCherry-bicoid
GFP
merged
mCherry-bicoid
GFP-CapuΔN
merged

Figure S3. Localization of fluorescent mRNAs in early stages of transport. Stage 9 egg chambers expressing MCP-mCherry and *grk*-$(ms2)_{12}$ (A), *nanos*-$(ms2)_{18}$ (B) or *bcd*-$(ms2)_{6}$ (C) mRNAs in combination with matα:GFP or matα:GFP-CapuΔN. MCP-mCherry is expressed from the ubiquitous hsp83 promoter whereas mRNAs are expressed only in the nurse cells. A nuclear localization sequence drives excess MCP-mCherry to the nucleus. (A) *grk* localizes normally around the oocyte nucleus forming a cap near the nucleus as has been shown (chevrons). Occasionally, matα:GFP-CapuΔN oocytes have decreased localization. Both *nanos* (B, chevron) and *bcd* (C, chevron) are localized normally in matα:GFP-CapuΔN oocytes.

Chapter 3: Characterization of Capu in tissue culture cells

Introduction

Actin nucleation and polymerization activities of formins are regulated by autoinhibition. This has been shown using biochemical assays (Chapter 1) as well as in tissue culture cells. Removal of the N-terminal half, GBD or DAD in the formins mDia1, FHOD1, FRL3 and DAAM1 results in increased number of actin filaments and stress fibers in mammalian cells (Alberts, 2001; Liu et al., 2008; Schulte et al., 2008; Vaillant et al., 2008; Watanabe et al., 1999). In some instances, expressing the DAD alone or having a point mutation in the DAD was sufficient to induce stress fiber formation, suggesting that autoinhibition is crucial for controlling actin polymerization activity in cells (Alberts, 2001; Liu et al., 2008). In addition, the cell culture assays showed that autoinhibition modulates membrane localization of formins (Schulte et al., 2008; Seth et al., 2006). The N-terminal half of FRL, mDia1 or FHOD1 was sufficient to localize these proteins to the plasma membrane. Furthermore, specific single point mutations that disrupted the autoinhibition also resulted in membrane localization of formins (Seth et al., 2006). In contrast full-length proteins that were autoinhibited had cytoplasmic localization.

Capu has primarily been studied in *Drosophila* egg development with little attention focused on its role in individual cells or in cell culture. Therefore, we wanted to characterize the activity and localization of Capu in *Drosophila* S2 cell lines and mammalian NIH3T3 cells. Studying Capu using cell culture will not only help us understand Capu's functions, it will give us an additional tool that is more accessible and easy to use compared to live imaging of *Drosophila* oocytes.

Results

Expression of Capu in *Drosophila* S2 cells

Previous studies showed that expression of FH1FH2 domains of formins in mammalian cells resulted in increased stress fibers. We asked whether expression of Capu-CT (467-1059), which has FH1, FH2 and Capu-Tail domains, would result in a similar phenotype. Since Capu is a *Drosophila* protein, we expressed Capu-CT and full-length Capu (FL) in the *Drosophila* S2 cell

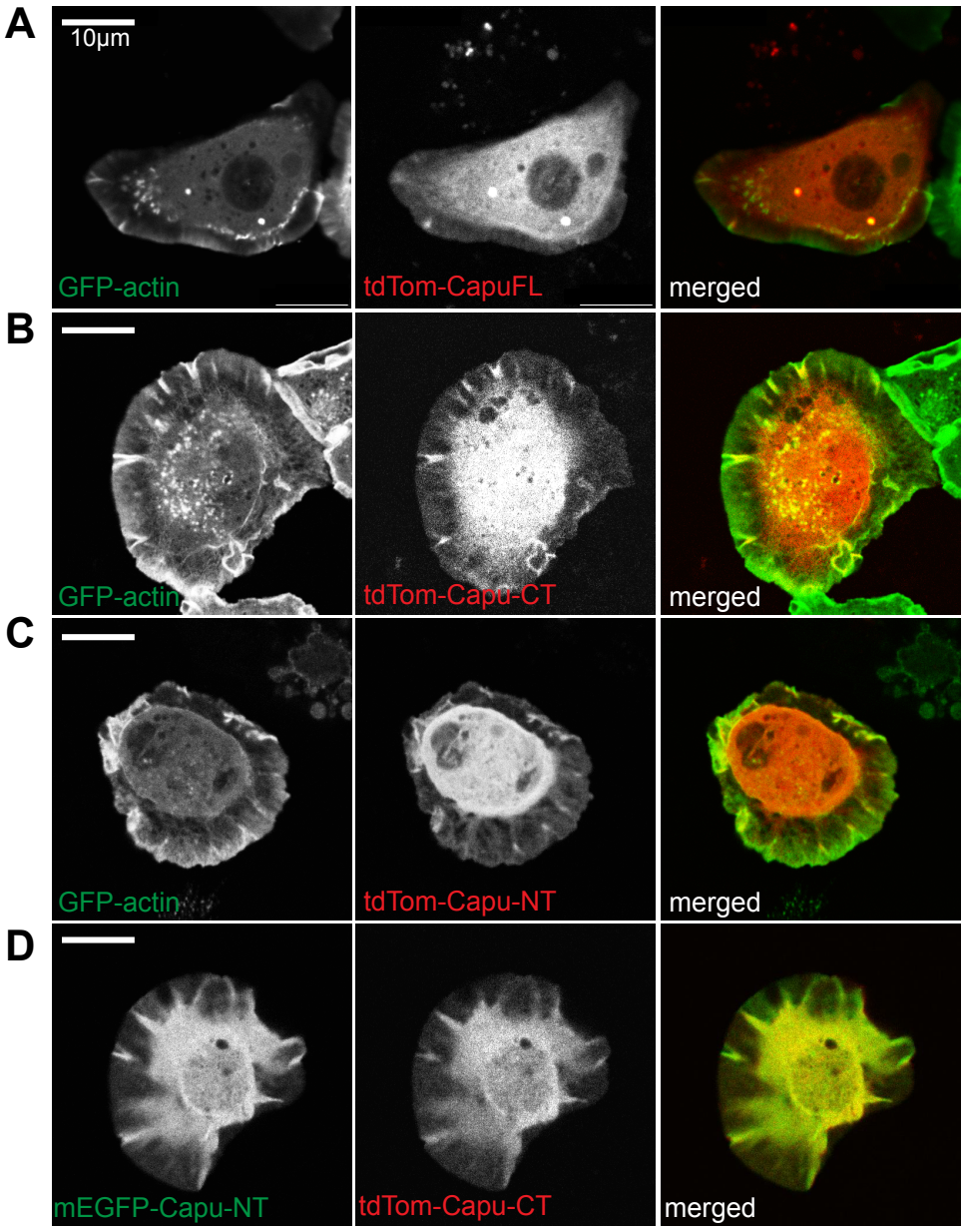

Figure 1. Localization of Capu-CT (467-1059) and Capu-NT (1-466) in *Drosophila* S2 cells. We transfected an S2 cell line that stably expresses GFP-actin with various Capu truncations (see methods). The first column of A, B and C is live imaging of GFP-actin. The second column of A, B and C is the live imaging of tandom Tomato (tdTom) tagged full-length Capu (FL), Capu-CT or Capu-NT. The last column is the merged images (green is actin and red is Capu). D shows the co-expression of mEGFP-Capu-NT and tdTom-Capu-CT. We acquired our S2 cell lines from the laboratory of Steve Rogers. All scale bars are 10 μm.

line. S2 cells have a “fried egg” like morphology when plated on concanavalin A due to its even spreading and protrusions and a yolk-like nucleus. Expression of both proteins had very similar localization in S2 cells, diffuse in the cell body and enriched in the protrusions and specific regions of lamella (Figure 1A,B).

Next we tested expression of Capu-NT (1-466) in S2 cells. We looked for an actin phenotype and for an unique localization pattern compared to Capu-CT. It has been shown that the N-terminal half of Capu and other formins are important for membrane localization of these proteins (Dahlgaard et al., 2007; Seth et al., 2006). When we expressed Capu-NT however we did not see localization to the membrane or a change in the actin cytoskeleton/morphology of the S2 cells (Figure 1C). We also expressed both Capu-CT and Capu-NT in S2 cells and observed diffuse localization similar to CapuFL, Capu-CT or Capu-NT alone (Figure 1D). Together, these data suggest that Capu-CT and Capu-NT have no or very minimal function in S2 cells.

While it has been previously shown that Capu is expressed in the oocyte (Quinlan et al., 2007) it is crucial to determine whether S2 cells also contain endogenous Capu or Spire (Spir) proteins since their presence could affect exogenous Capu’s function and localization. We analyzed Spir also because Capu and Spir are functional partners that cooperatively assemble and regulate actin filaments (Quinlan et al., 2007; Vizcarra et al., 2011). We looked at endogenous expression of Capu and Spir proteins in S2 cells using antibodies against these two proteins. We did not detect Capu by Western blot. We did detect bands using a anti-Spir antibody but they are much smaller than expected. Either Spir is breaking down rapidly or the cells lack Spir and these are non-specific bands. The antibody was shown to detect several non-specific bands in lysates of *Drosophila* oocytes (Quinlan et al., 2007). Thus, we suspect that S2 cells have very little or no endogenous Spir or Capu.

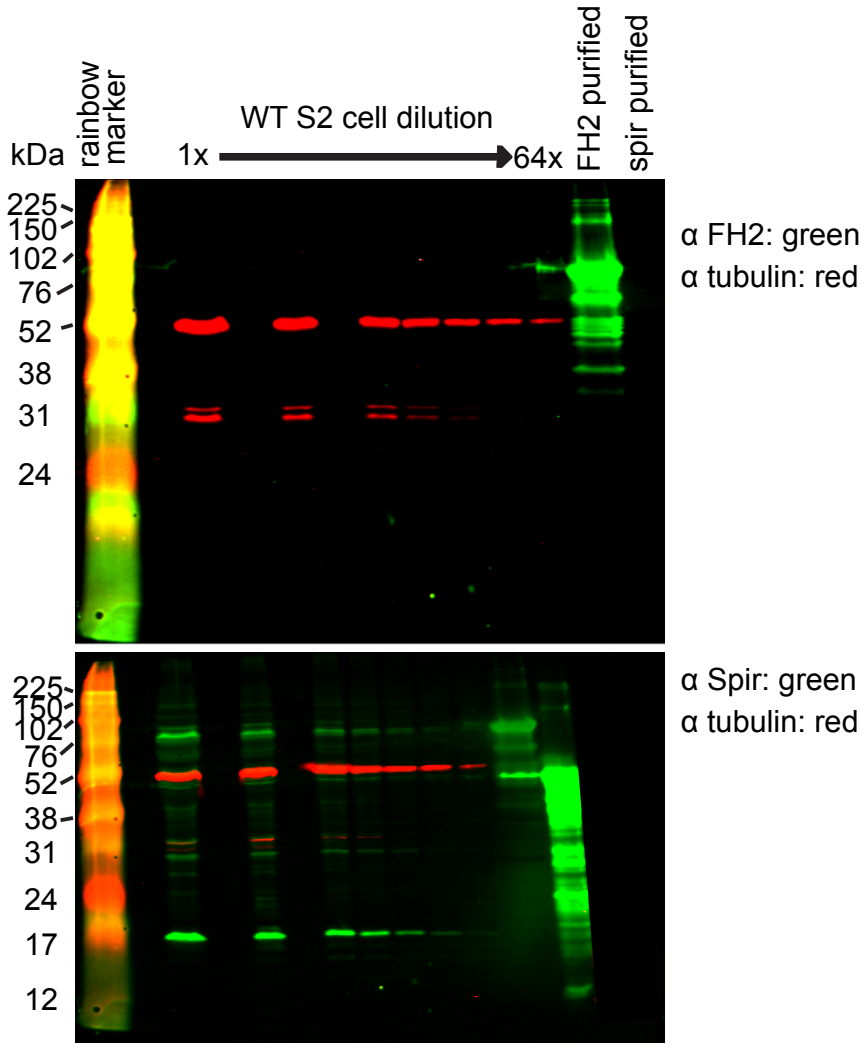

Figure 2. Western Blot analysis of endogenous Capu and Spir proteins in S2 cells. Top blot stained with antibodies against the FH2 domain of Capu. Bottom blot stained with antibody against against Spir. Green is anti-Capu or –Spire. Red is anti-tubulin staining for control. The last two lanes show the purified proteins (Capu-CT and Spir-NT) for positive controls.

Targeting Capu to the S2 cell plasma membrane

One of our goals was to ask whether Capu-CT and Capu-NT colocalize in S2 cells. However, because they localize very similarly when expressed individually (Figure 1B, C and D), we could not conclude that they are binding in S2 cells when expressed together. Our previous results (see Chapter 1 and 2) showed that Capu is autoinhibited through binding of Capu-CT and Capu-NT. To characterize Capu autoinhibition further, we tagged Capu-CT and Capu-NT with a plasma membrane signal sequence (myristoylation or CAAX sequences), which has been shown to facilitate membrane localization. Using these tags, we were able to target Capu-CT to the plasma membrane of S2 cells (Figure 3A). The images show that diffuse localization of untagged Capu-CT in the cytoplasm shifts to membrane localized, although some Capu-CT still remains in the cytoplasm. Due to the S2 cell spreading and "fried egg" like morphology on concanavalin A, the membrane-localized proteins look very weak and it is difficult to see the membrane enrichment. When we expressed untagged Capu-NT with the myr or CAAX tagged Capu-CT, we saw no depletion of Capu-NT from the cytoplasm (Figure 3B,C). Most of the Capu-NT remains in the cytoplasm whereas Capu-CT localizes to the plasma membrane. We also did the reciprocal experiment tagging Capu-NT with CAAX. Similar to Capu-CT-CAAX, Capu-NT-CAAX mostly localized to the membrane (Figure 3D). When we expressed Capu-NT-CAAX with untagged Capu-CT, Capu-CT was still localized to the cytoplasm (Figure 3E). Therefore, we successfully relocalize the cytoplasmic Capu-CT and Capu-NT to the plasma membrane, but the untagged Capu-NT and Capu-CT did not follow the localization to the membrane. This suggests that Capu-CT and Capu-NT either do not bind or these cells have a regulatory mechanism that prevents Capu-CT and Capu-NT from interacting. An alternative explanation is that cytoplasmic untagged protein is much greater than the membrane tagged protein, resulting in no depletion of the cytoplasmic pool, but visual inspection suggests that this not the case.

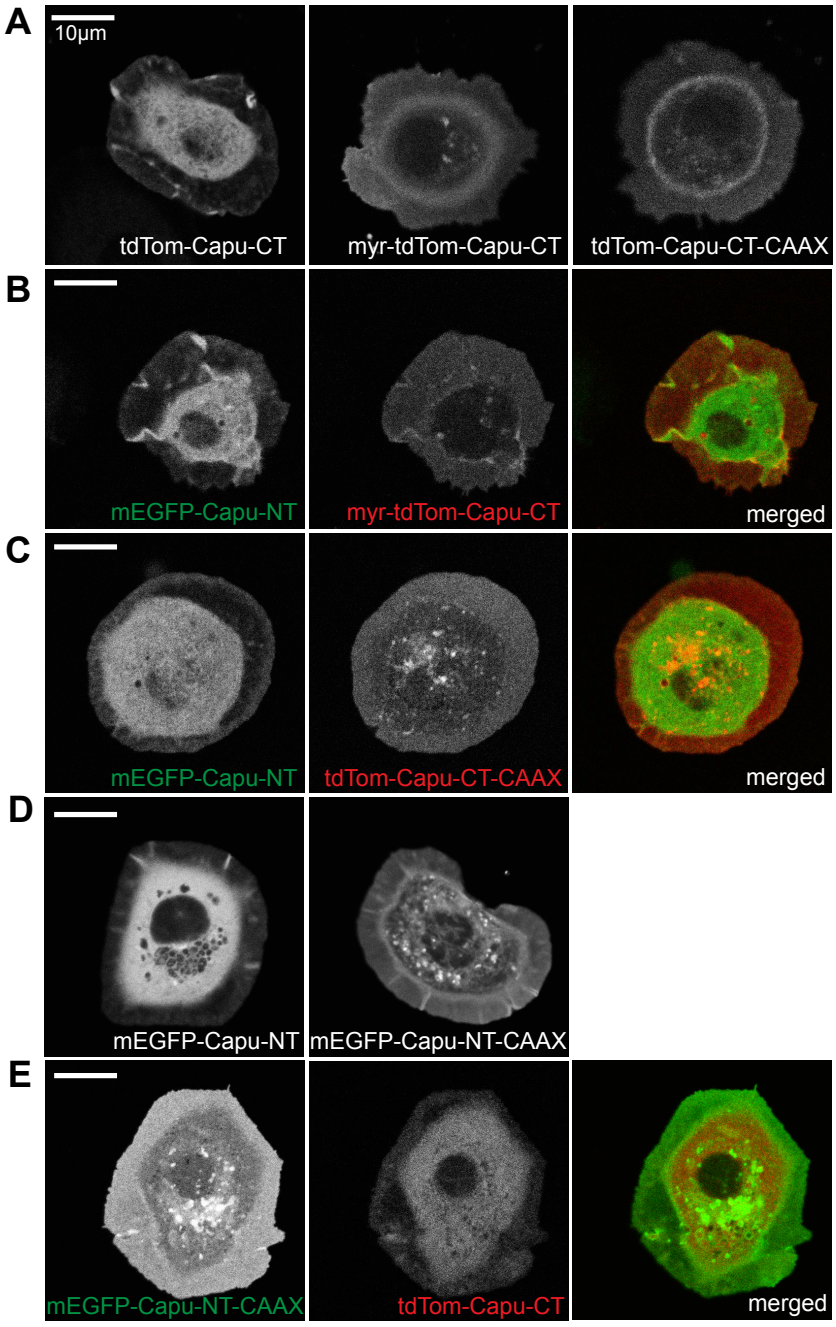

Figured 3. Targeting Capu-CT and Capu-NT to the plasma membrane of S2 cells. (A) Live imaging of S2 cells shows localization of tdTom-Capu-CT with or without myristoylation (myr) or CAAX membrane tags. (B, C) Expression of mEGFP tagged Capu-NT in the presence of either myr (B) or CAAX (C) tagged Capu-CT. (D) Live imaging of untagged or CAAX tagged Capu-NT. (E) Expression of untagged Capu-CT with CAAX tagged Capu-NT.

Expression of Capu in NIH3T3 cells

To further study the functional interaction between Capu-CT and Capu-NT, we also expressed these proteins in NIH3T3 cells. It was previously shown that expression of mDia1 C-terminal half (mDia1-CT) in NIH3T3 cells induces stress fiber formation. Therefore, we wanted to test whether Capu-CT has similar activity in NIH3T3 cells. As a positive control, we expressed mDia1-CT in NIH3T3 cells. Consistent with previous studies, we observed an increase in stress fiber formation in cells expressing mDia1-CT protein (Figure 4A). In contrast, when we expressed Capu-CT, we did not see any induction of stress fibers (Figure 4B). Capu-CT was diffuse throughout the cytoplasm similar to S2 cells. Expressing Capu-NT also had no effect on the actin cytoskeleton, and it localized similar to Capu-CT (Figure 4C). Finally, when we expressed both Capu-CT and Capu-NT, their localization remained cytoplasmic and we did not see any actin phenotype (Figure 4D). These results suggest that Capu has no activity in NIH3T3 cells in contrast to mDia1-CT.

Discussion

Despite our efforts, we were unable to show that Capu-CT induces accumulation of stress fibers or other actin structures in either S2 or NIH3T3 cells. Furthermore, both full-length and truncated Capu were diffuse in these cell lines. Interestingly, S2 cells do not have endogenous Capu. S2 cells are derived from *Drosophila* macrophages (Schneider, 1972). It seems likely that Capu does not play a role in regulating the actin cytoskeleton in these cells. Perhaps Capu does not function in these cells because its regulatory or partner proteins are not present.

We were able to target Capu-CT or Capu-NT to the S2 cell membrane using either a myristalyation sequence or CAAX tag. Because S2 cells were spread out and flattened, the membrane targeting was hard to visualize. The proteins did move to the membrane but they looked diffuse and not membrane rich due to the shape of the cells. However, when we co-

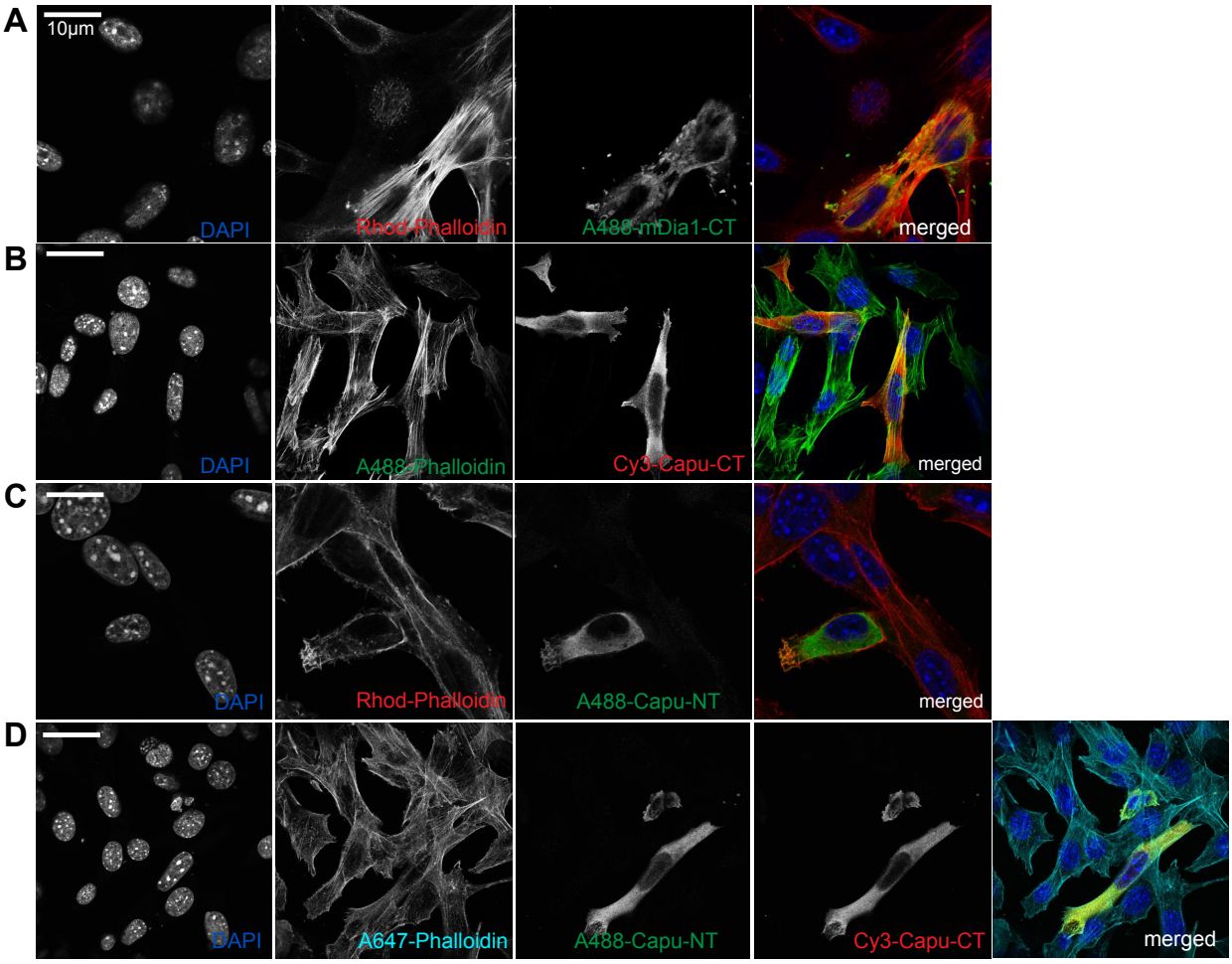

Figure 4. Localization of Capu-CT and Capu-NT in NIH3T3 cells. Fixed images of NIH3T3 cells expressing mEGFP tagged C-terminal half (CT) of mDia1 (A), tdTom tagged Capu-CT (B), mEGFP tagged Capu-NT (C) or both mEGFP tagged Capu-NT and tdTom tagged Capu-CT (D). These proteins were immunostained with anti-GFP or anti-dsRed primary antibody followed by Alexa488 (A488) or Cy3 conjugated secondary antibody respectively. The actin was either stained with Rhodamine-Phalloidin, Alexa488-Phalloidin or Alexa647-Phalloidin. The nucleus was stained with DAPI.

expressed the other half of the protein that is untagged, it does not follow the tagged protein to the membrane. This suggests Capu-CT and Capu-NT are not binding to each other. This could be explained by excess proteins that remain in the cytoplasm, or there is a regulator in the S2 cell that is inhibiting the interaction between Capu-CT and Capu-NT. We weren't able to distinguish between these possibilities.

Our main goal was to characterize Capu autoinhibition by exploring actin polymerization activity or membrane localization of Capu in S2 or NIH3T3 cells. However, because we could not get these activities/localization established in S2 or NIH3T3 cell lines, we were not able to characterize Capu autoinhibition. In the future, we need to try other *Drosophila* cell lines which may result in a better outcome.

Methods

Plasmids

We ligated HindIII-KpnI fragments of mEGFP-Capu(1-466), mEGFP-Capu(1-466)-CAAX, tdTomato-Capu(1-466), tdTomato-Capu(467-1059)-CAAX and myr-tdTomato-Capu(467-1059) in a pIZ/V5-His (Invitrogen) vector. The membrane targeting sequence of CVLS (CAAX) or Src64b was inserted at the C-terminal end of the Capu construct. pIZ was selected with zeocin and the genes were constitutively expressed with an OpIE2 promoter.

Cell culture

We obtained Schneider S2R+ insect cells (wild type and stably expressing GFP-actin) from Stephen L. Rogers at the University of North Carolina. They were cultured and maintained using standard conditions (Rogers and Rogers, 2008). Initially S2 cells were plated on concanavalin A coated plates and transfected with Capu and Spir constructs using Effectene reagent (Qiagen). After 6-18 hours of transfection, we re-plated the cells to concanavilin A coated glass bottom dishes (MatTek). After cells were attached to the cover slip (~1 hour), they were imaged on a Leica SPE I inverted confocal microscope.

NIH3T3 cells were transfected using Lipofectamine (Invitrogen). Cells were plated at $4x10^5$ density in 2 mL of growth medium without antibiotics overnight. 4 µg of DNA in 250 µL of medium was added to Lipofectamine and applied to the cells. The cells were incubated with the DNA mix for 18-48 hours before fixation. NIH3T3 cells were fixed using 3.7% paraformaldehyde and subsequently stained with primary (anti-GFP or anti-dsRed) and secondary (Alexa488 or Cy3 conjugated) antibodies as well as 0.1 µM labeled phalloidin.

Western blot

Spin down ~1 mL of 100% confluent wild type S2 cells at 500 xg for 10 minutes. Resuspend pelleted cells in 100 µL of SDS PAGE loading buffer. Boil and centrifuge sample at 15,000 xg for 5 min. Discard pellets and dilute supernatant 2, 4, 8, 16, 32 and 64-fold for analysis. Resolve the diluted supernatant by SDS-PAGE and transferred to nitrocellulose membrane (PVDF-FL Licor). Specific proteins were detected on membrane probed with anti-Spir or anti-Capu-FH2 at 1:2000 (Quinlan et al., 2007), together with fluorophore conjugated secondary antibody. Proteins bands were visualized by Licor Infrared Scanner.

Reference

Alberts, A. S. (2001). Identification of a carboxyl-terminal diaphanous-related formin homology protein autoregulatory domain. *J Biol Chem* **276**, 2824–30.

Dahlgaard, K., Raposo, A. A. S. F., Niccoli, T. and Johnston, D. S. (2007). Capu and Spire assemble a cytoplasmic actin mesh that maintains microtubule organization in the Drosophila oocyte. *Dev Cell* **13**, 539–53.

Liu, W., Sato, A., Khadka, D., Bharti, R., Diaz, H., Runnels, L. W. and Habas, R. (2008). Mechanism of activation of the Formin protein Daam1. *Proc Natl Acad Sci USA* **105**, 210–5.

Quinlan, M. E., Hilgert, S., Bedrossian, A., Mullins, R. D. and Kerkhoff, E. (2007). Regulatory interactions between two actin nucleators, Spire and Cappuccino. *J. Cell Biol.* **179**, 117–128.

Rogers, S. L. and Rogers, G. C. (2008). Culture of Drosophila S2 cells and their use for RNAi-mediated loss-of-function studies and immunofluorescence microscopy. *Nat. Protoc.* **3**, 606–611.

Schneider, I. (1972). Cell lines derived from late embryonic stages of Drosophila melanogaster. *J. Embryol. Exp. Morphol.* **27**, 353–365.

Schulte, A., Stolp, B., Schönichen, A., Pylypenko, O., Rak, A., Fackler, O. T. and Geyer, M. (2008). The human formin FHOD1 contains a bipartite structure of FH3 and GTPase-binding domains required for activation. *Structure* **16**, 1313–23.

Seth, A., Otomo, C. and Rosen, M. K. (2006). Autoinhibition regulates cellular localization and actin assembly activity of the diaphanous-related formins FRLalpha and mDia1. *J Cell Biol* **174**, 701–13.

Vaillant, D. C., Copeland, S. J., Davis, C., Thurston, S. F., Abdennur, N. and Copeland, J. W. (2008). Interaction of the N- and C-terminal autoregulatory domains of FRL2 does not inhibit FRL2 activity. *J Biol Chem* **283**, 33750–62.

Vizcarra, C. L., Kreutz, B., Rodal, A. A., Toms, A. V., Lu, J., Zheng, W., Quinlan, M. E. and Eck, M. J. (2011). Structure and function of the interacting domains of Spire and Fmn-family formins. *Proc. Natl. Acad. Sci.* **108**, 11884–11889.

Watanabe, N., Kato, T., Fujita, A., Ishizaki, T. and Narumiya, S. (1999). Cooperation between mDia1 and ROCK in Rho-induced actin reorganization. *Nat Cell Biol* **1**, 136–43.

Chapter 4: Capu binds and bundles actin filaments

Introduction

In addition to having well-conserved actin nucleation and elongation activities, formins can bind to the sides of pre-existing filaments and can cross-link (bundle) two or more filaments (Goode and Eck, 2007). Bundling activity however is not a universal function of formins. Previous *in vitro* studies showed that Arabidopsis formin AFH1, yeast formins Bnr1 and Fus1, and mammalian formins mDia2, FRL1 and INF2 bundle filaments, while a variety of fungal and mammalian formins (mDia1, Cdc12, For3, and Bni1) do not (Chhabra and Higgs, 2006; Harris et al., 2006; Michelot et al., 2005; Moseley and Goode, 2005; Scott et al., 2011). Bnr1 bundles using its FH1, FH2 and C-terminal domains, AFH1 and Fus1 need FH1 and FH2 domains for bundling, whereas FRL1 and mDia2 need only FH2 domain to bundle actin filaments, suggesting that different formins have distinct filament bundling domains. Whether side binding directly translates to bundling is still unclear. In addition, the FRL1, INF2, and mDia2 FH2 dimers can dissociate, suggesting that, in these cases, side binding involves filament encirclement, similar to barbed end binding (Gurel et al., 2014; Harris et al., 2006). Despite these findings, no study has shown directly that a formin's filament bundling activity is important for cellular processes. This is because no mutations have been described that specifically compromise bundling activity while leaving the nucleation and elongation activities unperturbed.

The *Drosophila* formin Cappuccino (Capu) also has been shown to bind and bundle actin filaments (Quinlan et al., 2007; Rosales-Nieves et al., 2006). Furthermore, Spir-KIND binding to Capu inhibits its filament binding and bundling activity. Spir-KIND binds to the Capu-Tail domain, suggesting Capu-Tail is important for Capu's filament binding and bundling activity (Vizcarra et al., 2011). However, it is still unclear how Capu binds actin filaments and subsequently bundles them. We addressed this question using *in vitro* biochemical assays on WT, mutated, truncated, and chimeric versions of Capu. We also had the goal of identifying genetic tools for separating bundling from nucleation and elongation activities of Capu *in vivo*.

Results

Capu-Tail is sufficient to bind the sides of actin filaments

To characterize Capu's filamentous actin (F-actin) binding capability, we used a high speed F-actin cosedimentation assay (see methods). In this assay, we kept the F-actin concentration constant and added increasing concentrations of different Capu constructs. Subsequent to centrifugation, we quantified the amount of Capu that co-pelleted with F-actin (Figure 1). These experiments showed that Capu-CT (aa 467-1059) binds to F-actin weakly, with 4.5 μM affinity, in contrast to previous results showing that Capu-CT binds F-actin with low nM affinity (Quinlan et al., 2007). The discrepancy is likely to be due to enhancement of F-actin binding by 6xHis labeling at the C-terminus where the Capu-Tail is located (see below). We also used the F-actin that was pelleted to quantify the ratio of Capu-CT dimer to F-actin monomer and it was about 0.5, suggesting that for every actin monomer 0.5 Capu-CT dimer bound on the filament (Figure 1). That is, essentially one Capu-CT monomer binds to one actin monomer on the filaments.

Previous studies suggested that Capu-Tail (aa 1029-1059) play a role in F-actin binding (Quinlan et al., 2007; Vizcarra et al., 2011). To test this hypothesis, we truncated the Capu-Tail domain from Capu-CT and asked if Capu(467-1031) or Capu(467-1047) can bind F-actin. Cosedimentation assays showed that these proteins had very little or no F-actin binding ability (Figures 1 and 2C, D), suggesting that Capu-Tail is crucial for Capu's F-actin binding. To test whether Capu-Tail alone is sufficient to bind F-actin, we employed two different approaches. First, we tested whether a GST-tagged Capu-Tail could bind F-actin. We expect GST-Capu-Tail to be a reasonable spatial approximation for Capu-Tail's position on the Capu-CT dimer (see Chapter 1). As expected, GST-Capu-Tail bound F-actin similar to Capu-CT, with 5.6 μM affinity. In contrast, GST alone did not bind to F-actin (Figure 1). Secondly, we analyzed the binding of monomeric Capu-Tail to F-actin. Because Capu-Tail is only 30 residues long, it was challenging to visualize it on an SDS-PAGE gel with various staining techniques (Coomasie, SyproRed and

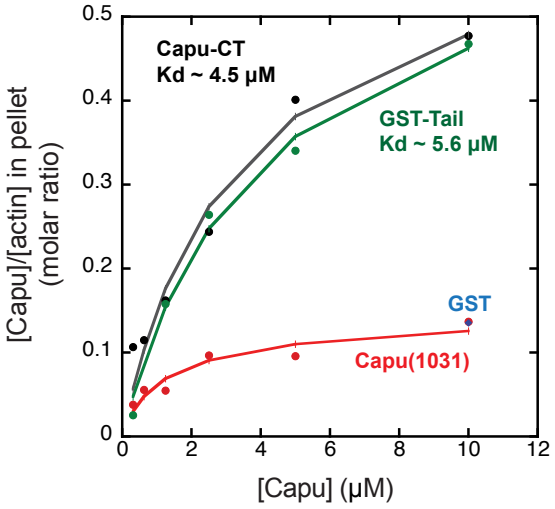

Figure 1. Filamentous actin side binding of Capu. Analyzing filament side binding of Capu-CT (467-1059, gray), Capu(467-1031) (red), GST-Tail (1029-1059) (green) and GST (blue) constructs using a high speed pelleting assay. We titrated in increasing concentrations of Capu to 0.5 µM of actin. Fitting and binding coefficients (Kd) were determined as described in Roth-Johnson *et al*., 2014.

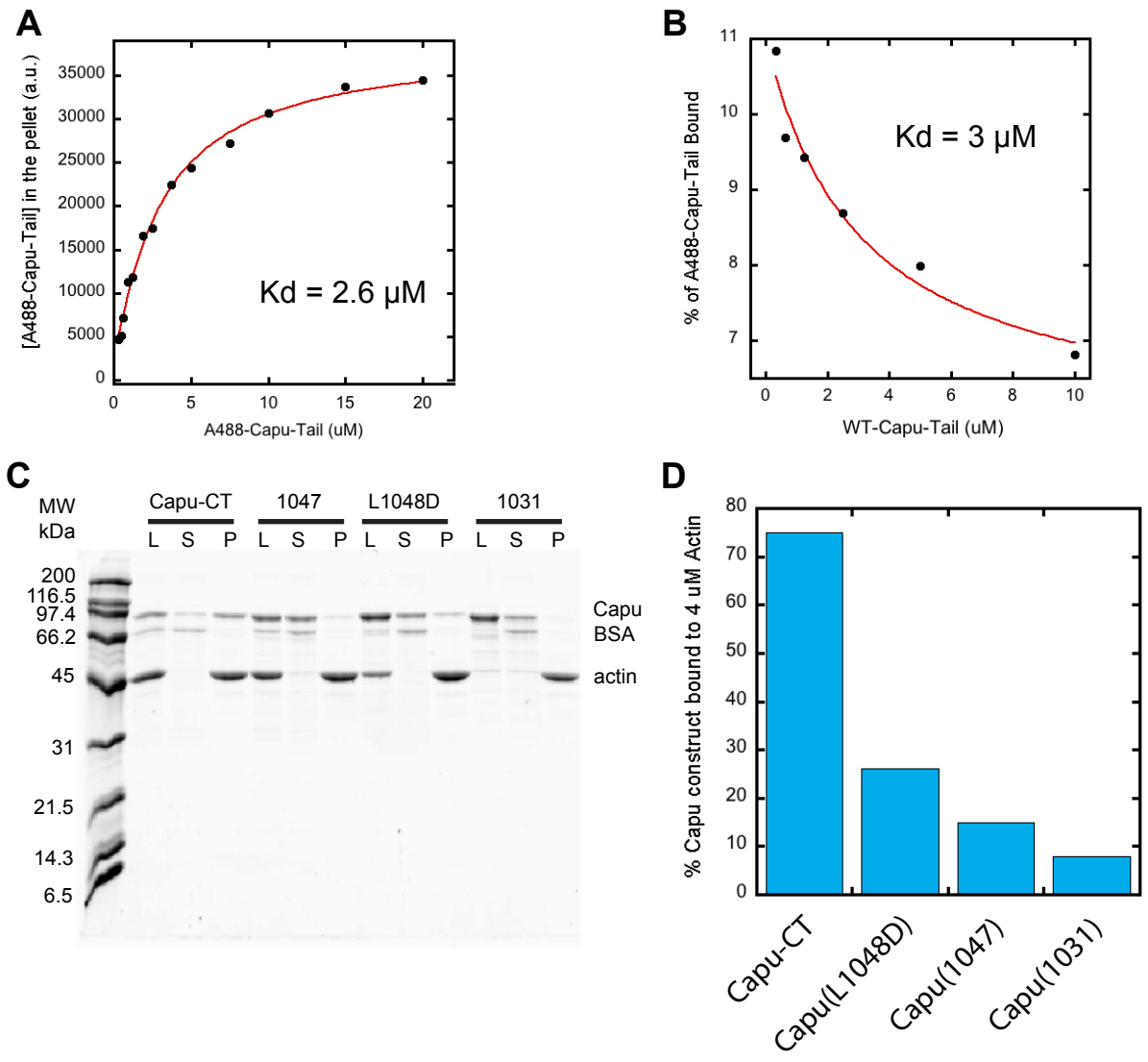

Figure 2. Capu-Tail (1029-1059) is sufficient to bind the sides of F-actin. (A) We quantified the F-actin binding of Alexa-488 (A488) labeled Capu-Tail. We used a fixed F-actin concentration (1µM) with increasing concentration of A488-Capu-Tail. (B) Competition experiment where A488-Capu-Tail was competed off from F-actin with wild type (untagged) Capu-Tail. (C) Gel of a high speed consedimentation assay with four different proteins: Capu-CT, Capu(467-1047), Capu-CT(L1048D) and Capu(467-1031). Load (L), Supernatant (S) and Pellet (P) are shown for each protein. (D) Quantification of proteins in C using Quantity One software.

SyproRuby). Therefore, we labeled the Capu-Tail with Alexa488 (A488) fluorophore and imaged the fluorophore to measure the amount of Capu-Tail that pelleted with F-actin. Using this assay, we determined that A488-Capu-Tail bound to F-actin with 2.6 μM affinity (Figure 2A). The binding was 2-fold lower than GST-Tail or Capu-CT but that could be due to labeling of the protein. To test this, we also carried out a competition-binding assay, where we competed off the F-actin bound A488-Capu-Tail with increasing concentrations of wild type (unlabeled) Capu-Tail. The resulting affinity (3 μM) was very similar to A488-Capu-Tail binding.

Our ultimate goal is to separate F-actin side binding activity from other Capu functions. When we mutated Leucine to Apartate at residue 1048, the Capu-CT binding decreased from ~75% to ~30%, suggesting that introduction of a negatively charged sidechain at residue 1048 is detrimental for F-actin binding (Figure 2C, D). However, this was the only point mutant we tested and we still need to look at other Capu mutants to completely map the residues responsible for F-actin binding. Therefore, F-actin binding activity of Capu-CT seems to be Capu-Tail specific and residue 1048 plays a crucial role in binding to F-actin.

Capu can bundle actin filaments

Since Capu-Tail can bind F-actin, and previous studies showed that Capu-CT can bundle two or more actin filaments (Quinlan et al., 2007), we wanted to further characterize the F-actin bundling activity of Capu-CT. Using a low speed cosedimentation assay (see methods), we analyzed the bundling activity of Capu-CT and various other Capu constructs. Consistent with previous results, Capu-CT was able to bundle 4 μM actin filaments (Figure 3A). As low as 60 nM Capu-CT was enough to start bundling filaments and by 200 nM, nearly all (4 μM) actin filaments were bundled (Figure 3A). Furthermore, Capu-CT-I706A and Capu-FH2 (aa 554-1059) were able to bundle actin filaments. The Capu FH2 knob mutation I706A abolishes Capu's nucleation activity (Quinlan, 2013) both *in vitro* and *in vivo*. This suggests that Capu's actin nucleation activity, and furthermore Capu's actin monomer binding capability is not necessary for Capu's F-actin bundling activity. The data for Capu-FH2 indicate that the FH1

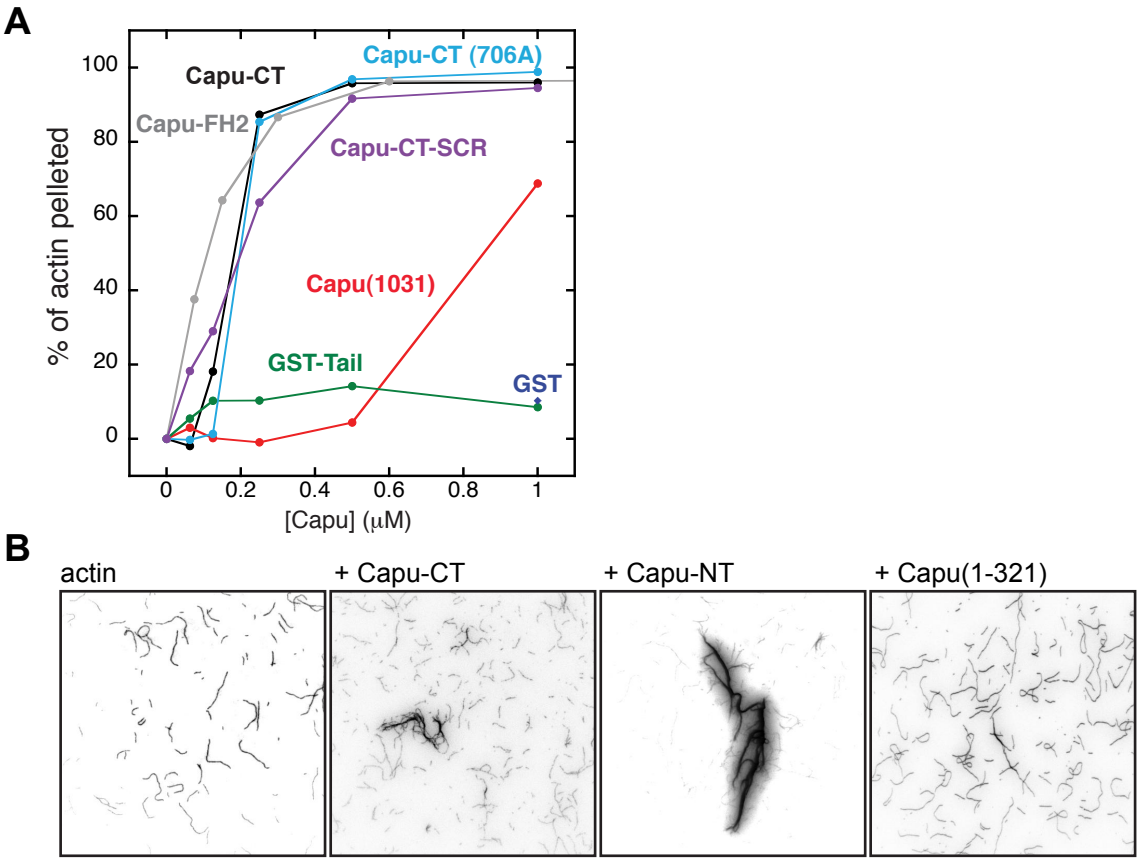

Figure 3. Capu bundles actin filaments. (A) Low speed cosedimentation experiment (see methods) shows that Capu-CT bundles actin filaments (black). I706A mutation in Capu-CT (light blue), a mutation that inhibits Capu's nucleation activity, and Capu-FH2 domain (554-1059, gray), a truncation that is missing the FH1 domain, were able to bundle actin filaments. Also Capu-CT with scrambled Capu-Tail region (Capu-CT-SCR, purple) was able to bundle actin filaments, suggesting residues within the Capu-Tail are important for bundling but not the sequence itself. Supporting that Capu-Tail is important for F-actin binding, truncating residues 1032-1059 severely reduced the F-actin bundling activity of Capu-CT (red). In contrast, GST or GST tagged Capu-Tail were not able to bundle F-actin (black). (B) TIRF microscopy assay (see methods) shows that Capu-CT and Capu-NT (1-466) bundle actin filaments but not Capu(1-321).

domain from Capu-CT is not needed for Capu's actin bundling activity. Since Capu-Tail is crucial for Capu's F-actin binding, we tested whether Capu-Tail is required for Capu's bundling activity. To that end, we truncated Capu-Tail domain and saw that Capu(467-1031) is a much weaker bundler than Capu-CT. We also scrambled the residues within the Capu-Tail (Capu-CT-SCR). To our surprise, Capu-CT-SCR still can bundle actin filaments (Figure 3A), suggesting that non-specific electrostatic charge mediates the interaction between Capu-tail and F-actin. In contrast, GST-Capu-Tail was not able to bundle F-actin (Figure 3A), suggesting GST cannot sufficiently mimic FH2 domain. GST alone was not able to bundle actin filaments. These results indicate that Capu-Tail is necessary for Capu's F-actin binding but not sufficient for bundling activity. Specifically the amino acid composition of the Capu-Tail, but not the sequence of the Capu-Tail, determines binding. The fact that, Capu-Tail alone cannot bundle actin filaments, suggests that the FH2 domain contributes.

We also looked at Capu's bundling activity using a TIRF microscopy assay (see methods). This assay showed that Capu-CT and Capu-NT (1-466) bundle actin filaments, but not Capu(1-321) (Figure 3B). We were not able to use the cosedimentation assay to test Capu-NT bundling because a significant amount of Capu-NT pellets on its own, obscuring the data. These results suggest that both Capu-CT and Capu-NT can bundle actin filaments. Within Capu-NT, residues 322-466 are necessary for the bundling activity because truncation of this region abolishes Capu-NT's bundling activity. We think this is do to loss of dimerzation because this region is also necessary for Capu-NT dimerzation (Chapter 1).

Discussion

Capu's mechanism of bundling

For Capu as well as other formins, the mechanism of F-actin bundling is still unclear. Capu seems to bind the sides of actin filaments using it C-terminal Capu-Tail domain. Interestingly, when we replaced the FH2 domain with GST, GST-Capu-Tail was able to bind actin filament sides similar to Capu-CT but was not able to bundle actin filaments, suggesting

that the FH2 domain is necessary for Capu's bundling activity. We speculate that dimeric FH2 domains force two Capu-Tail domains to bind different actin filaments, although this still needs to be illustrated. Dimeric FH2 domains of FRL1 and mDia2 can dissociate to clamp pre-existing actin filaments, suggesting one mechanism to bundle actin filaments (Harris et al., 2006). Perhaps Capu does the same thing, which explain why the FH2 domain is necessary. However, the dissociation capacity of the Capu-FH2 dimer still needs to be tested. The FH1 domain was dispensable for Capu's bundling activity. Capu has weak affinity to F-actin side binding but ~200 nM Capu-CT was sufficient to bundle 4 μM actin filaments, suggesting sparse decoration of actin filaments by Capu-CT is sufficient to bundle.

Capu bundling activity *in vivo*

Previous studies on formin bundling activity have focused mostly on *in vitro* characterization. The reason is that the nucleation and elongation activities of formin need to be uncoupled from the filament binding and bundling activity before we can test the affects *in vivo*. For Capu, this challenge is further complicated by Capu's F-actin binding domain being mapped to the Capu-Tail, which is important for interaction with Spir-KIND, Capu-NT, and microtubules (Bor et al., 2012; Roth-Johnson et al., 2014; Vizcarra et al., 2011). To distinguish these functions from Capu's bundling activity, we need to identify Capu-Tail mutants that affect only F-actin binding and bundling. The point mutant (L1048D) that we tested was a good start, but this mutation also affects Spir-KIND binding (Vizcarra et al., 2011). Point mutants such as R1034A and K1039A are good candidates because they have near wild type nucleation activity and do not affect Spir-KIND and Capu-NT binding (Bor et al., 2012). Such point mutations would help us to understand the role of Capu-mediated F-actin bundling during *Drosophila* oogenesis.

Methods

Actin Filament Binding and Bundling Assays

Amoeba actin (10 μM) was polymerized in 1x KMEH polymerization buffer (50 mM KCl, 10 mM HEPES, 1 mM $MgCl_2$, 1 mM EGTA, 0.5 mM Thesit) for 1 hour at room temperature (RT),

subsequently 1:1 ratio of phalloidin was added in the filamentous actin. During polymerization, Capu-CT or truncations were pre-cleared at 55,000 rpm for 20 min at 4°C. After polymerization, filaments were diluted to a final concentration of 0.5 μM in the presence of 0, 0.625, 1.25, 2.5, 5 and 10 μM Capu-CT, GST-Tail or Capu(467-1031) in 7x20 mm polycarbonate centrifuge tubes. The polymerized filaments were pipetted using cut tips to avoid shearing. The mixture was incubated for 20 min at RT, followed by centrifugation at 48,000 rpm for 10 min at 4°C using a TLA 100 rotor (Beckman Coulter). The supernatants were removed, and the pellets were resuspended in 12.5 μL polymerization buffer mixed with SDS-PAGE loading buffer. The pellets were resolved and visualized by SDS-PAGE gels and SyproRed (Invitrogen) staining, and subsequently quantified on a Pharos FX Plus Molecular Imager with Quantity One software (Bio-Rad). Actin bundling experiments were performed similarly to the actin binding experiments, with the exception that 8 μM actin was polymerized for 1 hour and diluted to a final concentration of 4 μM in the presence of varying concentrations of different Capu-CT truncations (Figure 1-1). The mixed filaments and proteins were incubated for 20 min at RT, followed by centrifugation at 19,000 rpm for 5 min at 4°C using a TLA 100 rotor. The filaments in the supernatant were analyzed similar to the binding assay.

TIRF microscopy assay

Cover slips (22x22 mm, #1.5, Corning) were coated with poly-L-lysine (Sigma) by incubating the cover slips with 1 mg/mL poly-L-lysine solution for 1-3 min. The cover slips were rinsed with distilled water three times and dried over night under UV light. Amoeba actin (30 μM) was polymerized for ~1 hour in 1x KMEH. After polymerization, an equimolar amount of AlexaFluor647-phalloidin was added. The polymerized filaments were pipetted using cut tips to avoid shearing. The phalloidin-actin was further diluted to a final concentration of 0.375 μM in the presence of control buffer or 2 μM Capu-CT, Capu-NT or Capu(1-321). Samples were incubated at RT for 15 min, diluted in 200 μL 1x KMEH, spotted on a microscope slide, and covered with a poly-L-lysine coated cover slip. Actin filaments and bundles were visualized

using a DMI6000 TIRF microscope (Leica) equipped with a 635 nm laser.

Reference

Bor, B., Vizcarra, C. L., Phillips, M. L. and Quinlan, M. E. (2012). Autoinhibition of the formin Cappuccino in the absence of canonical autoinhibitory domains. *Mol. Biol. Cell* **23**, 3801–3813.

Chhabra, E. S. and Higgs, H. N. (2006). INF2 Is a WASP homology 2 motif-containing formin that severs actin filaments and accelerates both polymerization and depolymerization. *J Biol Chem* **281**, 26754–67.

Goode, B. L. and Eck, M. J. (2007). Mechanism and Function of Formins in the Control of Actin Assembly. *Annu Rev Biochem* **76**, 593–627.

Gurel, P. S., Ge, P., Grintsevich, E. E., Shu, R., Blanchoin, L., Zhou, Z. H., Reisler, E. and Higgs, H. N. (2014). INF2-mediated severing through actin filament encirclement and disruption. *Curr. Biol. CB* **24**, 156–164.

Harris, E. S., Rouiller, I., Hanein, D. and Higgs, H. N. (2006). Mechanistic differences in actin bundling activity of two mammalian formins, FRL1 and mDia2. *J Biol Chem* **281**, 14383–92.

Michelot, A., Guérin, C., Huang, S., Ingouff, M., Richard, S., Rodiuc, N., Staiger, C. J. and Blanchoin, L. (2005). The formin homology 1 domain modulates the actin nucleation and bundling activity of Arabidopsis FORMIN1. *Plant Cell* **17**, 2296–2313.

Moseley, J. B. and Goode, B. L. (2005). Differential activities and regulation of Saccharomyces cerevisiae formin proteins Bni1 and Bnr1 by Bud6. *J. Biol. Chem.* **280**, 28023–28033.

Quinlan, M. E. (2013). Direct interaction between two actin nucleators is required in Drosophila oogenesis. *Dev. Camb. Engl.* **140**, 4417–4425.

Quinlan, M. E., Hilgert, S., Bedrossian, A., Mullins, R. D. and Kerkhoff, E. (2007). Regulatory interactions between two actin nucleators, Spire and Cappuccino. *J. Cell Biol.* **179**, 117–128.

Rosales-Nieves, A. E., Johndrow, J. E., Keller, L. C., Magie, C. R., Pinto-Santini, D. M. and Parkhurst, S. M. (2006). Coordination of microtubule and microfilament dynamics by Drosophila Rho1, Spire and Cappuccino. *Nat Cell Biol* **8**, 367–376.

Roth-Johnson, E. A., Vizcarra, C. L., Bois, J. S. and Quinlan, M. E. (2014). Interaction between microtubules and the Drosophila formin Cappuccino and its effect on actin assembly. *J. Biol. Chem.* **289**, 4395–4404.

Scott, B. J., Neidt, E. M. and Kovar, D. R. (2011). The functionally distinct fission yeast formins have specific actin-assembly properties. *Mol. Biol. Cell* **22**, 3826–3839.

Vizcarra, C. L., Kreutz, B., Rodal, A. A., Toms, A. V., Lu, J., Zheng, W., Quinlan, M. E. and Eck, M. J. (2011). Structure and function of the interacting domains of Spire and Fmn-family formins. *Proc. Natl. Acad. Sci.* **108**, 11884–11889.

Conclusion: Autoinhibition of Cappuccino

Combining *in vitro* and *in vivo* experiments, I was able to show that Capu can be autoinhibited. Although many formins are regulated by autoinhibition (Schönichen and Geyer, 2010), the formin group of formins were thought to be an exception due to the lack of N- and C-terminal sequence homology. Despite this hypothesis, I was able to show that Capu is autoinhibited (Bor et al., 2012). It is clear that Capu-NT can inhibit Capu-CT's actin polymerization activity in pyrene and TIRF microscopy assays as well as in *Drosophila* oocytes. We mapped the two interacting regions within the Capu N-terminus (CID) and C-terminus (Capu-Tail). They are in region similar to other formin's autoregulatory domains. I do not believe, however, that the CID and Capu-Tail domains are similar to DID and DAD domains because they have low sequence homology and my data suggests that the CID is structurally distinct from the DID. To address this further, future studies need to focus on a higher resolution structure of CID to determine how exactly CID and Capu-Tail interact and how this interaction inhibits Capu's function.

Furthermore, I was able to show that CID-truncated, constitutively-active Capu increases the density of the actin mesh in *Drosophila* oocytes. This increase subsequently inhibits cytoplasmic streaming. Correct timing of actin mesh and cytoplasmic streaming are crucial for establishing oocyte polarity and female sterility. Confirmingthis claims, we observe that expressing constitutively active Capu resulted in mis-localization of *osk*, *bcd* and *nanos* mRNAs as well as decreased female fertility. Therefore, Capu autoinhibition is crucial for regulating Capu's function both *in vitro* and *in vivo*.

Spire is a well known regulator of Capu and it is intriguing that both Spir-KIND and CID bind to the Capu-Tail domain (Bor et al., 2012; Quinlan, 2013; Quinlan et al., 2007; Vizcarra et al., 2011). This suggests Capu is either autoinhibited or bound to Spir but both cannot occur at the same time. I was able to find a Capu-Tail mutation that affects Spir-KIND binding but not CID binding. We were not able to find the converse mutation which affects CID binding but not Spir-KIND binding. The affinities of CID and Spir-KIND for Capu-Tail is very similar but CID is

part of Capu. Thus, autoinhibition is expected to be dominant over Spir-KIND binding. *Drosophila* studies, however, suggested that the Spir-KIND interaction might be dominant over autoinhibition during mid-oogenesis because expression of Capu-NT was not able to inhibit endogenous Capu protein. This could be explained by posttranslational modification of CID or Capu-Tail that inhibits Capu-Tail/CID interaction but not Capu-Tail/KIND interaction. Further experiments are needed to address how exactly Capu autoinhibition is regulated during *Drosophila* oogenesis so that normal cooperation of Capu and Spir can create the actin mesh.

In addition to Spir, Capu is also thought to be regulated by Rho GTPases (Goode and Eck, 2007). Specifically, Rho GTPase may bind near the CID domain (Rosales-Nieves et al., 2006) to inhibit interaction between Capu-Tail and CID. However, in our experiments, we did not see activation of Capu-CT when we added Rho GTPases in the presence of Capu-NT. This suggests Capu is not regulated by Rho GTPases or our *in vitro* conditions were not ideal for this kind of regulation. This hypothesis needs to be tested further.

Capu is the first member of formin family of formins for which autoinhibition has been studied in detail. It will be important to ask whether Capu's mammalian homologs are also autoregulated. Mammals have two Spire homologues, Spire-1 and Spire-2, and two Capu homologues, Formin-1 and Formin-2 (Higgs, 2005; Quinlan et al., 2007). There is evidence of Formin-1 autoinhibition *in vitro* but Formin-2 remains to be tested. The N-termini of these proteins are quite different, making experimental evidence of autoinhibition essential. Capu and Spire genes always exist together in metazoan genomes (Quinlan et al., 2007), and they have nearly identical expression patterns in the developing mouse embryo, suggesting their interaction is conserved (Schumacher et al., 2004). Furthermore, murine Formin-2 along with Spir-1 and Spir-2 are required for the correct positioning of the metaphase spindle, which ensures asymmetric cell division during meiosis I in oocyte development. Thus, the mammalian homolog of Capu is important in birth defects and infertility (Dumont et al., 2007; Leader et al., 2002; Pfender et al., 2011). Many stem cells use asymmetric cell division, and defects in these

cells could cause tumor development (Reya et al., 2001). Therefore, understanding the regulation of Capu and Spire will help us understand cancer biology and possibly offer a method to treat the disease state.

Reference

Bor, B., Vizcarra, C. L., Phillips, M. L. and Quinlan, M. E. (2012). Autoinhibition of the formin Cappuccino in the absence of canonical autoinhibitory domains. *Mol. Biol. Cell* **23**, 3801–3813.

Dumont, J., Million, K., Sunderland, K., Rassinier, P., Lim, H., Leader, B. and Verlhac, M.-H. (2007). Formin-2 is required for spindle migration and for the late steps of cytokinesis in mouse oocytes. *Dev Biol* **301**, 254–65.

Goode, B. L. and Eck, M. J. (2007). Mechanism and Function of Formins in the Control of Actin Assembly. *Annu Rev Biochem* **76**, 593–627.

Higgs, H. N. (2005). Formin proteins: a domain-based approach. *Trends Biochem Sci* **30**, 342–53.

Leader, B., Lim, H., Carabatsos, M. J., Harrington, A., Ecsedy, J., Pellman, D., Maas, R. and Leder, P. (2002). Formin-2, polyploidy, hypofertility and positioning of the meiotic spindle in mouse oocytes. *Nat Cell Biol* **4**, 921–8.

Pfender, S., Kuznetsov, V., Pleiser, S., Kerkhoff, E. and Schuh, M. (2011). Spire-Type Actin Nucleators Cooperate with Formin-2 to Drive Asymmetric Oocyte Division. *Curr. Biol.* 1–6.

Quinlan, M. E. (2013). Direct interaction between two actin nucleators is required in Drosophila oogenesis. *Dev. Camb. Engl.* **140**, 4417–4425.

Quinlan, M. E., Hilgert, S., Bedrossian, A., Mullins, R. D. and Kerkhoff, E. (2007). Regulatory interactions between two actin nucleators, Spire and Cappuccino. *J. Cell Biol.* **179**, 117–128.

Reya, T., Morrison, S. J., Clarke, M. F. and Weissman, I. L. (2001). Stem cells, cancer, and cancer stem cells. *Nature* **414**, 105–111.

Rosales-Nieves, A. E., Johndrow, J. E., Keller, L. C., Magie, C. R., Pinto-Santini, D. M. and Parkhurst, S. M. (2006). Coordination of microtubule and microfilament dynamics by Drosophila Rho1, Spire and Cappuccino. *Nat Cell Biol* **8**, 367–376.

Schönichen, A. and Geyer, M. (2010). Fifteen formins for an actin filament: A molecular view on the regulation of human formins. *BBA - Mol. Cell Res.* **1803**, 152–163.

Schumacher, N., Borawski, J. M., Leberfinger, C. B., Gessler, M. and Kerkhoff, E. (2004). Overlapping expression pattern of the actin organizers Spir-1 and formin-2 in the developing mouse nervous system and the adult brain. *Gene Expr. Patterns GEP* **4**, 249–255.